



Project Deliverable

Grant Agreement number	308952
Project acronym	OMSOP
Project title	OPTIMISED MICROTURBINE SOLAR POWER SYSTEM
Funding Scheme	FP7-ENERGY.2012.2.5.1:RESEARCH, DEVELOPMENT AND TESTING OF SOLAR DISH SYSTEMS
Work Package	WP1 – SYSTEM COMPONENT DEVELOPMENT
Deliverable number - title	D1.2 - REPORT ON SHORT TERM STORAGE TESTING AND EVALUATION
Lead Beneficiary	RO3
Dissemination level	PU
Delivery month	JULY 2015
Name, title and organisation of the scientific representative of the project's coordinator	Abdulnaser Sayma Professor of Energy Engineering City University London Tel: +44 (0)20 7040 8277 E-mail: a.sayma@city.ac.uk Project website address: www.omsop.eu

CONTENTS

INTRODUCTION.....
STATE OF THE ART.....
RO3 SHORT TERM STORAGE CONCEPT.....
THEORETICAL RECEIVER MODEL.....
TEST RESULTS.....
SHORT TERM & THERMAL STORAGE DESIGN.....
CONCLUSIONS.....
REFERENCES.....
ANNEX.....

INTRODUCTION

Concentrated Solar Energy Power Plants (CSEPP) equipped with turbomachinery based engines such as steam cycles; ORC and Brayton Cycles (BC) have shown some mechanical drawbacks owing to the oscillations of the Radiant Power (RP) reaching the Receiver [1, 2].

RP oscillations cause corresponding changes in the Engine Working Fluid inlet temperatures and consequently of the pressure. This produces pulsations on the trust bearings causing fatigue damages.

Phase Changing Materials (PCM) used as storage media can really be useful for this purpose when they work under two-phase state. In fact, under these circumstances, the engine working fluid flowing inside a tube bundle immersed in the two-phase state material, the working fluid temperature pulsations are damped and the engine behaviour becomes more regular as shown in figure 1 taken from [3]. If the PCM mass is sufficient and the PCM solid fraction approaches zero, a strong reduction of the DNI (also absence of the Sun) leads to increase the solid PCM fraction with reduced quick effects on the working fluid temperature. The same occurs when there is a sharp change in the DNI.

Numerous applications of PCM used as thermal storage have been successful for low temperatures [4, 5, 6, 7, 8, 9 and 10].

The search to have thermal storage at high temperatures suitable for Brayton Cycle based engines is ongoing [11, 12, 13, 14 and 15]. Difficulties arise because of the relatively high temperatures, higher than 800°C.

Today, Concentrated Solar Energy Micro Gas Turbine (CSEMGT) fed by Solar Dish can take benefit from the car engine turbocharger technology that being producing millions of units may really be cheap. Turbocharger technology allows running continuously to some 950 – 975°C and for short peaks can run up to some 1025°C. To take maximum energy benefit from such temperatures, it is necessary to think to PCM that melts at temperatures up to 1050 – 1100°C.

RO3 receiver concept is equipped with short-term thermal storage that has been made in agreement with the above concepts.

The thermal storage by PCM has been sized to allow:

- a minimum storage for 10 – 15 minutes just to dump compressed air pulsations and very short transient due to Sun unavailability;
- some 45 – 50 minutes to guarantee a longer heat supply to allow controlled shut-down of the connected processes. This solution may have also a fallout into various application fields.

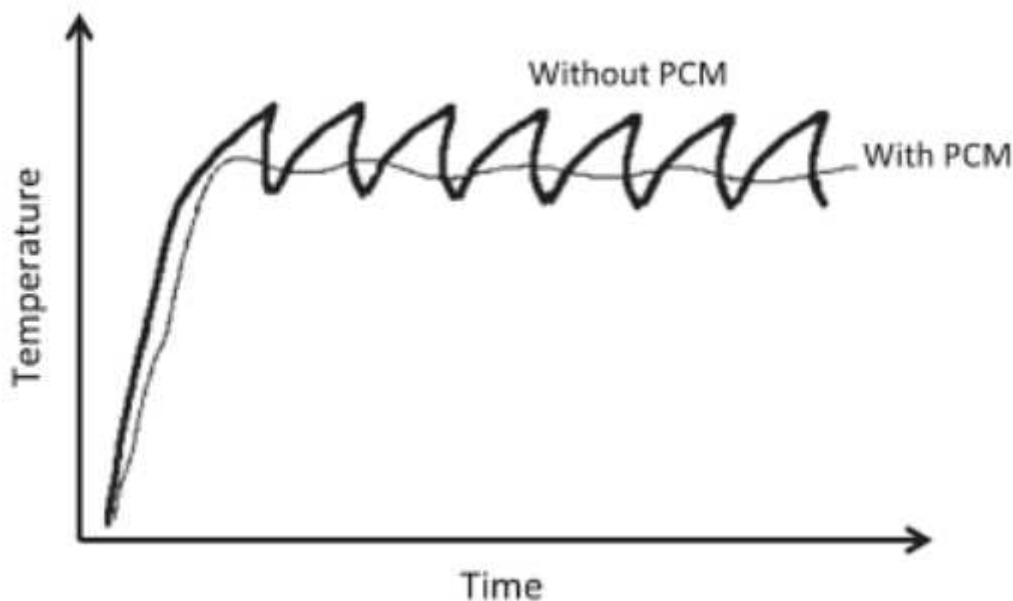


Figure 1: Trend of temperatures versus time with and without PCM

STATE OF THE ART

Thermal Energy Storage (TES) in Concentrated Solar Plants (CSP) is related to various aspects. The main one is connected with the possibility of feeding the Electrical Grid independently of the Sun availability and avoid a further backup engine to supply power during such an unavailability.

High temperature solar receivers, to feed Brayton and Stirling engines, have a long history. In the annex, a state of the art is reported.

Various projects have been carried out, they have analysed the concepts and their feasibility. Review papers and reports give an amply vision of the TES theoretical and practical aspects [16, 17, 18, 19, 20, 21].

Sensible heat thermal storage is widely used for ORC and steam solar fed power plants.

Typical temperature of the storage medium is in the order of 550°C when melted salts are used.

To increase such a temperature, various attempts have been made and research is still ongoing. Amply reviews have been published [22]. In addition, concrete and ceramic media have been studied.

Among the various CSP Fresnel linear reflectors, Parabolic Trough and Central Receiver Tower have been coupled with TES for plants whose generation power achieves 100s of MW [23].

Generally, sensible heat based TES have been explored and demonstrated.

Dish engine CSP's usually show a small scale, from a few kW (3-5 kW) up to 30-35 kW in a single module based on a Solid Mirror Dishes (SMD), Stirling and Brayton engines are the candidates. Dish based on Arrays have been demonstrated with Brayton engines for some 100 kW. In this project, only the Dish Engine systems based on Solid Dish having power ranging from 3 to 35 kw have been taken into consideration. OMSoP Project is for the demonstration of a Dish-Brayton Cycle (say Micro Gas Turbine (MGT) system).

Dish Engine System (DES) needs TES for reduced time intervals because the power backup can be made or by supplying fuel (heat) to the engine (so called hybrid systems) or by feeding electric batteries. However, Dish-Brayton Systems may need two levels of TES. One based on some 10-15 minutes to dump working fluid temperature oscillations at the receiver exit. This means that the PCM is used for thermal management application not as TES for power management. Another storage time interval concerns with 40 minutes to one hour. This TES is used for power management in some special applications.

RO3 SHORT TERM STORAGE CONCEPT

RO3 has proposed the development of a Solar Receiver (SR) made, according to the sketch of figure 2, of a tube bundle immersed in a PCM encapsulated in a container whose frontal area receives the concentrated Sun Rays from the Dish. The conceptual behaviour is that starting from cold conditions, the SR impinge onto the frontal plate surface making its temperature rise.

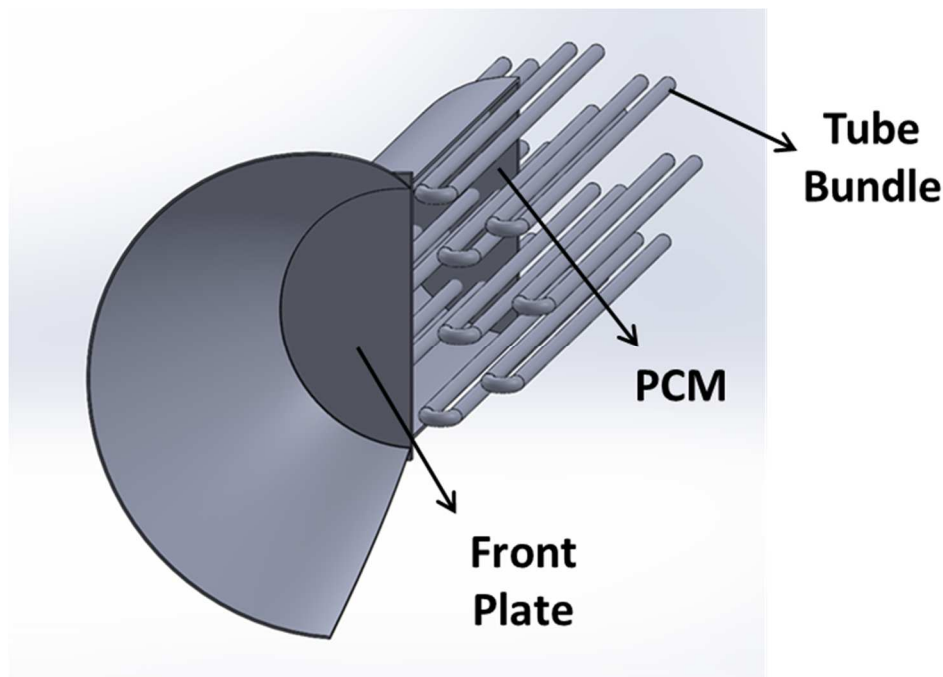


Figure 2: Sketch of tube bundle immersed in PCM

For this explanation, it is assumed that the Receiver heat power loss from the TES charge container is zero; moreover, no heat power is absorbed by the Engine Working Fluid (EWF). The heat power from the SR is transferred inside through the frontal plate thickness and by means of Solid Heat Pipes (SHP). During the regular behaviour, the internal TES charge, made of a suitable material, is heated up and its temperature increases up to the melting temperature. When the melting temperature is reached, the solid fraction $x_s = 1$ while the liquid fraction $x_l = 0$. After that instant, the solid fraction decreases until $x_s = 0$ while the liquid fraction increases till $x_l = 1$. After that condition, all the TES charge is completely melted and the liquid temperature starts to grow up.

The Receiver TES cavity contains also the tube bundle inside which the EWF is heated up. Making the EWF start flowing when the liquid fraction has reached a value higher than zero, the useful heat power reduces the rising rate of the liquid fraction while the temperature of the TES charge remains almost unchanged. Receiver irradiance oscillations are damped because of the thermal inertia of the TES charge that makes the internal temperatures stable.

The OMSoP Short Term Storage Receiver (STSR) has been designed. Its concept has been developed basing on modules to meet the needs of the demonstrator: (5 kW net electric power; single shaft MGT) and of the perspective engines that may be equipped with a multiple heating expander [24, 25]. The final choice is the adoption of 12 single bundles to meet the needs of up to four successive heating in the expansion.

Two possible solutions have been evaluated:

- the first one with longitudinal U tubes, see figures 2,3 and 4.

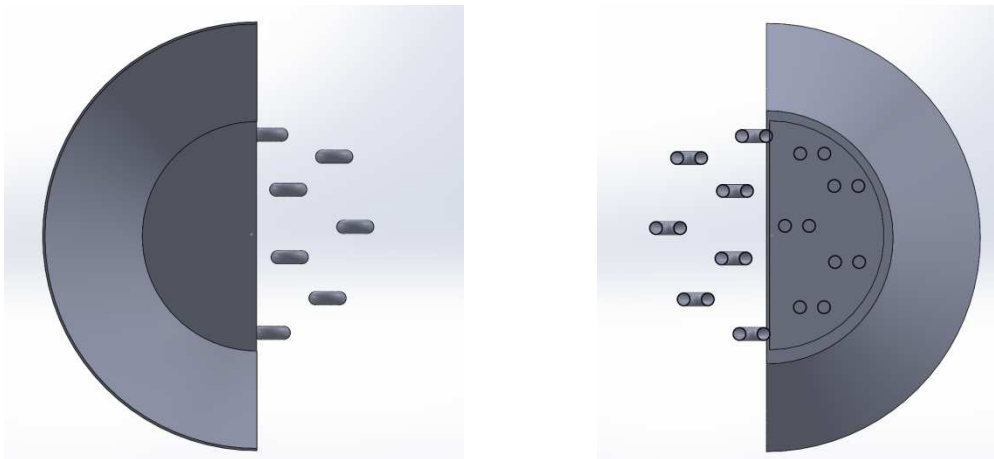


Figure 3: U Tubes Front Plate and Back Plate Views

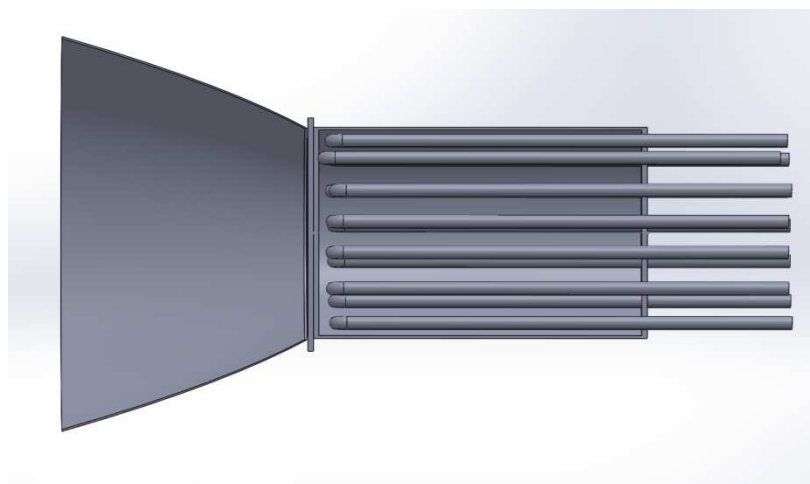


Figure 4: U Tubes Cross-Section Views

- the second one with tubes arranged in spirals (SPT) see figures 5, 6 and 7.

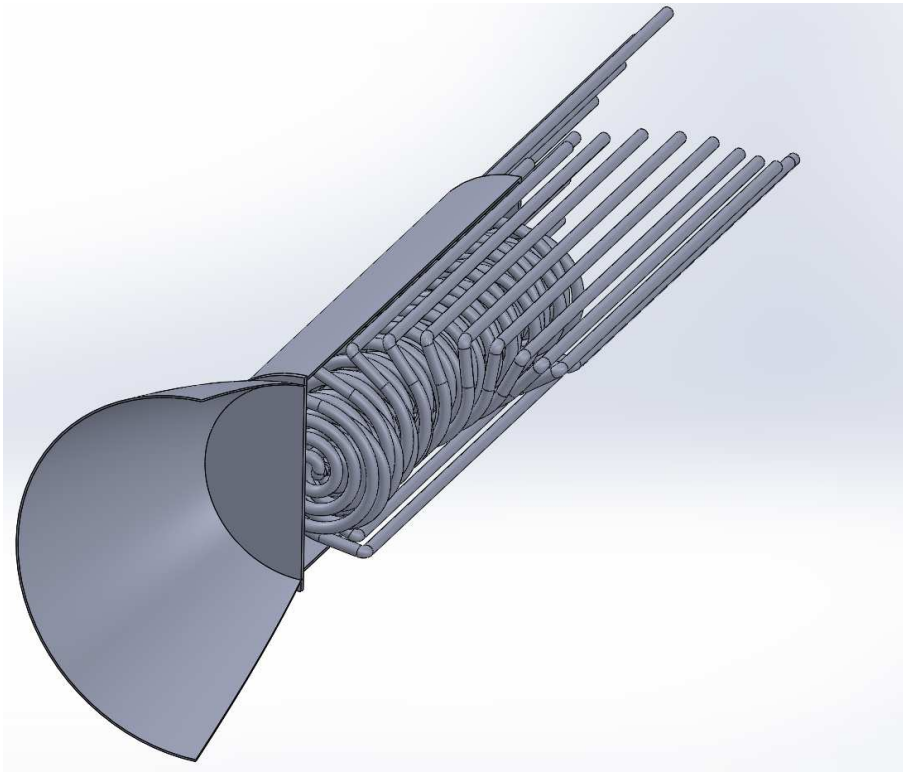


Figure 5: Spiral Tube Bundle Isometric View

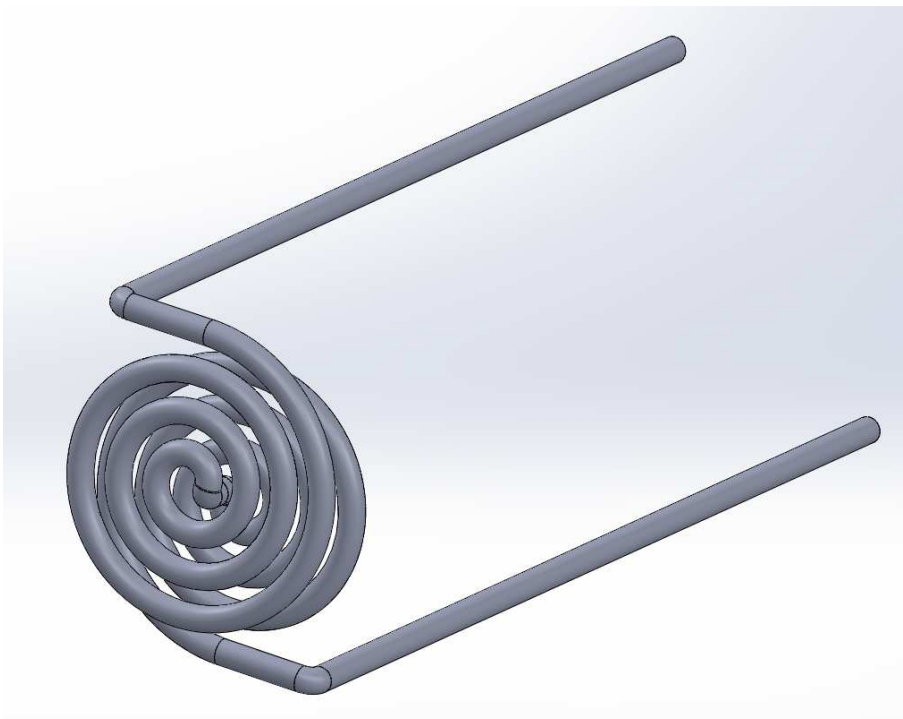


Figure 6: Two-Spiral Tube Bundle Isometric View

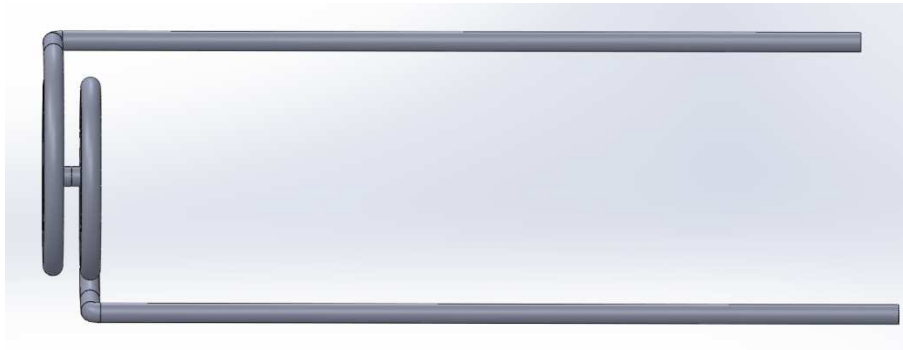


Figure 7: Two-Spiral Tube Bundle Cross Section

The scheme of the module to be tested in order to evaluate material temperature differences and heat transfer has been depicted in figure 8. Two experimental setups have been designed. The first one is with the internally smooth frontal surface while the second one has the inner frontal surface equipped with 25 Solid Heat Pipes made of corrugated surfaces to enhance the heat transfer. Figure 9 shows the two frontal plates on the side in contact with the PCM.

The two models have been filled with $\text{NaNO}_3 - \text{KNO}_3$ salt that melts at about 238°C furnished by ENEA.

The void volumes to be filled by the salt are 0,441 litres for the smooth plate and 0,434 for the SHP plate with the frontal plate having a diameter equal to 120 mm.

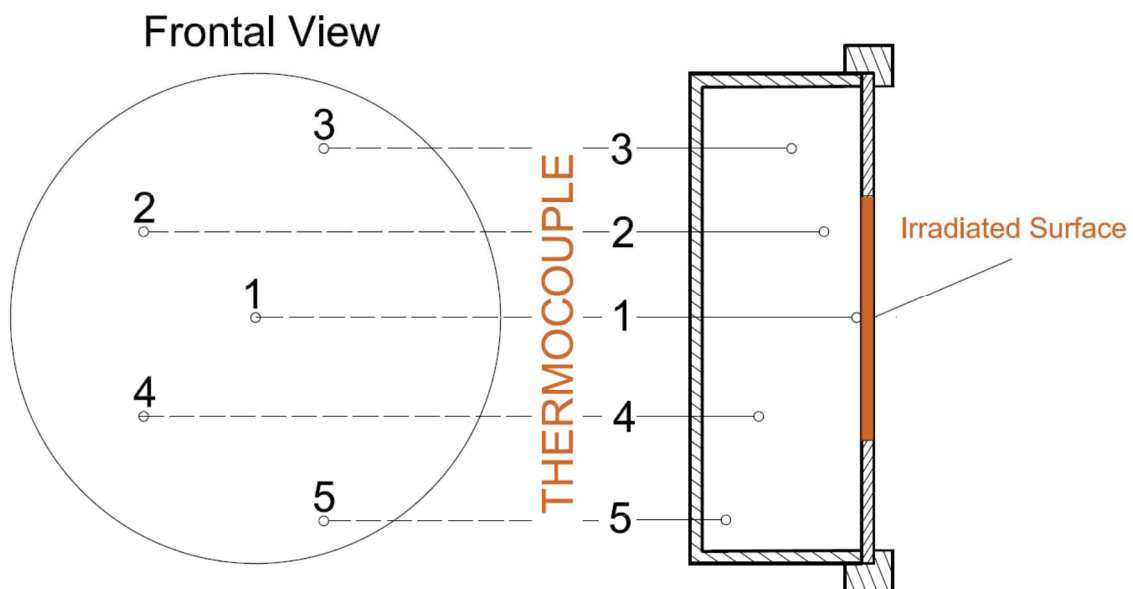


Figure 8: Sketch of the module used for tests



Figure 9: Picture of the two frontal disc – Smooth Surface (right) & Solid Heat Pipes (left) HEORETICAL RECEIVER MODEL

A simple model based on lumped parameters has been developed to estimate the time evolution and scale up the model test results. The model has been developed and used to perform calculations to forecast the response of the receiver for short-term storage. In figure 10, the scheme adopted for modelling the PCM based receiver is reported. Model is based on an approach that adopts lumped performance parameter (heat transfer coefficients, heat power, etc.) to describe the behaviour of the Receiver.

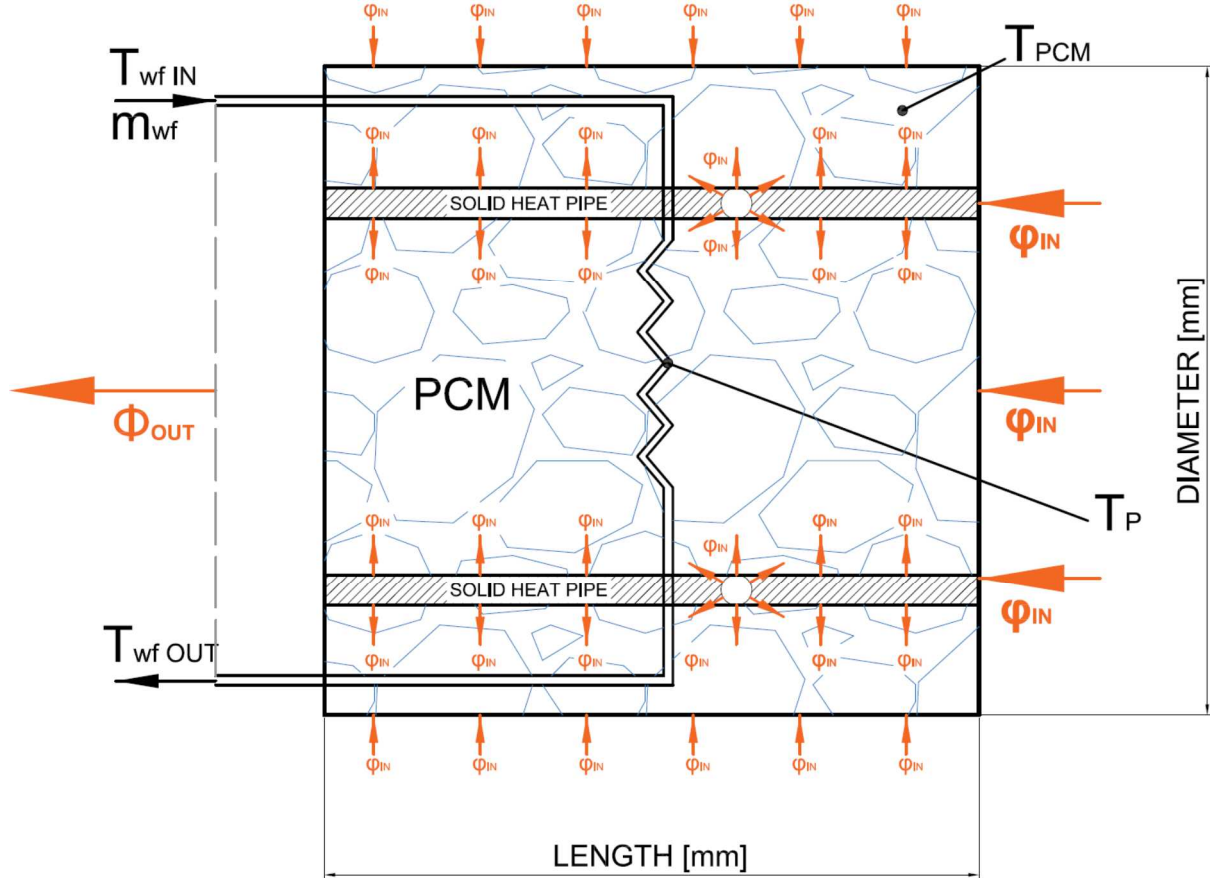


Figure 10: Scheme of the Short Term Storage Receiver based on PCM

Looking at the receiver sketch of figure 10, the heat power entering the receiver (Φ_{IN}) and the exiting one (Φ_{OUT}) are highlighted with orange arrows. The heat power Φ_{OUT} heats up the Engine Working Fluid (EWF) mass flow from inlet temperature (T_{WFIN}) to the WF outlet temperature (T_{WFOUT}). Accordingly, the heat power transferred to the working fluid is expressed by the rule (1):

$$\Phi_{OUT} = m_{WF} \cdot \bar{c}_p \cdot (T_{WFOUT} - T_{WFIN}) \quad (1)$$

The heat power enters into the PCM charge by means of solid surface made of the Solid Heat Pipes (SHP) and of the frontal plate inner surface. Taking heat fluxes φ_{IN} along the boundary surface σ into account, the heat power entering the receiver is (2):

$$\Phi_{IN} = \int_R \varphi_{IN} d\sigma \quad (2)$$

Looking at the Phase Change Material (PCM), the receiver volume is defined by the rule (3):

$$V_R \approx \frac{\pi \cdot D^2 \cdot L}{4} - \delta \cdot \frac{n_{SHP} \cdot \pi \cdot d_{SHP}^2 \cdot l_{SHP}}{4} \quad (3)$$

$$\begin{cases} \delta = 0 \Leftrightarrow \text{NO SHP} \\ \delta = 1 \Leftrightarrow \text{YES SHP} \end{cases} \quad (4)$$

D , L , d_{SHP} , l_{SHP} , n_{SHP} being the receiver diameter, the receiver length, the SHPs diameter, length and number of solid heat pipes, respectively. Coefficient δ is equal zero if the receiver is equipped without solid heat pipes. When SHPs exist $\delta = 1$ (4).

PCM density ρ_{PCM} can be assumed from literature [6, 8 and 17] for the materials that are employed for the thermal storage. Accordingly, the mass inside the receiver can be easily established by the rule (5):

$$M_R \approx V_R \cdot \rho_{PCM} \quad (5)$$

If the phase change material is a pure substance, its behaviour is characterized by the temperature-heat (T-H) diagram, given in figure 11.

According to such a scheme, it has been taken into consideration for modelling the heat transfer processes that take place when the PCM is in different phases:

- | | |
|-------------------------|-------------------------|
| 1. Solid Phase | $T_{PCM} < T_{Melting}$ |
| 2. Solid + Liquid Phase | $T_{PCM} = T_{Melting}$ |
| 3. Liquid Phase | $T_{PCM} > T_{Melting}$ |

It means that under the melting temperature (T_M) the phase change material is in the solid phase. Under these conditions, it is characterized by the solid specific heat c_S and heat transfer processes are characterized by conduction. PCM material temperature rises during heating and decreases during cooling. When temperature is higher than the melting one, the PCM is liquid and, in this case, heat transfer is characterized by prevalent convective processes. Also in these conditions, heating leads to a PCM temperature increase and cooling leads to a PCM temperature reduction. Correction has been adopted for taking the glide aspects being connected with the real phase change process of the PCM into consideration. In fact, the real behaviour of the system, in the melting region, depends strictly on the PCM composition. In many case the melting point temperature is not a point, but it is a range of temperature in which the two fractions change phase. It usually happens when the PCM is made of at least two components. As an example, a phase diagram of a two component PCM is depicted in figure 12.

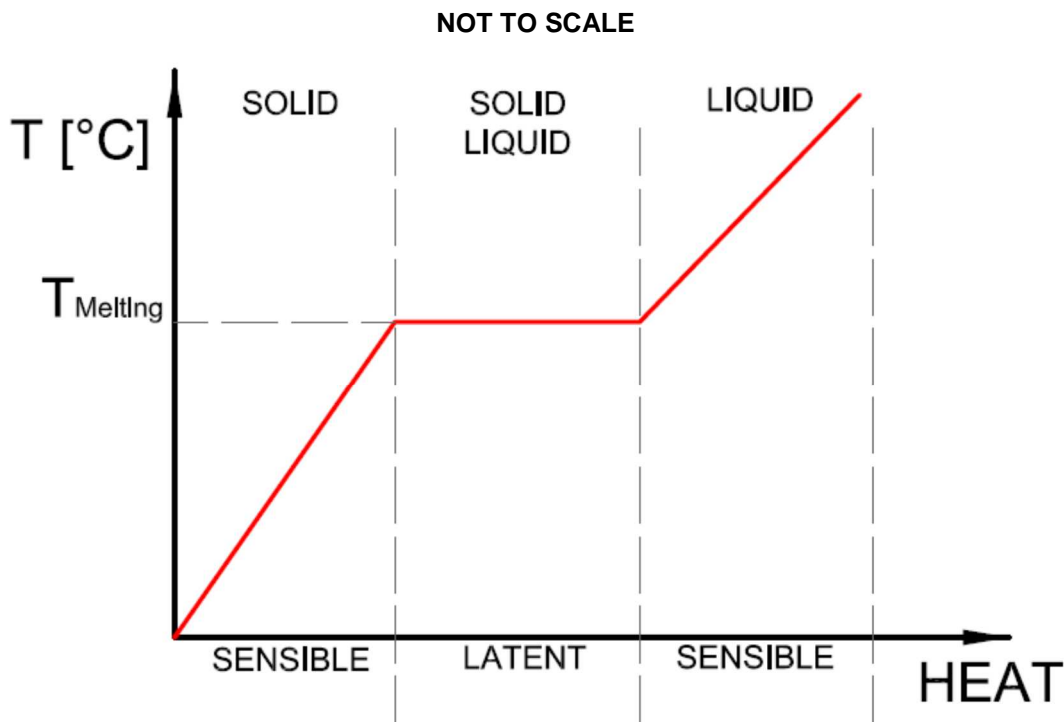


Figure 11: Typical PCM Phase Diagram – NOT TO SCALE

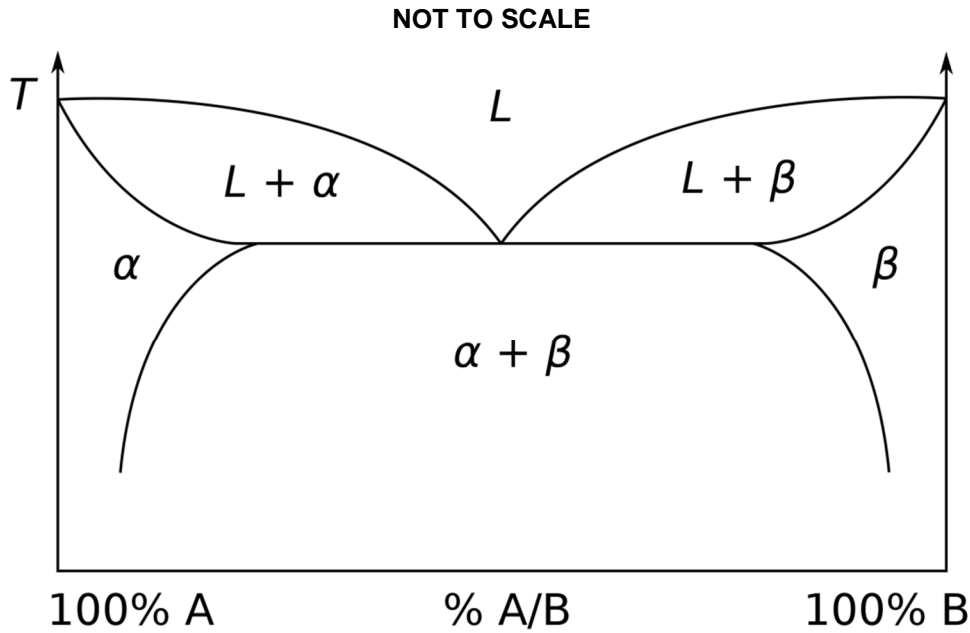


Figure 12: Example of a two components eutectic PCM – NOT TO SCALE

According to the above, the model has been developed taking into consideration three conditions, previously described. Concerning the mass of the system, two indexes have been introduced to describe the solidus (eq. 6) and liquid (eq. 7) fractions in the system.

$$\mu_s = \frac{M_s}{M_s + M_L} \quad (6)$$

$$\mu_L = 1 - \frac{M_s}{M_s + M_L} \quad (7)$$

By means of these indexes, it is possible to easily describe the heat transfer process in the three different cases. Heat transferred to the PCM Φ_{S-PCM} is established by coupling the model of the two sub-systems. One is the PCM charge; the other is the wall front disc that receives the impinging solar rays. Anyway, at this step, it is sufficient to say that (8):

$$\Phi_{IN} = \Phi_{S-PCM} \quad (8)$$

Heat power transferred between the PCM to the WF Φ_{PCM-WF} (9) can be correlated to specific quantities characterized the heat transfer processes.

$$\Phi_{OUT} = \Phi_{PCM-WF} = S_{TB} \cdot U_{TB} \cdot (T_{PCM} - T_{WF}) \quad (9)$$

U being the heat transfer coefficient, S being the heat transfer surface and T being the temperatures. Equation (9) takes the heat transfer process across the tube bundle surface, in which the WF flows. For establishing the heat transfer coefficients correlation of Nusselt, Reynolds, Grashof, Prantl, Stefan and others have been adopted, after a wide State of the Art investigation on such kind of applications. Moreover, the architecture and the geometries of the device influence significantly the heat transfer phenomena. Summarizing these concepts, the heat transfer coefficients (j -th) can be related to many quantities (10):

$$U_j = f(\text{Re}, \text{Gr}, \text{Pr}, \text{Pl}, \nu, \rho, s, \lambda, \mu, g, cp, \text{architecture}, \text{geom}, \dots) \Big|_j \quad (10)$$

Three heat transfer processes have been modelled:

1) Sensible Heat – Solid Phase

Under these conditions the fraction of the liquid is zero and the overall PCM mass is solid (eq. 11). Injection (or rejection) of some heat power on the PCM leads to an increase (or to a reduction) of PCM temperature.

$$M_{PCM} = (\mu_S + \mu_L) \cdot M_{PCM} \rightarrow \mu_L = 0 \& \mu_S = 1 \quad (11)$$

From energy conservation, it can be written (eq.12). It can be easily manipulated combining with (8) and (9) expressing the temperature variation in terms of the heat transfer processes.

$$(\Phi_{IN} - \Phi_{OUT}) = \Phi_{PCM} = M_S \cdot c_S \cdot \frac{dT_{PCM}}{dt} \quad (12)$$

2) Latent Heat – Solid + Liquid Phase

Under these conditions, the PCM temperature variation owing to positive and negative heat power contribution is negligible, because of the phase change. Accordingly, the mass of the system is constituted both from the liquid fraction and from the solid one (eq.13)

$$M_{PCM} = (\mu_S + \mu_L) \cdot M_{PCM} \rightarrow \mu_L, \mu_S \neq 0 \quad (13)$$

Also in this condition, taking into account energy conservation, it can be written (eq.14), that the heat power inject or rejected from the receiver, once the latent heat r [kJ/kg] of the PCM is given, leads to a variation of the liquid (or solid) fraction.

$$(\Phi_{IN} - \Phi_{OUT}) = \Phi_{PCM} = -r \cdot \frac{d\mu_S}{dt} \quad (14)$$

3) Sensible Heat – Liquid Phase

Under these conditions the fraction of the solid is zero and the overall PCM mass is liquid (eq. 15). Injection (or rejection) of some heat power on the PCM leads to an increase (or to a reduction) of PCM temperature.

$$M_{PCM} = (\mu_S + \mu_L) \cdot M_{PCM} \rightarrow \mu_L = 1 \& \mu_S = 0 \quad (15)$$

From energy conservation, it can be written (16) that the temperature variation on the PCM depends on the injection and rejection of heat power into the receiver.

$$(\Phi_{IN} - \Phi_{OUT}) = \Phi_{PCM} = M_L \cdot c_L \cdot \frac{dT_{PCM}}{dt} \quad (16)$$

Adoption of such a model, coupled together with well know ε -NTU model (effectiveness VS Number of Transfer Unit) has led to establish sizes of the receiver for given heat power (injection and rejection), for selected PCM (properties such as density, specific heat, latent heat, etc.) and for defined boundary conditions (inlet pressure, temperature, WF composition, etc.). Once sizes have been evaluated, performance at part load conditions have been performed.

TEST RESULTS

Tests on a module of the Receiver made by a container having a front plate, onto which the Sun Rays impinge, a back plate that allows the introduction of thermocouples to measure the temperatures at various distance from the front plate. Figure 13 shows the model to be tested. Thermocouples are included inside the charge.

The central thermocouple touches the back of the front plate (figure 8) and the others 4 thermocouples are spatially distributed. No tube bundle has been installed to perform the initial tests in order to

understand the temperature differences to transfer the heat power. Figures 8, 9 and 13 show the cross section drawing of the Receiver module and some photos of the details. The low power solar simulator test bench has been used to carry on the tests as shown in the photos of figures 14 and 15 that show AISI 316 used to build the body, the plates and the Solid Heat Pipes.

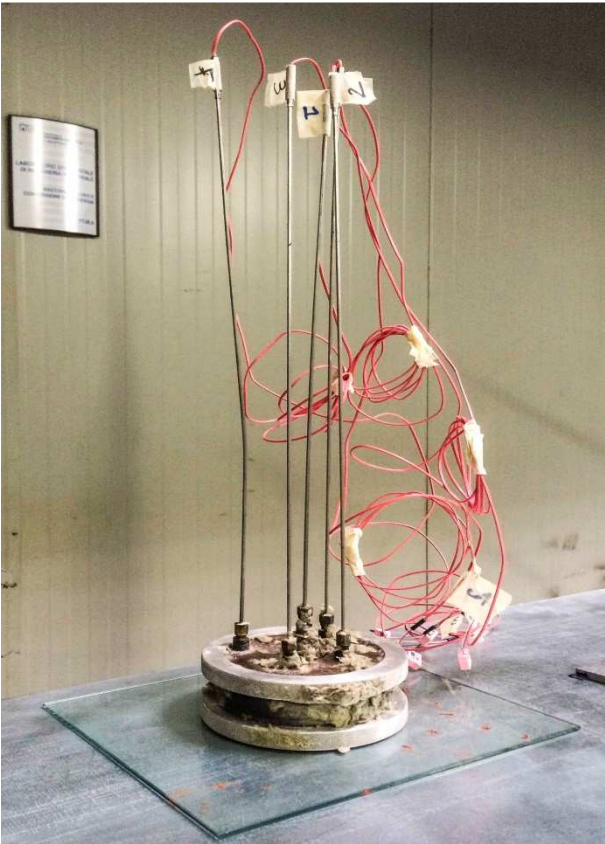


Figure 13: Picture of the model equipped with thermocouples used for tests



Figure 14: Picture of the low power test bench

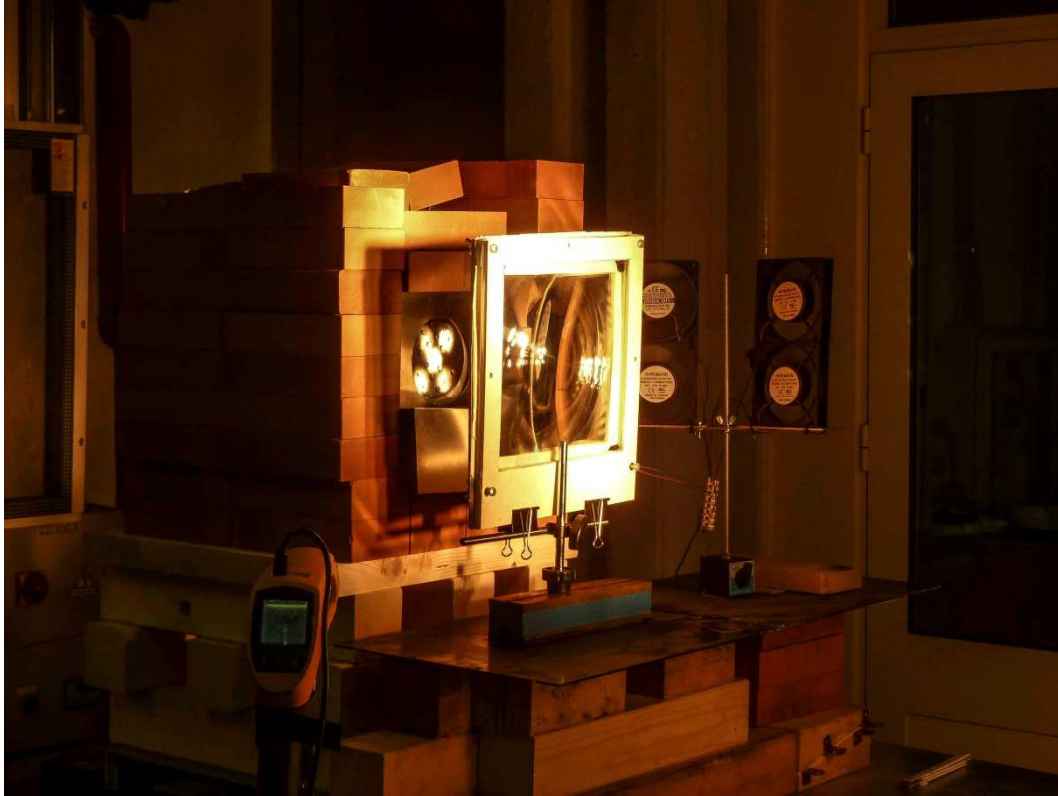


Figure 15: Picture of the low power test bench

The pyrometer that has been used to measure the front plate temperature in the area of the Sun Ray Spot. In this way, it has been possible to have the temperature difference across the front plate. The Receiver Module has been installed inside an insulation system made by porous wool high temperature materials and externally by refractory bricks. The system has been installed on a car platform able to move in the two axis in order to set the right position as shown in figure 16. During the tests, a thermographic camera has been used to check the level of the loss through the insulation. Photos in figure 17 show samples of such outcomes. The brick body outer surface temperature is very low demonstrating that the casing thermal losses are negligible.



Figure 16: Pictures of the target moving system

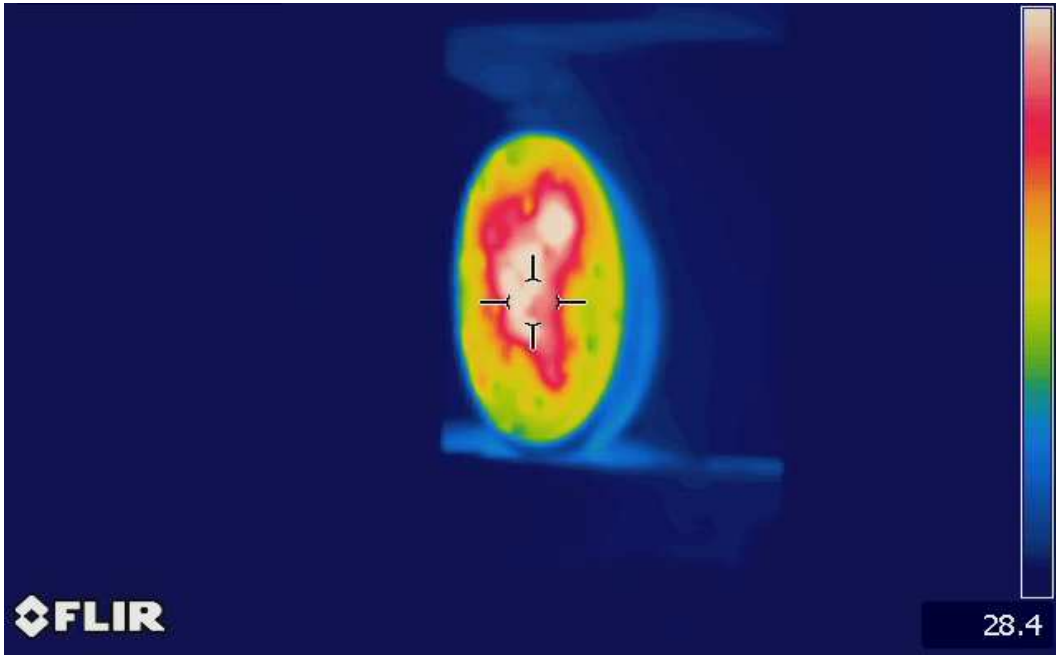


Figure 17: Thermographic camera outcomes

First results are shown in figure 18 where a comparison among the powder melting, the already melted and solidified salt, smooth front plate and front plate equipped with Solid Heat Pipes is given. Figure 18 shows non-dimensional temperature versus time for the three cases. The red solid line is for smooth front plate i.e. without SHP and power as charge. The green line is for front plate equipped with SHP and power as charge. It can be noticed a strong reduction of the peak temperature and the temperature difference in respect to the melting one. The blue line represents the data taken with front plate equipped with SHP and the already melted and solidified charge. In this last case, the peak temperature disappears and the temperature difference between the external front plate temperature and the melting one is reduced.

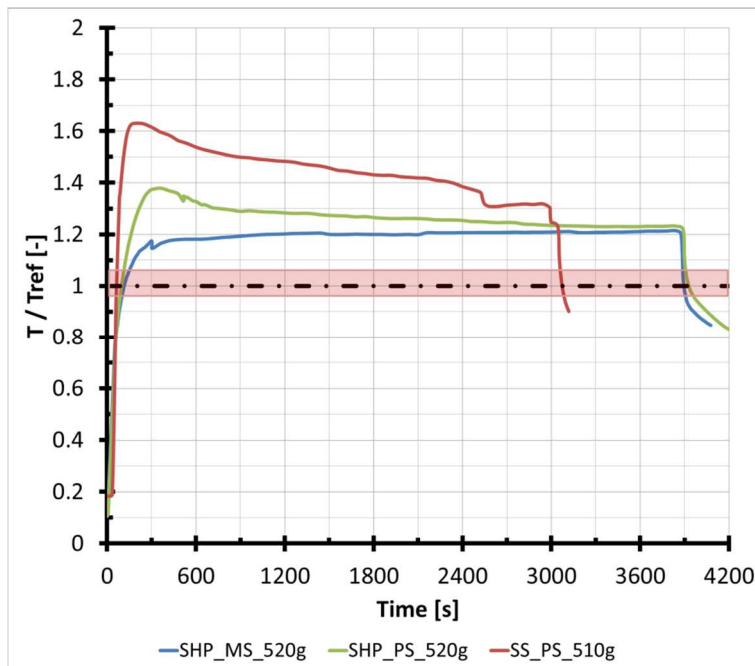


Figure 18: Non-dimensional temperature vs Time for different test bench setup

Lesson is that SHP strongly reduces the metal temperature and the charge has to be filled as liquefied material.

Photo of figure 19 shows the front plate temperature distribution that evidences the spot taken by using only one lamp.

The Model Receiver has been installed inside a cavity sized to avoid convective flows. In fact, figure 20 shows the absence of any velocity close to the front plate. Moreover, velocities measured by the hot wire anemometer range from 2 to 8 cm/s. The pyrometer temperature allows the calculation of the heat power transferred towards the outside.

Many tests have been carried on for long time to check repeatability and to compare results to be used for the receiver sizing. Tests have been carried on also by multiple spots on the front plate; a flat temperature distribution has been evidenced. Temperature versus time are given in figures 21, 22 and 23. Very high temperature gradients at the beginning of the test is evidenced. The charge temperature rises showing some temperature slope change around the expected melting start temperature. Figure 23 shows the discharging obtained by an instantaneous cut of the Rays. Temperature gradients of the metal parts and of the charge. It can be noticed the temperature inversion point, i.e. when the charge temperatures become equal to that of the internal surface of the front plate.

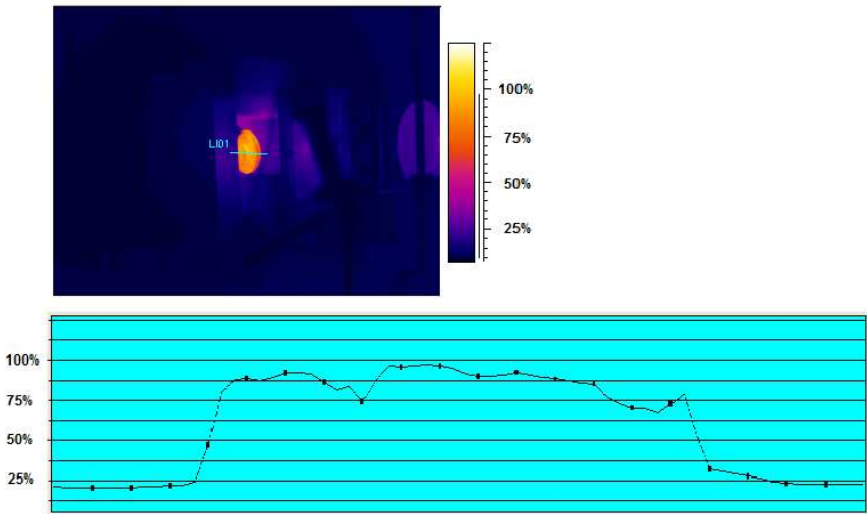


Figure 19: Thermographic camera outcome for using only one lamp



Figure 20: Speed measurement in the test bench cavity

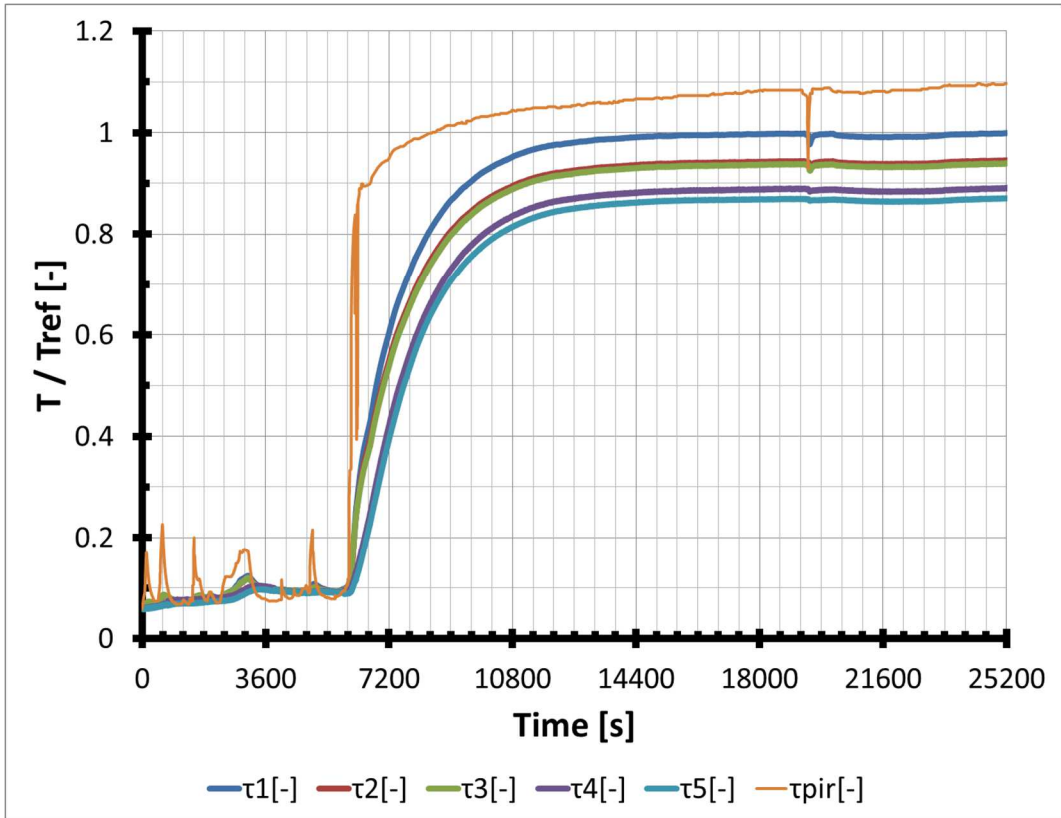


Figure 21: Non-dimensional temperature vs Time - Charging Test (1)

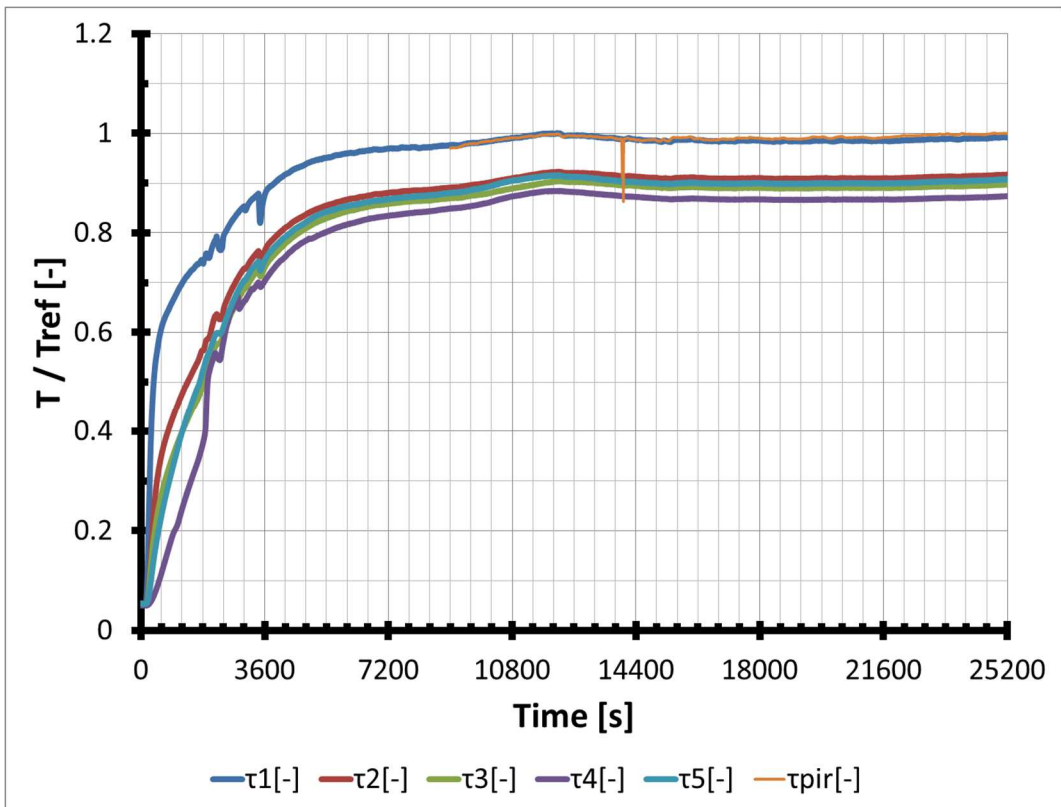


Figure 22: Non-dimensional temperature vs Time - Charging Test (2)

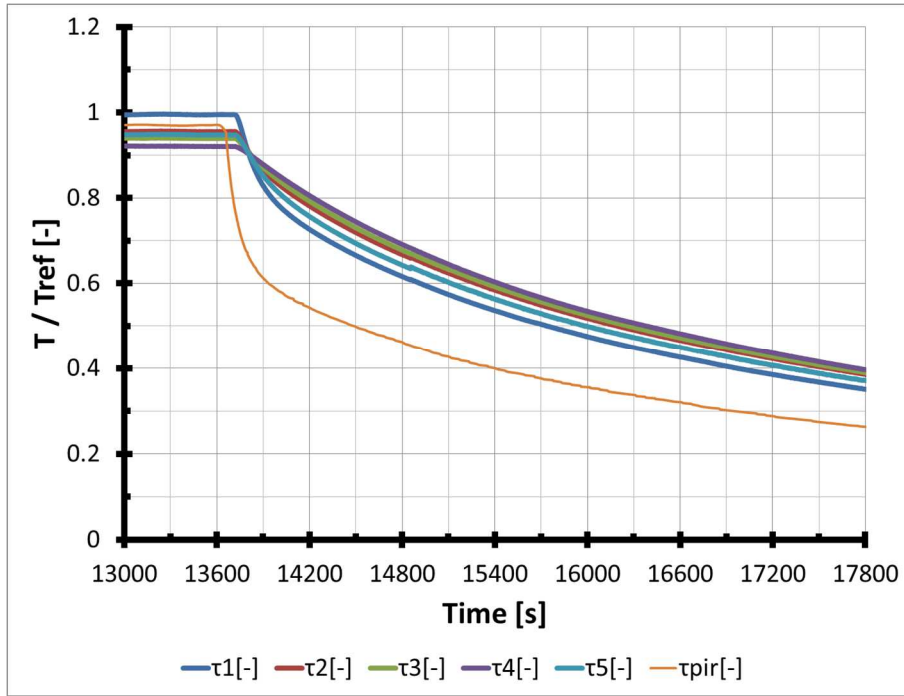


Figure 23: Non-dimensional temperature vs Time - Discharging Test

SHORT TERM & THERMAL STORAGE DESIGN

Time dependent results have been interpreted to evaluate the heat power entering the front disc, the inner heat transfer and the temperature at which the front face of the plate re-irradiates the impinging power. These tasks have been performed taking also the temperature gradients into consideration. According to the tests and selecting the following table charge materials, the final choice has been made taking the WF exit temperature into consideration. Thus, LiF has been chosen for 780 – 800°C Working Fluid Temperature (WFT). NaF for WF around 850 – 900 and CaSi and BeSi for the highest MGT temperatures always lower than 975°C. Materials selected according to the required WF Temperature have led to use volumes from 30 to 45 litres with a storage charge mass of 60 – 85 kg for 45 minutes storage. For 10 minutes storage, the charge volume ranges from 7 to 10 litres and the PCM mass ranging from 13 to 20 kg.

Table 1: Phase Change Material Specifications

PCM	Melting Temp.	Heat of Fusion [kJ/kg]	Density [kg/m3]	
	[°C]		Solid	Liquid
LiF	848	1044	2640	1875
Mg-Si	960	1212	N.A.	N.A.
NaF	995	789	2564	1949
Ca-Si	1023	1111	N.A.	N.A.
NaMgF3	1030	711	N.A.	N.A.
Be-Si	1090	1812	N.A.	N.A.
Mg2Si	1100	1118	1940	1900
Mn-Si	1142	1090	N.A.	N.A.
MgF2	1263	933	3180	2370

Twelve module tube bundles based on double spiral each to have the possibility of arranging various MGT options have been adopted.

Each spiral tube bundle is made of two spirals that are connected at the centreline and have the exit pipes at the opposite points of the circumference. Such bundle is shown in figures 6 and 7.

It has been designed to absorb 2.1 kW at the design condition and the tube diameter has been chosen to limit the pressure drop lower than 0.3 kPa. Figures 6 and 7 show the cross and the isometric view of the Double Spiral Tube Bundle. Moreover, in figures 24 and 25, the cross section and the isometric views of the Receiver are given.

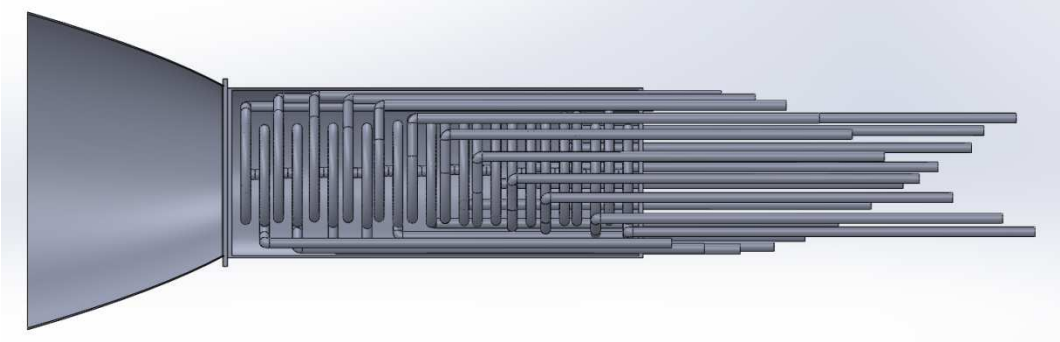


Figure 24: Spiral Tube Bundle Cross Section

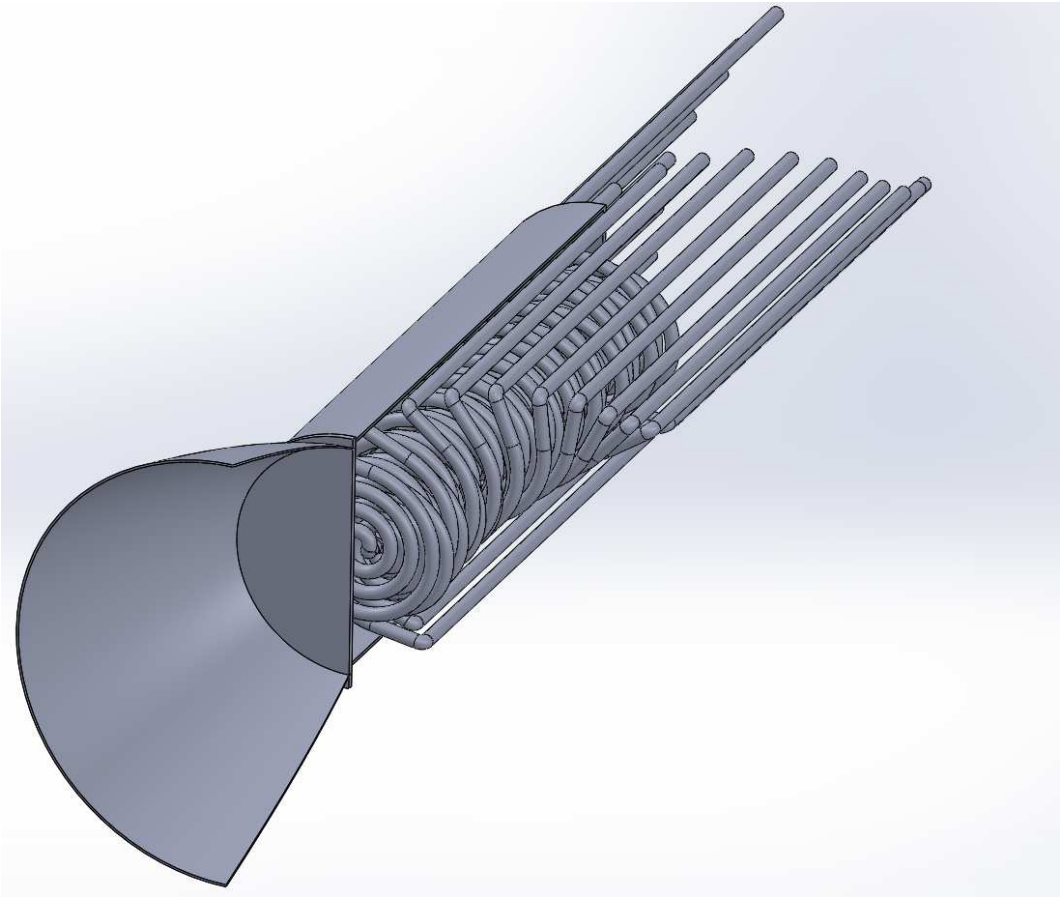


Figure 25: Spiral Tube Bundle Isometric View

To perform tests of the final design, a Module Receiver equipped with a double spiral sized according to similitude aspects has been designed and sized. The photo of such a Double Spiral Tube Bundle is given in figure 26.

CONCLUSIONS

A complete analysis of the short term Thermal Storage Solar Ray Receiver has been performed both theoretically and experimentally. The results have allowed the sizing of the final Receiver design as shown in figures 24 and 25 with the non-confidential details given in the Deliverable.

The module to be tested has been designed and sized for reduced power.

Future work will consist in making new part load and full load tests to confirm the final Receiver construction.

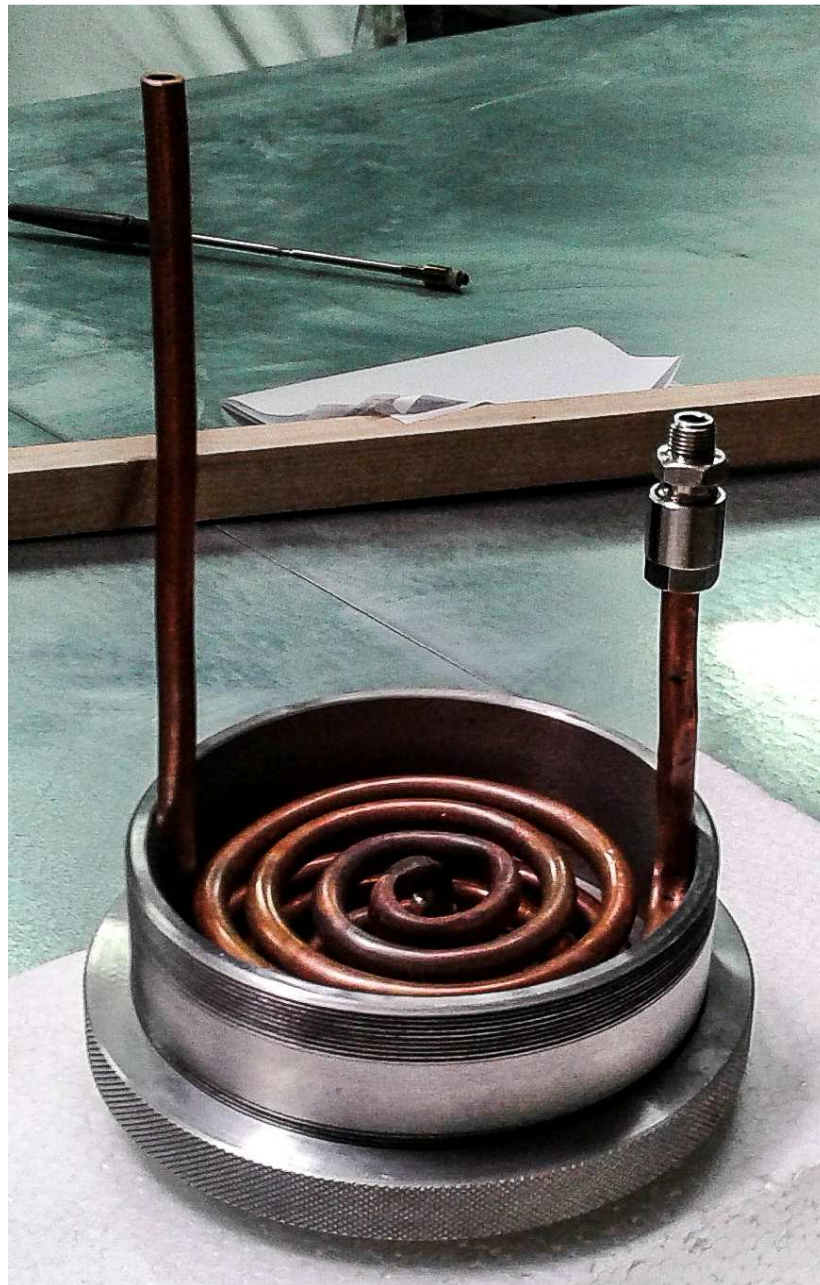


Figure 26: Picture of the two-spiral tube bundle device

REFERENCES

- [1] - Woodard M., Hudson H., '*Solar Oscillations Observed in the Total Irradiance*', Solar Physics 82 (1983)
- [2] – Lave Matthew, Kleissl J., '*Solar Variability of four Sites Across the State of Colorado*', Renewable Energy 35 (2010) 2867-2873, Elsevier
- [3] – Fleischer, AS., '*Thermal Energy Storage Using Phase Change Materials – Fundamentals and Applications*', Springer 2015
- [4] – Kuravi S., Goswami Y et Al., '*Thermal Energy Storage for Concentrating Solar Power Plants*', Clean Energy Research Center, California.
- [5] – Tamme R., Laing D., Steinmann WD., '*Advanced Thermal Energy Storage Technology for Parabolic Trough*', Proceedings of ISEC 2003, Hawaii, 15-18 March 2003
- [6] – Gil A., Medrano M., Martorell I., Lazaro A., Dolado P, Zalba B., Cabeza L., '*State of the art on high temperature thermal storage energy storage for power generation. Part 1 – Concepts, materials and modellization*', Renewable and Sustainable Energy Reviews 14 (2010) 31-55, Elsevier
- [7] –Medrano M., Gil A., Martorell I., Potau X., Cabeza L., '*State of the art on high temperature thermal storage energy storage for power generation. Part 2 – Case Studies*', Renewable and Sustainable Energy Reviews 14 (2010) 31-55, Elsevier
- [8] – Jonemann M., '*Advanced Thermal Storage with Novel Molten Salt*', NREL 2013
- [9] – Nkewtta D., Haghghat F., '*Thermal energy storage with phase change material – A State of the Art review*', Sustainable Cities and Society 10 (2014) 87-100, Elsevier
- [10] – Cirocco L., Belusko M., Bruno F., Boland J., Pudney, '*Optimization of Storage for Concentrated Solar Power Plants*', Challenges 2014
- [11] – Gui X., Song X., Li T., Tang D., '*Influence of void ratio on phase change of thermal energy storage for heat pipe receiver*', Thermal Science Vol19, N³, pp.967-976, 2015.
- [12] – Hall C.A., Glakpe E.K., Cannon J.N., '*Modeling Cycle Phase Change and Energy Storage in Solar Heat Receivers*', NASA Technical Memorandum 1997
- [13] – Hall C.A., Glakpe E.K., Cannon J.N., '*Thermal State of Charge in Solar Heat Receivers*', NASA Technical Memorandum 1998
- [14] – Nithyanandam K., Pitchumani R., Mathur A., '*Analysis of a Latent Thermocline Energy Storage System for Concentrating Solar Power Plants*', ASME Proceedings, ES2012, San Diego, USA
- [15] – Cameron H., Mueller A., Namkoong D., '*Preliminary Design of a solar Heat Receiver for a Brayton-Cycle Space Power System*', NASA Technical Memorandum 1972
- [16] – Gomez J., '*High-Temperature Phase Change Materials (PCM) Candidates for Thermal Storage (TES) Applications*', NREL 2011.
- [17] – Heinz A., Streicher W., '*Application of Phase Change Materials and PCM-Slurries for Thermal Energy Storage*', Institute of Thermal Engineering, Graz Austria.
- [18] – Zalba B., Marin J.M., Cabeza L, Mehling H., '*Review on thermal storage with phase change: materials, heat transfer analysis and applications*', Applied Thermal Engineering 23 (2003) 251-283, Elsevier

- [19] – Strumpf H.J., Krystkowlak C., Klutcher B.A., '*Design of the Heat Receiver for the US/RUSSIA Solar Dinamic Power Joint Flight Demonstration*', AlliedSignal Aerospace Equipment Systems, California.
- [20] – Khare S., Dell'Amico M., Knight C., McGarry S., '*Selection of Materials for High Temperature Latent Heat Energy Storage*', Solar Energy Materials and Solar Cells, Volume 107, December 2012, Pages 20–27, Elsevier.
- [21] – Petrasch J., Tan M., '*Testing of a Cavity-Type Metal Phase Change Thermal Storage Unit for CSP Applications*'.
- [22] – Sharma A., Tyagi V.V., Chen C.R., Buddhi D., '*Review on Thermal Energy Storage with Phase Change Materials and Applications*', Renewable and Sustainable energy Reviews 13 (2009) 318-345, Elsevier.
- [23] – IRENA, '*Thermal Energy Storage – Technology Brief*', IEA-ETSAP&IRENA 2013
- [24] - Alavi B., Bernardini I., Cerri G., Chennaoui L., Mazzoni S.: SASEC 2015, '*Power, Cool and Water Production by Innovative Cycles Fed by Solar Energy*', South Africa May,11-13,2015
- [25] - Alavi B., Cerri G., Chennaoui L., Giovannelli A., Mazzoni S.: SEEP 2014, '*MGT Cycles for Solar Dish Applications*', Proceedings of SEEP 2014, 23-25 November 2014, Dubai

D.1.2. ANNEX

TITLE

**High Temperature Solar Receivers for Brayton and Stirling
Engines for Space Application**

RO3 INTERNAL REPORT

Scientific Responsible:

Prof. Giovanni Cerri

INDEX

1. Introduction.....	6
1.1 Classification of receivers.....	6
1.2 Description of solar receiver as a solar chemical reactor.....	7
2. State Of The Art (Solar Reactors).....	10
2.1 Introduction.....	10
2.2 List Of Articles	10
3. State Of The Art (Solar Engines).....	67
3.1 Introduction.....	67
3.2 List Of Articles	68
4. Conclusions.....	106
4.1 Results & Discussions For Solar Receivers.....	106
4.2 Results & Discussions For Solar Engines.....	107

List Of Figures

Fig. 1.1 Solar Receiver.....	6
Fig. 1.2 Types Of Cavity Reactor.....	7
Fig. 2.1.1 Min. Blow parameter required for steady state v/s viscosity temp. exponent	14
Fig. 2.1.2 B as function of relative temp. increase $w=0$	14
Fig. 2.2.1 Efficiency as a function of dimensionless temp. for uniform irradiance.	15
Fig. 2.2.2 - Efficiency v/s dimensionless temp. (Gaussian irradiance distribution)	16
Fig. 2.3.1 - Dimensions of window in mm.....	17
Fig. 2.3.2 - Schematic of secondary concentrator, light extractor receiver, Kohinoor light extractor.	17
Fig. 2.4 Schematic cross section view of the receiver.....	18
Fig. 2.5.1 - Scheme of the surface absorber	20
Fig. 2.5.2 - Thermal efficiency of absorbers with radiative losses as a function of t_f , the ratio of the exit temperature to the stagnation temperature	20
Fig. 2.7 Schematic of a latent thermal energy storage system composed of multiple individual storage cells.	22
Fig. 2.8.1 The frustum-like high-pressure (FLHIP) window.....	24
Fig. 2.8.2 Geometry of the window.....	25
Fig. 2.9.1 The porcupine volumetric solar absorber concept.....	26
Fig. 2.9.2 The porcupine absorber Experimental setup.....	26
Fig. 2.9.3 Incident radiation and flow directions in absorbers.....	27
Fig. 2.10.1 Thermodynamic cycle for closed Brayton engine integrated with solar heat receiver.	28
Fig. 2.10.2 Solar heat receiver of GTD system.....	28
Fig. 2.11.1 Assembly of the concentrator array and pre-heaters.....	29
Fig. 2.11.2 Receivers in the partitioned receiver system.....	30
Fig. 2.13.1 Optimized non-regular polygonal concentrators.....	32
Fig. 2.13.2 Flux distribution.....	33
Fig. 2.14 Scheme of the improved SynMet Vortex-flow solar chemical reactor.	34

Fig. 2.15.1 Symmetric receiver design at 10kW power level.....	36
Fig. 2.15.2 Asymmetric receiver design at 50 kW power level.....	36
Fig. 2.16 Schematic representation of the two-step water-splitting cycle using the Zn/ZnO redox system for the solar production of hydrogen.	37
Fig. 2.17 Reflectivity at temperature.....	39
Fig. 2.18.1 Solar air preheating system.....	39
Fig. 2.18.2 Modular receiver arrangement.....	40
Fig. 2.18.3 REFOS Receiver Module.....	40
Fig. 2.19.1 SBP/LCS 10 KW Dish/Stirling system.....	42
Fig. 2.19.2 Hybrid heat pipe receiver with combustion system.....	42
Fig. 2.19.3 Scheme of hybrid heat pipe receiver.....	43
Fig. 2.20.1 Reactor model M2b-CPC assembly.....	45
Fig. 2.20.2 Reactor model.....	46
Fig. 2.22.1 Variation of the exergy output with efficiency for $B = 0.06$	49
Fig. 2.22.2 Variation of the maximum exergy output with dimensional depth for $B = 0.06$.	49
Fig. 2.23 Schematic diagram of the physical problem.....	50
Fig. 2.24.1 Dish Stirling system components.....	51
Fig. 2.24.2 Bio-Dish hybrid receiver.....	53
Fig. 2.24.3 DLR pressurized volumetric air receiver.....	53
Fig. 2.25 Geometric layout of solar particle receiver.....	54
Fig. 2.26.1 Schematic view of a DIAPR-type reformer.....	56
Fig. 2.26.2 Representative module (unit cell) of the computational control volume in the Porcupine absorber.	56
Fig. 2.27 Schematic of solar thermal fluid wall aerosol flow reactor	57
Fig. 2.28 Schematic representation of the indirect heating the multitube rotary kiln.	58
Fig. 2.29.1 Principle scheme of the electrical set-up.....	60
Fig. 2.29.2 Typical axial temperature distributions of the heater obtained at different times during the heating process.	61
Fig. 2.30 Experimental setup for CO ₂ reforming by the double-walled reactor tube with the Na ₂ CO ₃ composite material.	63
Fig. 2.31 Solar test reactor at DLR in Cologne, Germany.....	64
Fig. 2.32.1 Schematic of the fluidized bed reactor assembly.....	65
Fig. 2.32.2 Actual reactor assembly interfaced with the NREL solar furnace.	66
Fig. 3.1.1 Brayton cycle space power system.....	70
Fig. 3.1.2 Stirling cycle space power system.....	71
Fig. 3.1.3 Baseline Receiver.....	72
Fig. 3.2.1 100 kW system design layout.....	74
Fig. 3.2.2 550 kW System design layout.....	75
Fig. 3.3.Effect of surface modification on the emittance of Haynes 188.	76
Fig. 3.4 Advanced solar simulator verses classical solar simulator.	78
Fig. 3.5 Advanced Solar Simulator.....	79
Fig. 3.6.1 Block diagram of SD system.....	81

Fig. 3.6.2 Complete solar heat receiver.....	82
Fig. 3.7.1 Solar dynamic flight demonstration hardware.....	83
Fig. 3.7.2 Heat receiver.....	84
Fig. 3.8.1 Schematic diagram of solar simulator.....	85
Fig. 3.8.2 Pattern of nine beams overlapping at the centre.....	86
Fig. 3.8.3 Flux variation with radial position.....	87
Fig. 3.8.4 Flux distribution at the optical control surface located at the concentrator.	87
Fig 3.10.1 Receiver cross section.....	90
Fig. 3.10.2 Containment Canister Configuration.....	90
Fig. 3.11.1 SDGTD receiver.....	91
Fig. 3.11.2 Receiver assembly overview.....	92
Fig. 3.11.3 Receiver gas circuit.....	92
Fig. 3.11.4 Outer shell assembly.....	92
Fig. 3.11.5 Receiver aperture assembly.....	92
Fig. 3.13.1 Schematic of encapsulated PCM tube configuration with annular gas flow.	94
Fig. 3.13.2 Comparison of numerical and experimental results for the receiver gas exit temperature	94
Fig. 3.14.1 SDFD hardware on moon.....	95
Fig. 3.14.2 SDFD Receiver.....	95
Fig. 3.14.3 SDFD Aperture Shield.....	95
Fig 3.15.1 Solar Heat Receiver concept Diameter 6.1 ft Length 9.8 ft.	97
Fig 3.15.2 Solar Receiver Layout (Dim in inches).....	98
Fig 3.15.3 Receiver Tube Configuration.....	99
Fig. 3.15.4 PCM Containment Canister.....	99
Fig 3.15.5 Solar Receiver with Aperture Plate Assembly Overall Dimension Diameter 1.86m Length 2.99m.	100
Fig 3.15.6 Advanced Developer Receiver Design Configuration.....	102
Fig 3.15.7 Advanced Development Receiver prior to testing in vacuum chamber.	102
Fig 3.15.8 Receiver manifolding.....	103
Fig 3.15.9 Receiver Structure.....	103

List Of Tables

Table 3.3 Summary of the effect of Surface Modification on Optical properties of Haynes 188	77
Table 3.5 Solar Simulator Characteristics.....	79
Table 3.15.1 : CBC Receiver Design Attributes.....	98
Table 3.15.2 : CBC Receiver Mass Summary.....	99
Table 3.15.3 Receiver Dimension.....	104
Table 3.15.4 Receiver Thermal Performance Summary.....	104
Table 3.15.5 Receiver Mass Breakdown.....	105

1. Introduction

This report analyzes in depth the current state of the art, challenges faced and the future work related to the study of high temperature solar receivers/ reactors and solar engines, described briefly in the following paragraphs. It is divided into two parts, first part discussing the state of the art and specific problems and complications faced in the development of the solar receiver and the solar engine respectively, through articles written by well-known authors in the field of solar energy. It is a comprehensive collection of a large number of articles, organized in a chronological order which will help in understanding how solar reactors, engines evolved and the state of the art, the problems related and suggest solutions which could help in the development of solar receivers and engines.

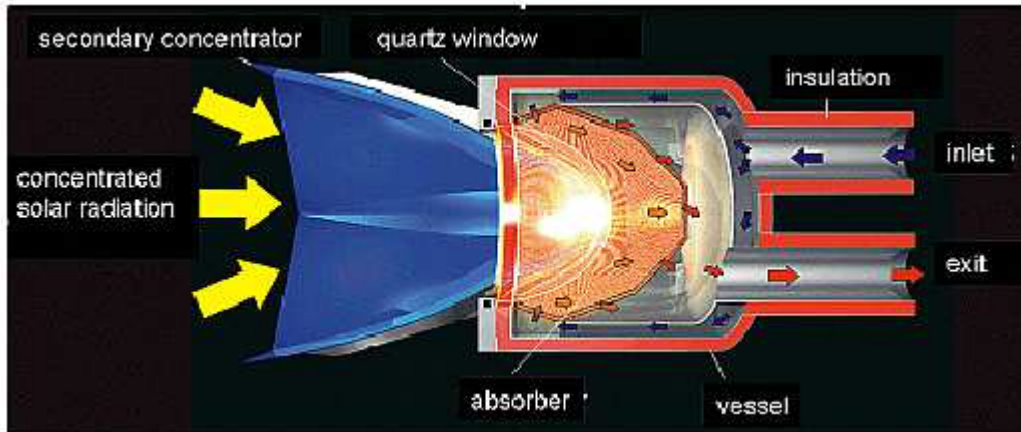


Fig. 1.1 - Solar Receiver

A Solar Receiver is the component of a solar-thermal system where concentrated light, provided by the primary collectors - and sometime a secondary concentrator - is absorbed and converted to thermal energy or chemical potential, as required by the system. The receiver design depends on the type of collector (e.g., trough, parabolic dish, central receiver), the working fluid, and the operating ranges of temperature, pressure and radiation flux. As the temperature, pressure and solar flux increase, it becomes more difficult to effectively handle the intensified solar energy provided by the optical system, and the receiver design poses a greater challenge. Material properties, for example, determine the maximum receiver temperature, and may also force the designer to lower the working pressure, as the receiver temperature increases.

1.1 Classification of receivers

Most of the receivers can be classified as either Indirectly Irradiated, or Directly Irradiated (Volumetric). The common characteristic of the Indirectly Irradiated receivers is that the heat transfer to the working fluid does not take place upon the surface which is exposed to incoming solar radiation. Instead, there is an intermediate wall, which is heated by the irradiated sunlight on one side and transfers the heat to a working fluid on the other side. The two main groups of Indirectly Irradiated receivers are the Tubular Receivers and the Heat Pipe Receivers. All of these receivers are limited to working fluid temperatures of below 1000°C and a solar flux of less than 1000 kW/m^2 . Due to material and design limitations, as the operating temperature increases, the solar flux and working pressure must be reduced; these can not exceed 600 kW/m^2 and 10 Atmosphere, respectively, at the upper temperature range ($T > 800^{\circ}\text{C}$).

The general characteristic of the 'Volumetric', or Directly Irradiated receiver, is that the heat transfer to the working fluid takes place upon the surface which is heated directly by

incoming radiation. Receivers of this diverse group have been developed for both, parabolic dish and central receiver systems.

In general, the performance of these receivers did not exceed that of tubular receivers until the recent development of the Directly Irradiated Annular Pressurized Receiver (DIAPR), which produces a working gas temperature of up to 1300°C, while operating at an average aperture solar flux of 5,000-10,000 kW/m² and a pressure of 15-30 bar

1.2 Description of solar receiver as a solar chemical reactor

Solar thermo-chemical processes use concentrated solar energy to drive endothermic chemical reactions. Therefore, the solar receiver serves as the solar chemical reactor. Cavity-type receivers have turned out to be appropriate geometries for conducting a variety of chemical reactions because of the capability of capturing incoming solar radiation efficiently.

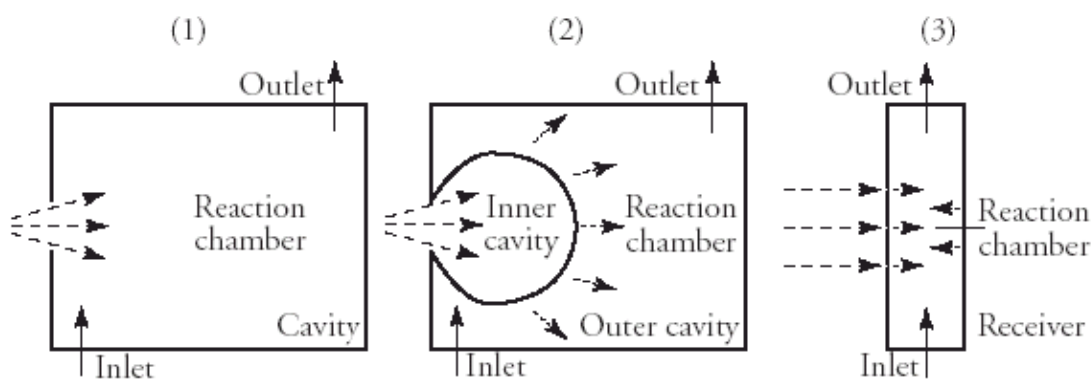


Fig. 2-2: Chemical reactor concepts which have turned out to be operable in lab-scale and pilot plant scale: (1) One-cavity type reactor; the reaction chamber is directly irradiated, (2) Two-cavity type reactor; the incident radiation is absorbed by an inner cavity which emits the energy into an outer cavity where the reaction chamber is irradiated indirectly, (3) Another concept of indirect irradiation where a receiver serves as absorber, typically a cylinder which emits the energy into the reaction chamber.

Figure 1-2 shows three chemical reactor concepts which have turned out to be operable in lab-scale and pilot plant scale. The task of a solar reactor is to efficiently transfer solar energy to the cavity and to the reacting system (gases and solids), while minimizing heat losses. Basically two concepts of heat transfer are distinguished, namely, direct irradiation Figure 1-2 (1) and indirect irradiation Figure 1-2 (2, 3). The advantage of direct irradiation is that it provides a very efficient means of heat transfer directly to the reaction site. A drawback is the requirement of a transparent window at the aperture (the small opening) closing the reactor's atmosphere. This window is a critical component because contamination by dust may occur disturbing the radiation entering the reactor. Furthermore, this window is exposed to concentrated radiation. This radiation is absorbed partly by the window leading to elevated temperatures. In addition, when operating the reactor at excess pressure, the shape and thickness of the window need to be adjusted .

A benefit of solar reactors irradiated indirectly is the protection of the window by the inner cavity. The inner cavity is irradiated directly by the solar radiation entering through the aperture that is closed by a window if need be. The temperature of the inner cavity is raised by absorption, thus its walls emit to all directions. The emitted radiation is either reflected and absorbed within the outer cavity (reaction chamber) or lost through the aperture. Thus, the

window at the aperture is separated completely from the reacting chemical environment inside the outer cavity .

Another concept where the reaction chamber is irradiated indirectly is (3) in Figure 1-2. Typically, a cylinder serves as radiant absorber and radiant emitter through which the reactants flow while the chemical reaction is taking place ([12]-[14]). A preferred material to construct a cavity or absorber is graphite due to its high absorptivity and emissivity. Additionally, it is resistant to thermal shocks, has a fairly good thermal conductivity, and allows operations at temperatures up to 3500 K in oxygen-free atmospheres.

All the concepts described above theoretically allow the use of any mixture of solid particles and gases introduced by the inlet stream. Even concepts where parts of the cavity are rotating during operation have been tested successfully ([28], [48]). With a rotating cavity, the solid particles, which are conveyed onto the cavity, are distributed more equally. This leads to a more efficient radiation heat transfer, a better contact with the gaseous reactants, and as a consequence, to a faster chemical reaction. Furthermore, the solid particles protect the cavity walls from the concentrated radiation. In principle, any kind of endothermic chemical reaction is suitable to be conducted in a solar chemical reactor.

Photovoltaic systems have been relatively low power, 10 kW or less. Future NASA, military, and commercial space missions will require much higher power levels. In low earth orbit (LEO) more efficient power systems with their smaller drag areas will result in lower orbit maintenance propellant requirements. Advanced Solar Dynamic (ASD) systems can provide high power efficiently and reliably in a compact, lightweight manner. These systems can operate in any orbit because they will not be affected by high radiation levels. Advanced concepts for the key components of ASD systems will be pursued and related technologies developed. These components are the concentrator, receiver, radiator, and thermal energy storage material.

The Advanced Solar Dynamic (ASD) Power systems offer the potential for efficient, lightweight, survivable, relatively compact, long-lived space power systems applicable to a wide range of power levels (3 to 300 kW), and a wide variety of orbits. The successful development of these systems could satisfy the power needs for a wide variety of these projected missions.

The availability of space power systems with high power capability would enable missions with requirements for 75 kW or more. ASD systems do provide a non-nuclear alternative. They also provide power for military missions such as Space Defense Initiative (SDI) systems, surveillance satellites, and housekeeping power for weapon platforms.

2. State Of The Art (Solar Reactors)

2.1 Introduction

The solar receiver mainly consists of two components, the Absorber - which absorbs direct, concentrated sunlight and transports its energy to a working fluid flowing within and over it. In different designs, the absorber is either located adjacent to the receiver aperture, or deeper in the receiver cavity. It is either a stationary matrix (grid, wire-mesh, foam, honeycomb, etc.), or moving (usually solid) particles.

Often the operating conditions demand that the absorber be physically separated from the ambience; e.g., when the flow is pressurized, or the working fluid is not air. In these cases the receiver must be equipped with the 2nd main component - transparent 'window', which allows concentrated light to enter the receiver, while separating between the working gas and the ambient air. The window also permits the receiver cavity to be pressurized, if necessary.

In most of the known windowed receivers, the window is made of fused silica (fused quartz), which, like many other transparent materials, has high transmittance to sunlight, but absorbs much of the re-radiation spectrum. In some designs the cold working gas entering the receiver cavity can be directed to flow over the inner surface of the window, cooling it before extracting heat from the absorber. The window may then be significantly colder than the absorber, thus re-radiation and convection losses can be reduced substantially.

The window poses a difficult design problem because it must be highly transparent, yet strong and durable at high temperatures. Several attempts to develop a workable window for Volumetric receivers failed, or had to settle for lower operating pressure, temperature and general performance than originally planned. Consequently, the need for a window was considered the main draw back of Directly Irradiated (Volumetric) receivers until the development of the DIAPR.

2.2 LIST OF ARTICLES (Cavity Reactor)

Authors, Topic, Journal	Page No.
(1)Kribus A., Ries H., Spirkl W. Inherent Limitations of Volumetric Solar Receivers ASME journal of solar engineering. May 1995	14
(2)Ries H., Kribus A., Karni J. Non-isothermal Receivers ASME journal of solar engineering. Vol. 117 August 1995	15
(3)Karni J., Kribus A., Doran P., Rubin R., Fiterman A., Sagie D..... The DIAPR: A High-Pressure, High-Temperature Solar Receiver ASME journal of solar engineering. Vol. 119, February 1997	16
(4)Doron, P., Kribus, A..... The effect of irradiation directional distribution on absorption in volumetric solar receivers Journal of Solar Energy Engineering Vol. 119, February 1997	17
(5)Spirkl W., Ries H., Kribus A..... Performance of Surface and Volumetric Solar Thermal Absorbers ASME journal of solar engineering. Vol. 119, May 1997	19

(6)Ries H., Tschudi H. R. and Spirkl W.....	21
On the stability of solar chemical particle receivers	
Journal of Solar Energy Engineering Volume 120, 1998	
(7)Aceves S.M., Nakamura H., Reistad G.M., Martinez-Frias J.....	21
Optimization of a class of latent thermal energy storage systems	
with multiple phase-change materials	
Journal of Solar Energy Engineering Vol. 120, February 1998	
(8)Karni J., Kribus A.....	23
A high-pressure window for volumetric solar receivers	
Journal of Solar Energy Engineering Vol. 120, May 1998	
(9)Karni J., Kribus A., Rubin R., Doron P.....	25
The "Porcupine": A Novel High-Flux Absorber For Volumetric	
Solar Receivers	
Solar Energy Engineering Vol.120 / 85-95, 1998	
(10)Hall C. A., Glakpe E. K., Cannon J. N. and Kerslake T. W.....	27
Thermodynamic analysis of space solar dynamic heat receivers	
with cyclic phase change	
Journal of Solar Energy Engineering Volume 121, 1999	
(11)Kribus A., Doron P., Rubin R., Karni J., Reuven R., Duchan S.,	29
Taragan E.	
A Multistage solar receiver: The route to high temperature	
Solar Energy Vol. 67, Nos. 1–3, pp. 3–11, 1999	
(12)Fletcher J. Miller and Roland W. Koenigsdorff, Professor	30
Thermal Modeling of a Small-Particle Solar Central Receiver	
Journal of Solar Energy Engineering Volume 122, February 2000	
(13)Kribus A., Huleihil M., Timinger A., Benmair R.	31
Performance of a rectangular secondary concentrator with an	
asymmetric heliostat field	
Solar Energy Vol. 69, No.2, pp. 139-151, 2000	
(14)Kräupl S. and Steinfeld A.....	34
Experimental Investigation of a Vortex-Flow Solar Chemical	
Reactor for the Combined ZnO-Reduction and CH ₄ -Reforming	
Journal of Solar Energy Engineering Volume 123 2001	
(15)Kribus A., Doron P., Rubin R., Taragan E., Duchan S., Karni J.	35
Performance of the Directly-Irradiated Annular Pressurized Receiver	
(DIAPR) Operating at 20 Bar and 1200°C	
Journal of Solar Energy Engineering Vol. 123, February 2001	
(16)S. Möller and R. Palumbo	36
The Development of a Solar Chemical Reactor for the	
Direct Thermal Dissociation of Zinc Oxide	

Journal of Solar Energy Engineering Volume 123, May 2001	
(17)Joseph A. Bonometti, Clark W. Hawk.....	37
High Temperature Solar Absorber Material Measurement Technique	
Journal of Solar Energy Engineering Volume 123, August 2001	
(18)Reiner Buck, Thomas Bräuning, Thorsten Denk,	39
Markus Pfänder, Peter Schwarzbözl and Felix Tellez	
Solar-Hybrid Gas Turbine-based Power Tower Systems (REFOS)	
Journal of Solar Energy Engineering Volume 124, February 2002	
(19)Doerte Laing and Magnus Pålsson	42
Hybrid Dish/Stirling Systems: Combustor and Heat Pipe	
Receiver Development	
Journal of Solar Energy Engineering Volume 124 May 2002	
(20)Abraham Kogan, Meir Kogan.....	44
The Tornado Flow Configuration—An Effective Method	
for Screening of a Solar Reactor Window	
Journal of Solar Energy Engineering Volume 124, August 2002	
(21)Abraham Kribus, Andreas Timinger.....	47
Optical In-Situ Assessment of a Non-imaging Secondary	
Concentrator in a Solar Tower	
Journal of Solar Energy Engineering Volume 124, August 2002	
(22)Alejandro Londoño-Hurtado, Alejandro Rivera-Alvarez.....	48
Maximization of Exergy Output From Volumetric Absorption Solar Collectors	
Journal of Solar Energy Engineering Volume 125, February 2003	
(23)Pai-Chuan Liu.....	49
Temperature Distribution in a Porous Medium Subjected to	
Solar Radiative Incidence and Downward Flow: Convective Boundaries	
Journal of Solar Energy Engineering Volume 125 May 2003	
(24)Thomas Mancini, Peter Heller, Barry Butler, Bruce Osborn,	51
Wolfgang Schiel, Vernon Goldberg, Reiner Buck, Richard Diver,	
Charles Andracka, and James Moreno	
Dish-Stirling Systems: An Overview of Development and Status	
Journal of Solar Energy Engineering Volume 125, May 2003	
(25)Bertocchi R., Karni J., Kribus A.	53
Experimental evaluation of a non-isothermal high temperature solar	
particle receiver	
Energy 29, 2004	
(26)Rachamim Rubin, Jacob Karni	55
Chemical Kinetics Simulation of High Temperature	
Hydrocarbons Reforming in a Solar Reactor	

Journal of Solar Energy Engineering Volume 126, August 2004

(27)Jaimee K. Dahl, Alan W. Weimer, Andreas Z'Graggen and Aldo Steinfeld.....56
Two-Dimensional Axi-Symmetric Model of a Solar-Thermal
Fluid-Wall Aerosol Flow Reactor

Journal of Solar Energy Engineering Volume 127, February 2005

(28)Anton Meier, Wojciech Lipinski, Enrico Bonaldi and Gian Mario Cella58
Multitube Rotary Kiln for the Industrial Solar Production of Lime

Journal of Solar Energy Engineering Volume 127, August 2005

(29)Irina Vishnevetsky, Michael Epstein, Rahamim Rubin.....59
Simulation of Thermal and Chemical Processes

in Annular Layer of ZnO–C Mixtures

Journal of Solar Energy Engineering Volume 127, August 2005

(30)Tsuyoshi Hatamachi, Tatsuya Kodama, Yuki Isobe,61
Daisuke Nakano, Nobuyuki Gokon

Double-Walled Reactor Tube with Molten Salt Thermal Storage
for Solar Tubular Reformers

Journal of Solar Energy Engineering Volume 128, May 2006

(31)Martin Roeb, Christian Sattler, Ruth Klüser, Nathalie Monnerie,63
Lamark de Oliveira, Athanasios G. Konstandopoulos, Christos Agrafiotis,

V. T. Zaspalis, L. Nalbandian, Andrew Steele, and Per Stobbe

Solar Hydrogen Production by a Two-Step Cycle Based on Mixed Iron Oxides

Journal of Solar Energy Engineering Volume 128 May 2006

(32)Lock, J.P. , Peterson, B.L., Weimer, A.W.,Pitts, R.J., Bingham,65
C.E. and Lewandowski

Aluminum nitridation in a solar-heated vibrating fluidized bed reactor

Journal of Solar Energy Engineering Volume 121

(1)Kribus A., Ries H., Spirkel W

Inherent Limitations of Volumetric Solar Receivers

ASME journal of solar engineering. May 1995

Many experiments with open receivers (volumetric absorbers) have suffered from non-uniform flow conditions and persistent local overheating, leading to failure of absorber due to melting or cracking. The failures can be overcome by compensating hydraulic resistance at different locations across the absorber. The variation of fluid's dynamic viscosity with temperature plays a significant role in determining the maximum allowable irradiation on the absorber.

The investigation of flow in volumetric absorbers points out that the heat extracted safely by the absorber is limited by flow-related constraints. Multiple steady solutions exist for certain parameter values (due to the variation of viscosity): a "fast" solution corresponding to a low exit temperature, a "slow" solution which is unstable, and a "choked" solution for which the absorber is near to stagnation temperature. The existence of multiple solutions may lead to abrupt local "switching" and absorber failure. For a given irradiance applied to the absorber,

the existence and the character of the solutions are referred to a single dimensionless parameter, the Blow parameter B. Neglecting the variation of the hydraulic resistivity with temperature may lead to a dangerous overestimation of the receiver's ability to sustain irradiation. For reasonable efficiencies control of mass flow or outlet temperature of the absorber, rather than pressure control, may be required.

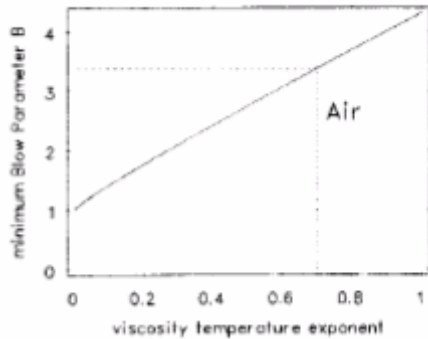


Fig. 2.1.1 -
Min. Blow parameter required for
steady state v/s viscosity temp. exponent.

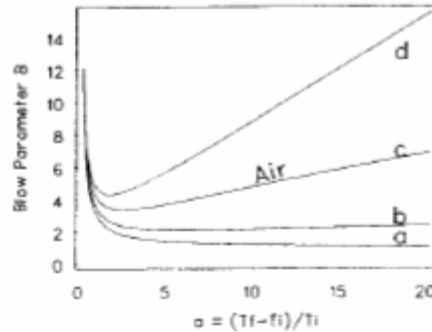


Fig. 2.1.2 -
B as function of relative temp. increase
 $w=0$ (a), 0.3 (b), 0.7 (c), 1 (d).
For a given B smaller value represents
"fast" solution, larger "slow" solution.

(2)Ries H., Kribus A., Karni J.

Non-isothermal Receivers

ASME journal of solar engineering. Vol. 117, August 1995

The main loss of energy from a high-temperature solar receiver is by thermal emission (re-radiation) as a consequence of Kirchhoff's Law of radiation. Non-isothermal receivers are compared to an isothermal receiver, where all parts of the receiver are at the same temperature. A receiver approaches this limit when the heat exchange between different parts of the working fluid as well as between absorbing surfaces and working fluid is very good. Cavity receivers are nearly isothermal because of efficient internal radiative heat transfer. The re-radiation is uniform over the aperture and mainly determined by the maximum temperature.

The re-radiation losses, inherent to every thermal receiver, can be significantly reduced by exposing the working fluid to monotonously increasing irradiance and preventing energy exchange between parts of the receiver that are at different temperatures. In this way the highest temperatures are reached only near the end of the working fluid's path. The improvement is much more pronounced for non-uniform irradiance as compared to uniform one. For a Gaussian distribution of irradiance improvements exceeding a factor of two for the efficiency at a given temperature (0.8 of the peak stagnation temperature), and for the temperature at a given efficiency of 0.8 have been calculated. These results are independent of the peak irradiance and of the width of the distribution. Even a coarse partitioning into two mutually isothermal parts can already produce a significant improvement over the totally isothermal receiver.

Objective of this work is to show how a black flat receiver can be constructed to best make use of an available irradiance distribution produced by a solar concentrator.

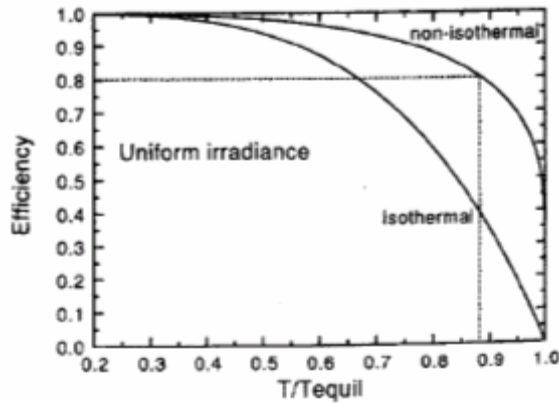


Fig. 2.2.1 Efficiency as a function of dimensionless temp. for uniform irradiance.

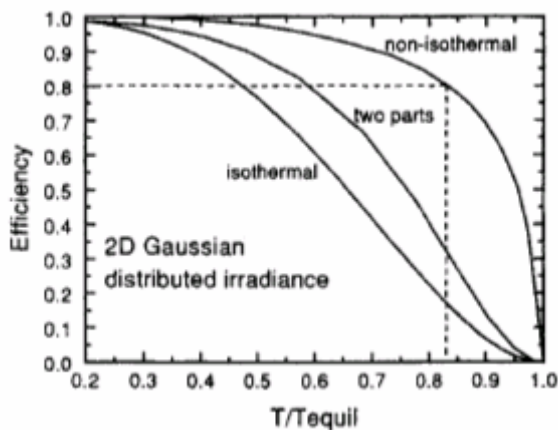


Fig. 2.2.2 - Efficiency v/s dimensionless temp. (Gaussian irradiance distribution)

(3)Karni J., Kribus A., Doran P., Rubin R., Fiterman A., Sagie D.
The DIAPR: A High-Pressure, High-Temperature Solar Receiver
 ASME journal of solar engineering Vol. 119, February 1997

The Directly Irradiated Annular Pressurized Receiver (DIAPR) is a volumetric (directly irradiated), windowed cavity receiver that operates at aperture flux of up to 10 MW/m². It is capable of supplying hot gas at a pressure of 10-30 bar and exit temperature of up to 1300 °C. The three main innovative components of this receiver are:

- a Porcupine absorber, made of a high-temperature ceramic (e.g., alumina), which has a pyramid frustum shape with its heat transfer elements facing the axis. Its purpose is to absorb concentrated sunlight and transfer its energy to the working fluid.

Its advantages: radiation penetrates in a way such that absorption process is spread over a large heat transfer area, it provides an effective heat transfer to the working fluid, and its flexible structure prevents the development of thermal stresses.

- a Frustum-Like High-Pressure (FLHP) window, made of fused silica, which separates the receiver cavity from ambient air allowing operation at high pressure and minimizing reflection losses. It is cooled by the working fluid and capable of withstanding pressure of over 50 bar.
- a two-stage secondary concentrator followed by the Kohinoor light extractor, the secondary

concentrator includes three optical stages: (i) a reflective Compound Parabolic Concentrator (CPC), (ii) a dielectric Total Internal Reflection (TIR) concentrator, made of fused silica and (iii) the Kohinoor light extractor, which extracts concentrated sunlight from the high index-of-refraction medium of the TIR concentrator into the receiver cavity, while minimizing back reflection losses.

DIAPR at power level of 100 kW could be used with a parabolic concentrating dish to supply power to a Brayton cycle and can also be used for reforming hydrocarbons.

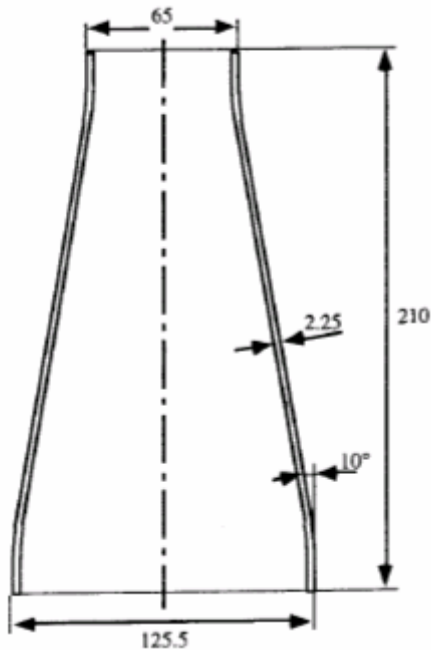


Fig. 2.3.1 – Dimensions of window in mm.

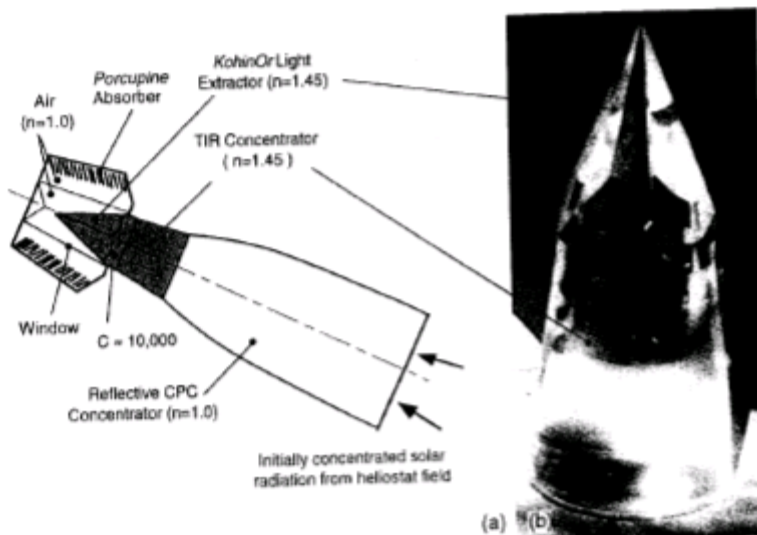


Fig. 2.3.2 - Schematic of secondary concentrator, light extractor receiver, Kohinoor light extractor.

(4)Doron, P., Kribus, A.

The effect of irradiation directional distribution on absorption in volumetric solar receivers

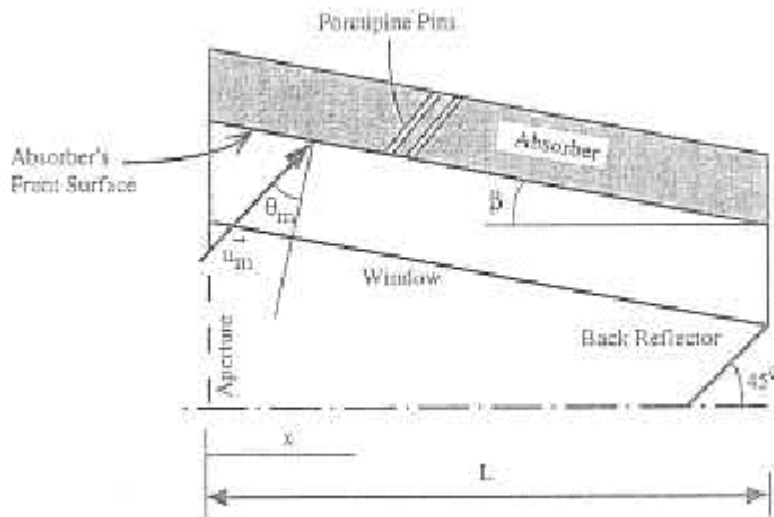
Journal of Solar Energy Engineering Vol. 119, Feb 1997

Volumetric solar absorbers are designed to enable the penetration of radiation deep into the absorber in order to improve the efficiency of the energy transfer from incoming radiation to the working fluid. The character of the incoming radiation is one of the most important considerations in the design and analysis of solar receivers, especially the absorber. Only the distribution of the radiative energy flux on the front of the absorber is considered. The direction of the radiation is used only to determine the reflection coefficients. In volumetric absorbers the direction of radiation is used only should be considered since it affects the absorption process. The absorbers optical density is also affected by the directional distribution, and hence should be taken into account. This work only considers the geometrical effects related to the incoming radiation impinging on the exposed surface of a volumetric absorber. The design of such absorbers is usually based on the irradiation energy flux distribution. The authors show that the directional features of the irradiation also affect the absorption characteristics of volumetric absorbers, present criteria for the characterization of directional attributes, and describe a method for their calculation. The directional information should be used to promote the matching of the absorber's microstructure to the incoming radiation:

The effective extinction coefficient of the absorber varies significantly with location, and depends on design details, it is affected by the local mean incidence angle and the distribution width. Maintaining a uniform optical thickness may require adjusting the absorber elements' density and the absorber's physical thickness.

The local principal direction of an anisotropic absorber should be aligned with the mean direction of incident radiation. This allows maximum penetration of the irradiation into the absorber.

The significance of the directional data is demonstrated for two types of volumetric absorbers. Receiver design and modeling guidelines are presented. The next step would be the coupling of radiative transport to conduction and convection inside the receiver, and simultaneous solution of the energy conversion process.



The DIAPR: (a) schematic cross-section view of the receiver;

Fig. 2.4

(5)Spirk W., Ries H., Kribus A.
Performance of Surface and Volumetric Solar Thermal Absorbers
 ASME journal of solar engineering. Vol. 119, May 1997

For systems with a large difference between inlet and outlet temperature, e.g., for systems with secondary processes having large temperature spread or for open systems using the inlet fluid at ambient temperature, the effective temperature of the absorber's re-radiation can be brought as near as possible to the inlet temperature, which could be performed utilizing a surface absorber where different parts of the aperture area are at different temperatures (Bejan, 1988; Ries et al., 1995), or by employing a volumetric absorber where the temperature increases along the depth of the absorber from inlet to outlet temperature.

Thermal surface absorbers convert all incident radiation to heat at a single local temperature. The fluid flows perpendicular to the radiation's propagation direction. In contrast, in volumetric absorbers the fluid flows parallel to the radiation's propagation direction, and the absorber may exhibit temperature stratification along the radiation's direction. This raises the question whether re-absorption of parts of the thermal emission coming from the hotter absorber sections renders the volumetric absorber superior to the surface absorber.

The volumetric absorber is shown to be less efficient, but closely approaches the performance of the ideal non-isothermal surface absorber. Since the volumetric absorber provides a much larger heat transfer area, non-perfect heat transfer degrades the performance of a surface absorber much more than it degrades that of a volumetric absorber. In real absorbers, the volumetric design may therefore be equal or even superior to the surface absorber. The benefit of volumetric absorbers does not consist then in recycling of radiative losses, but rather in more efficient heat transfer between absorber and fluid.

The isotropic volumetric absorber is less efficient than the surface absorber, since the volumetric absorber necessarily shows radiative interaction between different sections. However, in the region of outlet temperatures of 60-80% of the stagnation temperature, the efficiencies are far better than for the isothermal absorber. The counter-current operation of the volumetric absorber is slightly superior to co-current operation. Practical considerations, but not reduction of radiative losses, might prefer the co-current operation. Convective losses should favour co-current versus counter-current operation due to lower front surface temperatures.

The surface absorber, which may be considered as a crosscurrent heat exchanger, has the highest efficiency. Conclusion is that the volumetric absorber with one-dimensional flow may be viewed as a slightly non-perfect non-isothermal absorber. However, a hypothetical volumetric absorber with directional selectivity such that in each slab only a certain incidence angle is absorbed can exactly match the efficiency of the surface absorber.

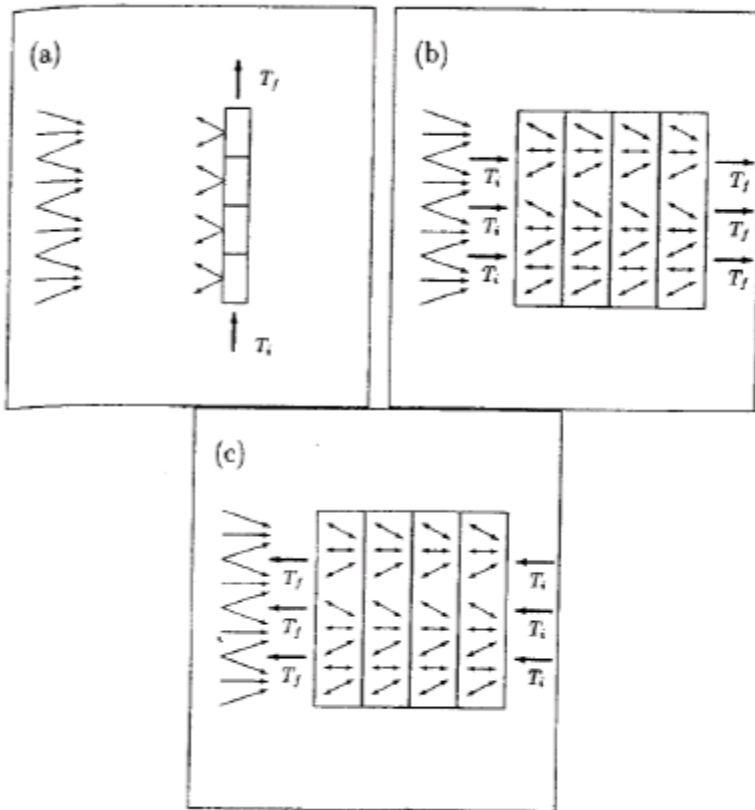


Fig. 2.5.1 - Scheme of the surface absorber (a) and of the volumetric absorber in co-current operation (b) and in counter-current operation (c) Thin arrows correspond to radiation, thick arrows to fluid flow. The absorbers are divided in sections along the direction of fluid flow.

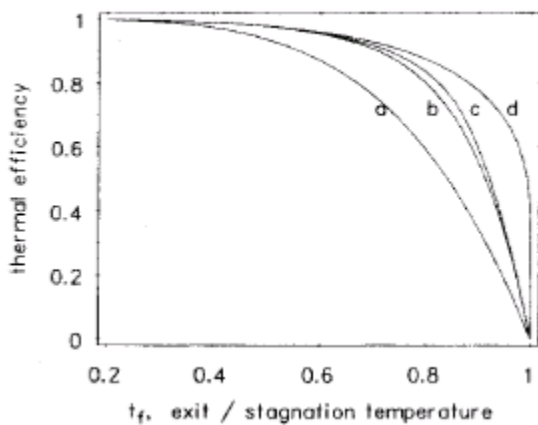


Fig. 2.5.2 - Thermal efficiency of absorbers with radiative losses as a function of t_f , the ratio of the exit temperature to the stagnation temperature, (a) for an isothermal absorber, (b) for a volumetric absorber according to the two-flux model, in co-current operation, (c) in counter-current operation, (d) for a surface absorber. For the cases (b), (c), and (d) the normalized inlet temperature t_i , was set to 0.2.

(6)Ries H., Tschudi H. R. and Spirkl W.
On the stability of solar chemical particle receivers

Journal of Solar Energy Engineering 1998 Volume 120 Issue 2 pp 96-100

Almost all reactions proposed and studied so far for high-temperature application involve the decomposition of a solid into one or more gaseous compounds. If the solid is fluidized with a carrier gas then the produced gas can act as feedback for certain configuration of volumetric solar reactors and affect their stability allowing for a volumetric absorption of the solar radiation. It was found that in volumetric thermal receivers where a gaseous heat transfer fluid is passed through a porous matrix, the expansion of the gas in conjunction with viscous drag can cause a positive feedback and limit stable operation. Viscosity is not an issue and neither does it determine the inflow. Instead the gas produced by the chemical reaction produces a similar feedback on flow rate. Instability means that a receiver operating in steady state may change its mode of operation to unsteady state. It is undesired as it leads to inhomogeneous product, lower efficiency and the failure of the entire system.

We model the decomposition reaction of a solid powder into a solid plus gas in a mixed homogeneous open solar reactor and derive criteria for stability. Instability may occur via a feedback mechanism whereby gas produced in the decomposition reaction reduces the inflow, which leads to even higher reaction rate. For a variety of reactions proposed for solar application, the limits of stable operation are listed as the maximum fraction of solid educt in the input carrier gas both for complete as well as for partial decomposition.

(7)Optimization of a class of latent thermal energy storage systems with multiple phase-change materials

Journal of Solar Energy Engineering Vol. 120, Feb 1998

Efficiency and environmental concerns have resulted in an increased importance of thermal energy storage (TES) systems. Among the available technologies for TES latent thermal energy storage (LTES) systems have been studied because they offer the theoretical possibility of storing a great amount of thermal energy in a small volume, and with a relatively small temperature swing.

This paper presents an analysis of a class of latent thermal energy storage (LTES) system. The analysis is based on a simplified model that allows the system performance to be evaluated in terms of a small set of parameters, while still retaining the main thermodynamic aspects associated with their operation. This analysis therefore permits the broad-based application potential of these systems to be viewed. The paper also discusses the applicability of the model to practical systems. This paper analyzes LTES with multiple energy storage cells and multiple phase-change materials (PCMs). The most general case of infinite energy storage cells and PCMs is solved, for the charge process only, as well as for the overall charge-discharge process. The results yield the optimum phase change temperature, expressed as a continuous function of position along the LTES. The method is equally applicable to the case of a finite number of storage cells. An example of the application of the method to this case is also included. The results show the optimum phase change temperatures for each of the problems being considered, along with the corresponding optimum exergetic efficiencies. The solutions to the optimization problems are surprisingly simple to express, considering the difficulty of the problems, and indicate the potential advantages of using LTES with multiple PCMs.

This analysis permits the broad-based application potential of the systems to be viewed. The model is useful because it sets upper bounds for system performance, and provides an easy method for evaluating the effect of system parameters on performance. The solutions to the optimized problems indicate the potential advantages of using LTES with multiple PCMs. The main results are :

The optimization of the charge process is done with variation calculus. The resulting optimum phase-change temperature is an exponential function of the axial position align the LTES. The solution is expresses in terms of an integration constant, which is evaluated from an algebraic equation.

The problem of the charge-discharge process can be reduced to a single differential equation by using the cyclic operation constraint, which requires each cell to discharge the same amount of energy that is originally stored. The resulting phase-change temperature profile is also exponential.

The problem of finite number of energy storage cells is presented as a set of $3n$ equations in terms of $3n + 1$ free variables, where n is the number of energy storage cells. The set of $3n$ equations can be used to write the exergetic efficiency in terms of a single free variable, which can then be found by optimizing the exergetic efficiency.

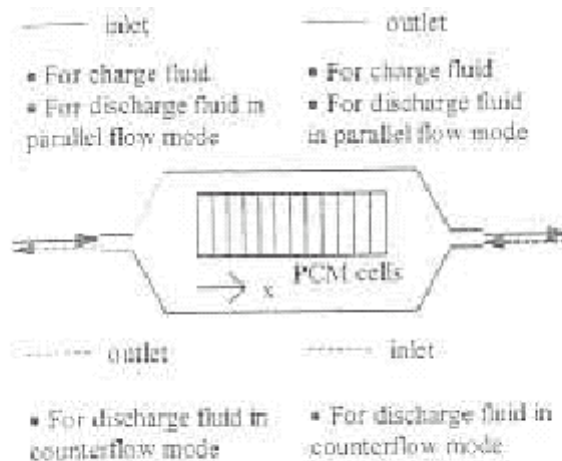


Fig. 1. Schematic of a latent thermal energy storage system composed of multiple individual storage cells

Fig. 2.7

(8)Karni J., Kribus A.

A high-pressure window for volumetric solar receivers

Journal of Solar Energy Engineering Vol. 120, May 1998

The absorbing matrix of a volumetric (directly irradiated) solar receiver must be exposed to the concentrated incoming sunlight. Most applications require that the receiver operates at an elevated pressure and in many cases the working fluid is not air. These requirements can be met only if the receiver is equipped with a transparent window. A novel frustum-like high-pressure (FLHIP) window, made of fused silica, is presented. Optical, mechanical, and thermal analyses, over 1,000 hours of accelerated life-time tests and several hundred hours of tests in a solar receiver, show that this window satisfies the required criteria for operation in a volumetric solar receiver whose operating pressure and peak absorber temperature reach 30 bar and 1700 C respectively.

An effective window must satisfy the following criteria for a long period of time :

Good optical properties: minimize reflection and absorption of incoming light.

Mechanical strength: ability to endure stress caused by the receiver operating pressure and temperature conditions.

High variable working temperatures: operate at a continuous window temperature of upto 800° C, peak temperature of 1000° C, and thermal gradients of upto 25°C/mm.

Reliable stress-free installation and sealing: prevent placement-induced stresses and leaks of the pressurized working gas.

Cooling capacity: inner receiver temperatures could reach 1500-1700°C, i.e., a few hundred degrees higher than the maximum allowable window temperature, therefore the window must be cooled.

Prevent dust accumulation: settling of dust could reduce the window optical performance and cause overheating.

Simple Low-cost production: the window should be made in a relatively simple method, using inexpensive method.

Because of its optical, mechanical and thermal properties, fused silica, a vitreous material which is readily forged and used ordinarily in the furnace industry, has been the material of choice.

The successful development of the FLHIP window opens numerous possibilities for volumetric receiver applications.

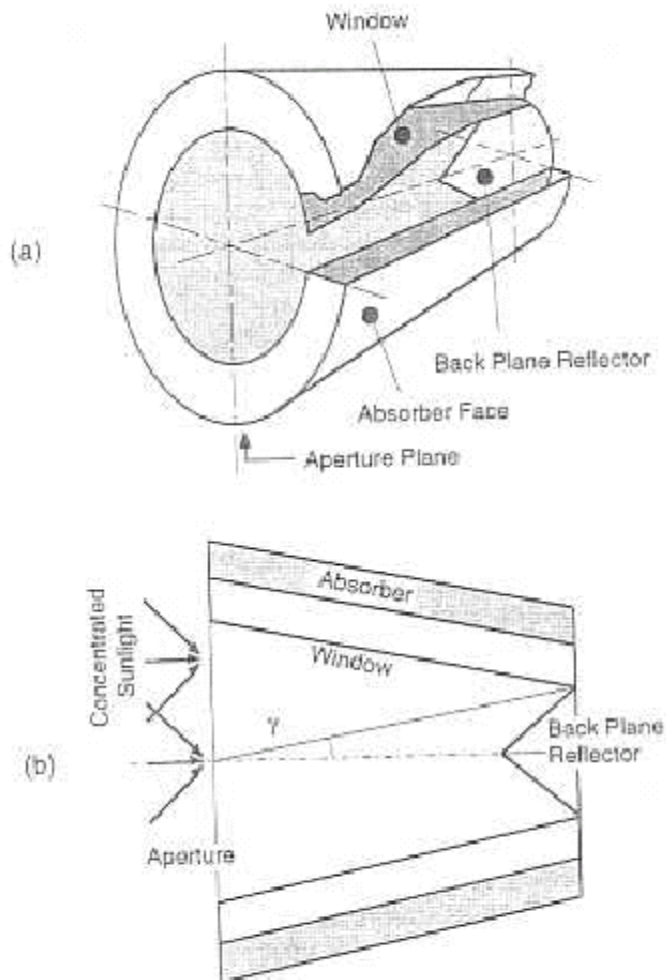


Fig. 2 Geometry of the window; (a) cutaway view of an annular solar receiver with a FLHIP window, (b) receiver cross section and the angle parameter γ (after Kribus, 1994)

Fig. 2.8.2

(9)Karni J., Kribus A., Rubin R., Doron P.
The "Porcupine": A Novel High-Flux Absorber For Volumetric Solar Receivers
 Solar Energy Engineering Vol.120 / 85-95, 1998

A new Volumetric (Directly-Irradiated) solar absorber at a power level of 10kW was tested at the Weizmann Institute's Solar Furnace. It can endure a concentrated solar flux of 4 MW/m² and produce working gas exit temperatures of 940°C. It sustained an irradiation solar flux level 4 times higher than that sustained by other Volumetric absorbers (foam and honeycomb matrices) yielding twice the power output of the other absorbers while its exit gas temperature being 300-350°C higher.

The Porcupine absorber aims at producing an absorber matrix capable of operating over large and variable conditions with the following characteristics:

- allow penetration of incident radiation into it and provide good radiative exchange between the absorbing elements, so that the absorption process is spread over a large heat transfer area and local overheating is prevented;

- introduce an effective convection heat transfer, with strong 3D flow mixing; the convective cooling pattern should match the distribution of the absorbed radiation;
- be durable and minimize the development of thermal stresses.

The performance of the Porcupine absorber is sensitive to the details of the fluid inlet and the pins layout. The Porcupine design therefore provides a means for matching between the irradiation intensity distribution and the distribution of convective cooling, consequently, local overheating is reduced. The Porcupine structure of mechanically independent members annuls thermal stresses development; consequently, cracking of the absorber material is prevented. The basic Porcupine structure provides convective and radiative energy transport between the matrix elements, therefore alleviating the development of flow instabilities; this phenomenon causes local overheating and restricts the operation of other Volumetric matrices.

A Porcupine absorber was subsequently incorporated into the Directly Irradiated Annular Pressurized Receiver (DIAPR), where it has been operating at an incident flux of several MW/m² and temperatures of up to 1700°C. Temperature gradients of about 800°C/cm, which developed in early tests, did not damage the Porcupine matrix. None of the Porcupine absorbers showed any signs of deterioration after hundreds of operating hours.

Porcupine performance can be further improved by increasing the operating temperature, especially its ability to allow penetration of incident radiation into it and provide good radiative exchange between the absorbing elements.

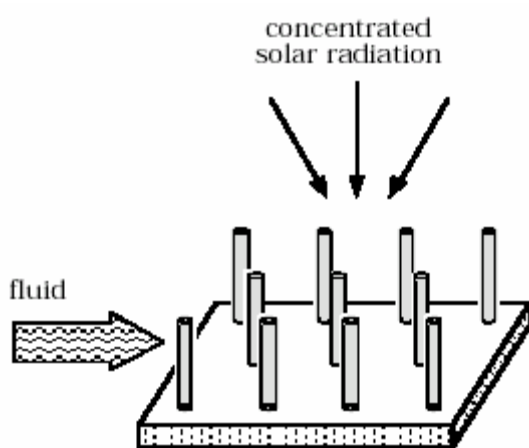


Fig. 2.9.1 - The porcupine volumetric solar absorber concept.

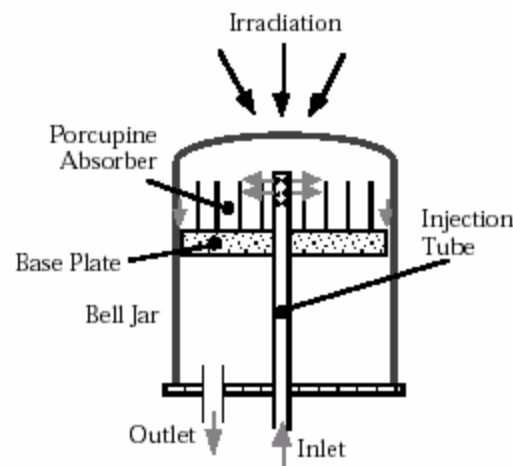


Fig. 2.9.2 -The porcupine absorber Experimental setup.

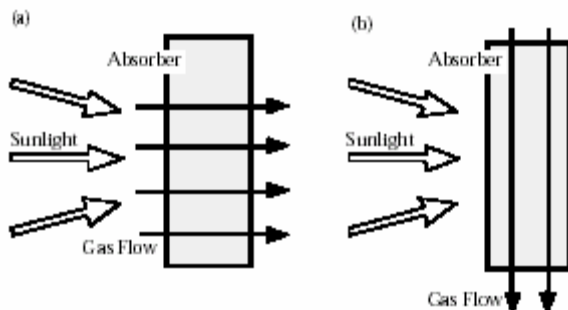


Fig. 2.9.3 Incident radiation and flow directions in absorbers

- (a) the incoming sunlight and the working-fluid flow are in the same general direction, as in Foam, Honeycomb, Grid, etc.;
- (b) the flow is perpendicular to the irradiation, as in the Porcupine.

(10)Hall C. A., Glakpe E. K., Cannon J. N. and Kerslake T. W.

Thermodynamic analysis of space solar dynamic heat receivers with cyclic phase change

Journal of Solar Energy Engineering 1999 Volume 121 Issue 3 pp 133-144

Solar heat receivers with solid-liquid phase change storage are viable options for space power management schemes during traverse of low earth-orbit (LEO) spacecraft into the eclipse phase of their orbit cycles. Solar Dynamic Power (SDP) systems use solar heat receivers with high-melting point phase change materials (PCMs) to produce continuous electric power throughout a spacecraft's entire orbit cycle. As shown in following figure

a typical SDP consists of :

- 1) a concentrator to collect and focus the incident energy onto the aperture plane of a central receiver
- 2) a central receiver to collect and distribute the reflected energy
- 3) working fluid tubes along the periphery of receiver to absorb the distributed energy.
- 4) a turbine to expand the high temperature working fluid to produce mechanical work via a rotating shaft.
- 5) a compressor to circulate the working fluid through the working fluid tubes.
- 6) an alternator to convert the mechanical shaft motion into the electric power
- 7) a radiator to reject the remaining cycle waste heat.

In the figure, a recuperator is added to increase the thermal efficiency of the thermodynamic cycle , which is typically a closed Brayton cycle.

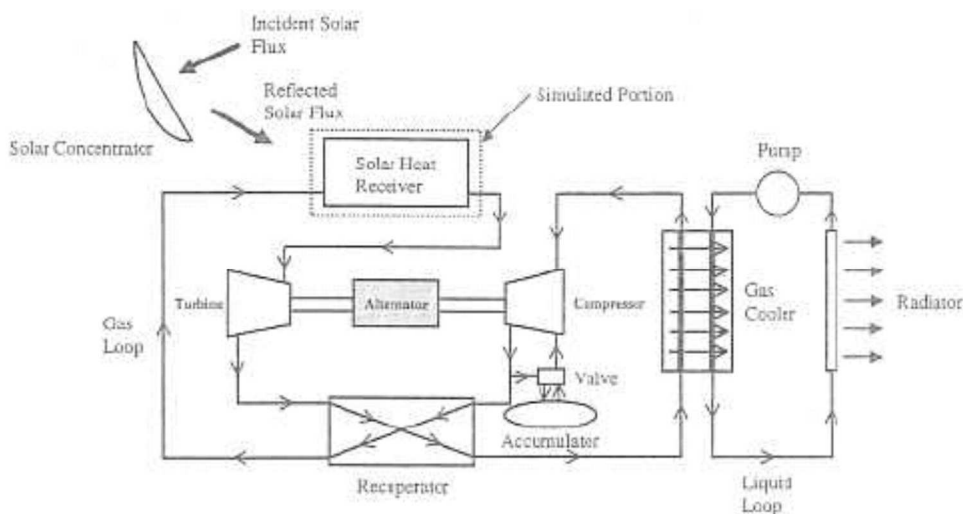


Fig. 2.10.1 Thermodynamic cycle for closed Brayton engine integrated with solar heat receiver

A physical and thermodynamic model of space solar dynamic heat receivers employing solid-liquid phase change storage is developed. Generalized first and second law efficiencies are defined for cyclic operation. The solar heat receiver of NASA Glenn Research Center's Solar Dynamic Ground Test Demonstration System is used to generate numerical results from start-up through balanced-orbit (asymptotic) conditions.

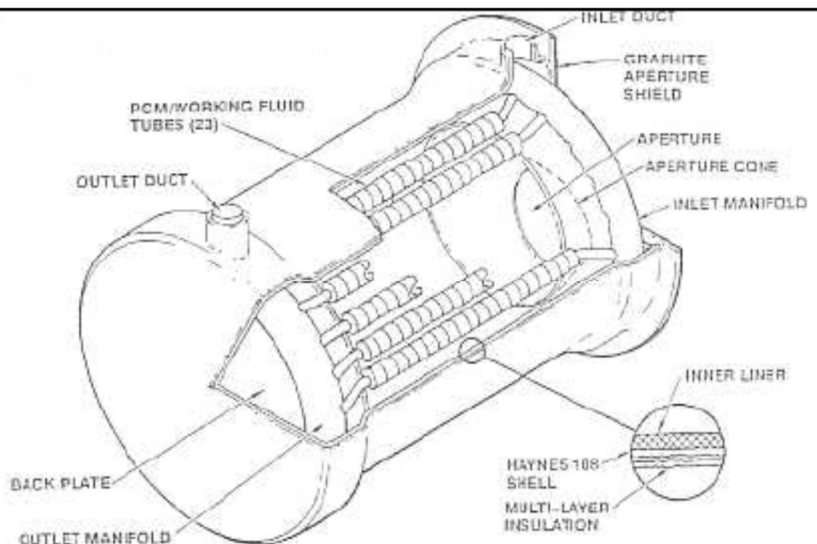


Fig. 2.10.2 Solar heat receiver of GTD system

In addition, a parametric study is performed to assess changes in receiver first and second law efficiencies due to changes in various system measurable parameters. Although the NASA receiver configuration is not optimized for cyclic thermodynamic performance, the cycle-integrated first and second law efficiencies compare favourably with steady-state numerical and experimental first and second law efficiencies.

(11) Kribus A., Doron P., Rubin R., Karni J., Reuven R., Duchan S., Taragan E.
A Multistage solar receiver: The route to high temperature

Solar Energy Vol. 67, Nos. 1–3, pp. 3–11, 1999

A high-temperature solar thermal receiver based on new concepts has been constructed at the Weizmann Institute's Solar Tower. It consists of a partitioned system in which the working fluid is gradually heated as it passes through a sequence of receiver elements with increasing irradiance levels. This configuration has been chosen to minimize the temperature-dependent emission and convection losses.

A device composed by two heating stage has been set up and tested. The high-temperature receiver stage, which accepts radiation from the central, high flux region of the aperture plane, is the Directly Irradiated Annular Pressurized Receiver (DIAPR - Karni et al.1997). The low-temperature stage is implemented as a partial ring of intermediate-temperature cavity tubular receivers (Pre-heaters) surrounding the central high-temperature stage.

Tests on both receiver stages has been performed including a total of about 40 solar hours. Maximum working fluid (air) temperature was up to 1000 °C, with the pre-heaters supplying about 650-750 °C at the inlet of the DIAPR. The power output was in the range of 30-60 kW. Operation of the partitioned receiver system was at pressures in the range of 16-19 bar.

A larger partitioned receiver system (Yogev et al ., 1999) is being currently developed which includes a large DIAPR rated at 500 kW, and several pre-heaters that bring the total receiver system output to about 800 kW, which will supply thermal energy to a small gas turbine in hybrid (solar/fuel) operation.

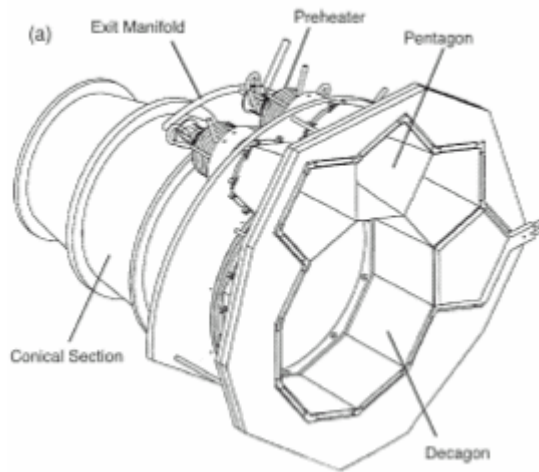


Fig. – 2.11.1 Assembly of the concentrator array and pre-heaters

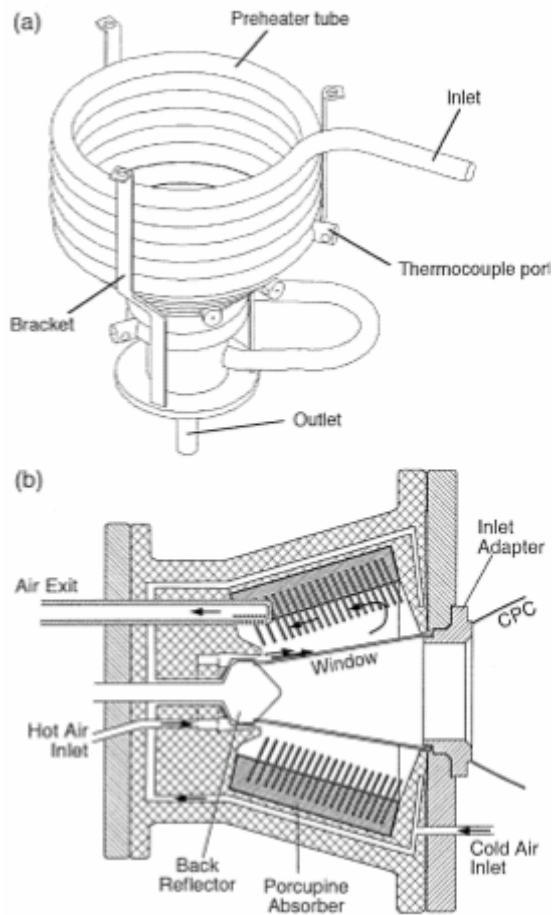


Fig. 2.11.2 - Receivers in the partitioned receiver system.
 (a) The light reflected temperature receiver (pre-heater);
 (b) high-temperature receiver (DIAPR).
 Arrows indicate direction of air flow.

Thermal Modeling of a Small-Particle Solar Central Receiver

Journal of Solar Energy Engineering Volume 122 February 2000

One of the limitation of solar central receiver designs is to absorb the high radiant fluxes that large heliostat fields are capable of delivering. One way to overcome this is to directly absorb the incident radiation volumetrically in the working medium. This paper presents a thermal model of a solar central receiver that volumetrically absorbs concentrated sunlight directly in a flowing gas stream seeded with submicron carbon particles. The heat transfer advantage of such a receiver is that the particles have a large surface area and are in the intimate contact with the gas. By proper choice of the particle loading and receiver shape and dimensions, the radiation can be absorbed throughout the given volume. The effect is that the gas has same temperature as the particles in contrast with the other receivers, leading to lower thermal losses.

The simplified receiver design consists basically of an insulated box with aperture on one side to admit concentrated light from the northern heliostat field. A gas particle mixture (i.e. dense smoke) flows in the bottom of the box, absorbs the light, and exits through the top. The particle flow is from bottom to top because buoyancy aids the flow in that direction as the gas heats.

A modified six-flux radiation model is developed and used with the energy equation to calculate the three-dimensional radiant flux and temperature distributions in a cavity-type particle receiver.

The model accounts for the spatial and spectral distribution of the incident sunlight and includes the effect of scattering and emission from the receiver walls and the participating working medium. A simultaneous solution of the energy equation for the flow through the receiver is used to determine the temperature distribution. The article includes one simple chemical reaction, namely that of carbon particles oxidizing as they traverse the receiver, but the model allows for the addition of more general chemistry.

Results indicate that the receiver is capable of withstanding very high incident fluxes and delivering high temperatures and has high efficiencies. The receiver efficiency as a function of mass flow rate as well as the effect of particle oxidation on the temperature profiles can be derived.

From a thermal point of view, this makes the receiver an ideal candidate for electricity generation, fuel/chemical processing, or hazardous waste destruction. In order to design such a receiver, issues such as how to form the particle mixture and how to incorporate a window (or not) need to be addressed. Further work on receiver modelling in the areas of fluid dynamics and radiation transfer would also help the design process.

(13) Kribus A., Huleihil M., Timinger A., Benmair R.

Performance of a rectangular secondary concentrator with an asymmetric heliostat field

Solar Energy Vol. 69, No.2, pp. 139-151, 2000

Secondary concentrators (used to increase the flux density of the radiation on the receiver, which increases the receiver efficiency and subsequently the overall system performance by reducing the size of the thermal receiver) with non-regular cross section permit additional degrees of freedom in heliostat field design, free of the limitations imposed by conventional rotationally symmetric concentrators.

A new class of concentrators with a rectangular cross section having an elliptic contour with

high eccentricity was constructed and tested at the Weizmann Institute, where the heliostat field has a strong asymmetry and is poorly suited for symmetric (having regular cross section) concentrators.

The performance of the new concentrator has been tested using calorimetric and radiometric measurements. The tests were carried out for several heliostats, located in representative positions relative to the predicted acceptance contours of the concentrator. The results of the tests validate the new design for use with highly eccentric fields. A more general conclusion is the validation of the approach of optimizing faceted secondary concentrators with flexible geometry to match heliostat fields having a wide range of possible contours.

An appropriate non-regular optical solution can be derived for many types of asymmetric fields using the optimal receivers. The severe restrictions placed on high-performance field design by symmetric secondary concentrators are therefore alleviated, and additional degrees of freedom are now available for field design and optimization.

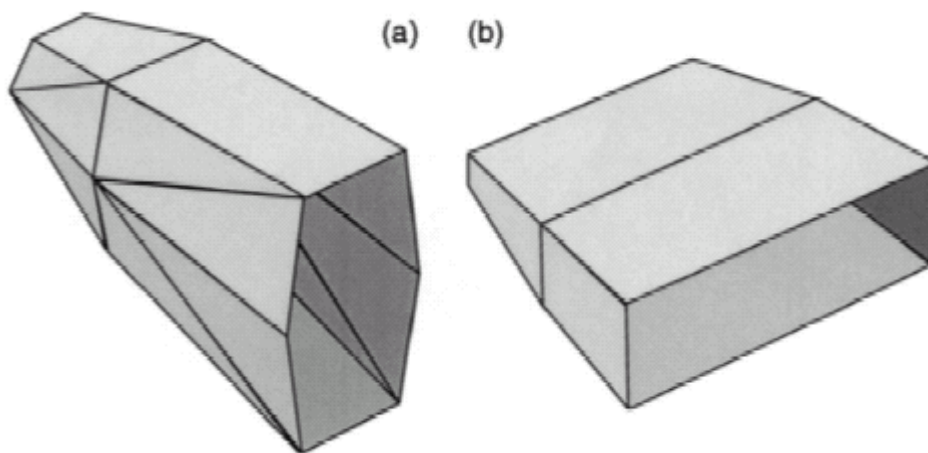


Fig. 2.13.1 - Optimized non-regular polygonal concentrators.

- (a) Hexagonal concentrator with an irregular entrance and a regular exit aperture;
- (b) rectangular concentrator with irregular entrance and exit apertures.

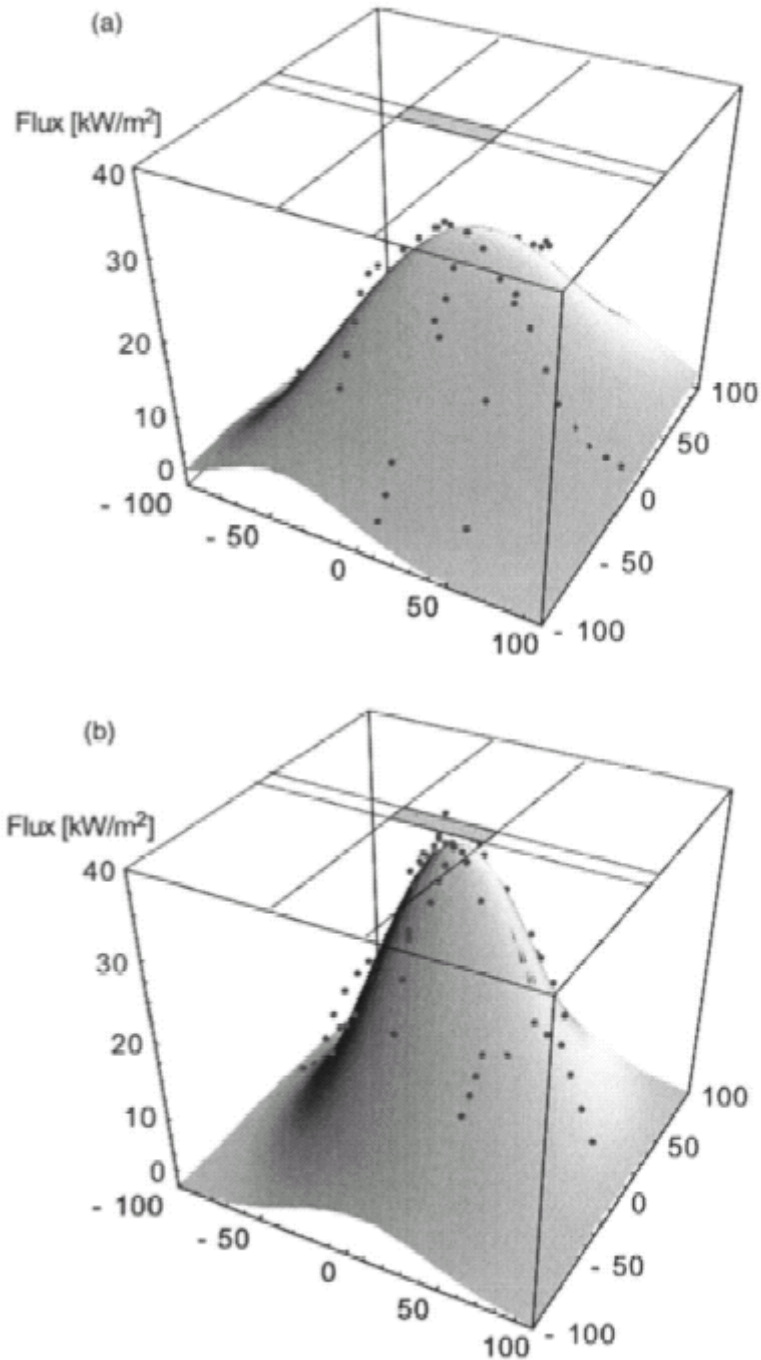


Fig. 2.13.2 - Flux distribution of (a) heliostat 100 and (b) heliostat 201. The dots are the measured, averaged and scaled radiometer data; the surface is the fitted Gaussian function. Some of the data dots are hidden below the surface. The lines on the top surface indicate the extent of the concentrator inlet aperture. Target dimensions are in centimetres.

(14)Kräupl S. and Steinfeld A.

Experimental Investigation of a Vortex-Flow Solar Chemical Reactor for the Combined ZnO-Reduction and CH₄-Reforming

Journal of Solar Energy Engineering Volume 123 pp 237-243 2001

The co-production of Zn and synthesis gas by the combined reduction of ZnO and reforming

of CH₄ has been performed using a vortex-flow chemical reactor in a high-flux solar furnace. The overall stoichiometric reaction is

$$\text{ZnO} + \text{CH}_4 \rightleftharpoons \text{Zn} + 2\text{H}_2 + \text{CO}$$

The 5 KW Vortex flow chemical reactor operating temperature ranged between 1221 and 1481 K for an input solar power of 2.3 to 4.6 kW and mean solar flux intensities of 810 to 1609 kW/m². The performance of the reactor was determined by conducting a complete mass and energy balance for the chemical process. The chemical conversion ranged between 83-100%. The thermal efficiency, defined as the portion of input solar power absorbed as sensible and process heat, was in the range 11-28%. The exergy efficiency for the closed cycle, defined as the ratio of the maximum amount of work that the products leaving the reactor could produce if were re-combined to the input solar power, was in the range 0.3-3.1%.

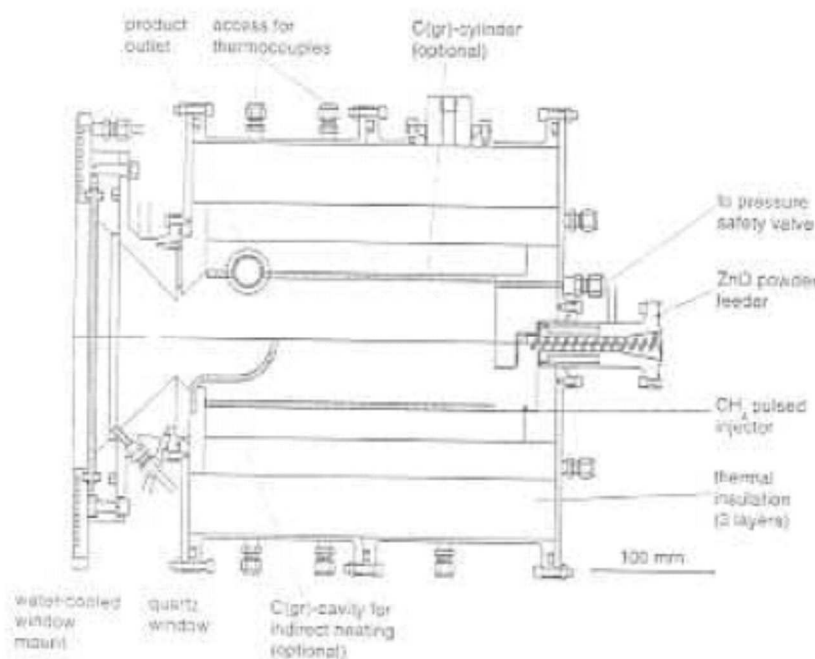


Fig. 2.14 Scheme of the improved SynMet Vortex-flow solar chemical reactor

The SynMet process offers the possibility of storing and transporting solar energy. The calorific value of zinc and syngas is increased above the value of the initial reactants by the solar input in an amount equal to the enthalpy change of the reaction. Since the cost incurred by the solar concentration system correspond to about half of the total investment for the entire solar chemical plant, the higher the energy conversion efficiency, the lower is the solar collection area for producing a given amount of solar fuel, and eventually the more favourable become the economics of the solar process.

Major sources of energy loss are re-radiation heat transfer through the reactor aperture, conduction heat transfer through the reactor walls, and the quenching of the reaction products.

(15)Kribus A., Doron P., Rubin R., Taragan E., Duchan S., Karni J.
Performance of the Directly-Irradiated Annular Pressurized Receiver (DIAPR)
Operating at 20 Bar and 1200°C

Journal of Solar Energy Engineering Vol. 123, February 2001

The Directly Irradiated Annular Pressurized Receiver (DIAPR) is a volumetric (directly irradiated) windowed cavity receiver. It integrates two innovative components which allow good receiver performances:

A Porcupine ceramic volumetric absorber, which absorbs concentrated sunlight and transfers its energy as heat to the working fluid.

Frustum-Like High Pressure fused silica window closing the cavity to reduce the reflective losses.

The receiver is designed for operation at a pressure of 10–30 bar, exit gas temperature of up to 1300°C, and aperture radiation flux of up to 10 MW/m². Inlet aperture flux can reach up to 5 MW/m²; exit air temperatures of up to 1200 °C can be obtained, with operating pressures of 17–20 bar. The receiver efficiency is in the range of 0.7–0.9. The absorber and window temperatures of 200–400°C, below the permitted maximum indicate that higher air exit temperatures can be reached.

Tests verify receiver stable operation and durability under continuous high load and under rapid heating-cooling cycles. These encouraging results have led to the develop a larger partitioned system which includes a DIAPR rated at 50 kW and several pre-heaters. This receiver has been designed to supply thermal energy to gas turbines in solar and fuel operations.

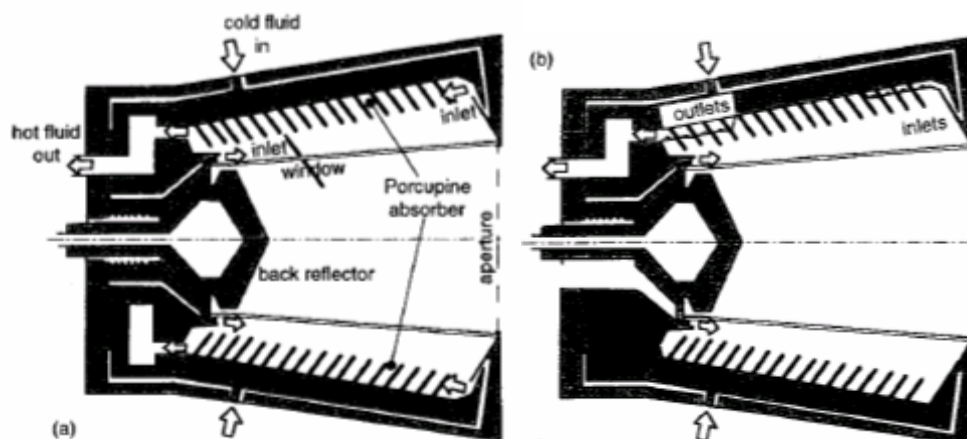


Fig. 2.15 -
Symmetric receiver design at 10kW
power level

Asymmetric receiver design at 50 kW
power level

(16)S. Möller and R. Palumbo

The Development of a Solar Chemical Reactor for the Direct Thermal Dissociation of Zinc Oxide

Journal of Solar Energy Engineering May 2001 Volume 123 Issue 2 pp 83-90

The direct solar thermal composition of ZnO to its elements is an attractive process for the storage of solar energy. In this process, concentrated sunlight provides high temperature

process heat for the endothermic reaction
 $\text{ZnO(s)} \rightleftharpoons \text{Zn(g)} + 0.5\text{O}_2 \text{ (T>2000K)}$

At temperatures near 2000K the reaction proceeds. Solar radiation is thereby directly converted into the chemical energy of Zn and O₂. To avoid their recombination at high temperature, the gaseous products can be separated by gas phase electrolysis or quenched. The solar energy stored in the condensed Zn phase may be used as the fuel in a fuel cell or battery. When H₂ is the desired fuel, it has also been suggested that the Zn be used to split the water in an exothermic reaction. In either scenario, the ZnO is recycled to the solar furnace. Following figure shows a schematic representation of the two-step water-splitting cycle using the Zn/ZnO redox system for the solar production of hydrogen.

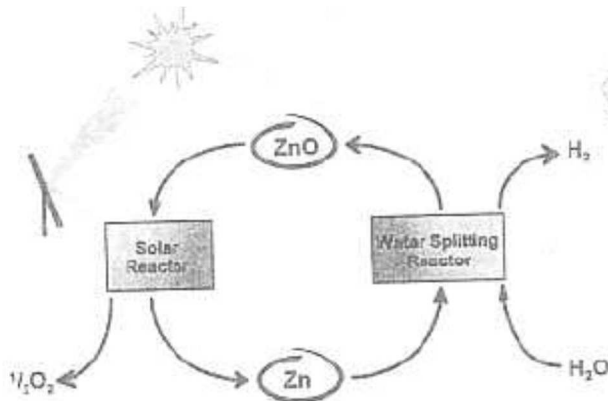


Fig. 2.16 Schematic representation of the two step water-splitting cycle

Directly heating the reactants means the window through which the concentrated sunlight enters the reactor must be protected from the deposition of Zn or ZnO. The need is to protect the window with a curtain of inert gas. There is no known special formula or dimensionless number one can use to design the flow patterns or flow rates required to keep the window clean. Computer fluid dynamic modelling is an important design tool that can be used in conjunction with experimental work.

A solar chemical reactor was designed, constructed and tested for the direct thermal decomposition of zinc oxide at temperatures as high as 2250 K using concentrated sunlight. Along with the reactor, a 1-dimensional numerical model was developed to predict the reactor's thermal performance under various solar flux levels and to identify the physio-chemical properties of ZnO that are critical for designing the reactor. An experimental study was also conducted to ascertain how best to employ a curtain of inert gas to keep the reactor's window clean of Zn and ZnO. The reactor proved to be a reliable research tool for effecting the decomposition reaction and it possesses many features characteristic of a reactor scale-able to an industrial level: it is resilient to thermal shock; it has a low effective thermal inertia, and it can operate in a continuous mode when ZnO as a powder is fed to the reactor. Furthermore, experimental work led to insight on how best to keep the window clean in the course of an experiment. Also, comparisons between output from the numerical model and experimental results show that the solar flux and the ZnO's thermal conductivity and emissivity are the most critical variables affecting the exergy efficiency of the reactor and the mass flux of product gases. The comparison further reveals the need to investigate whether or not the magnitude of the published pre-exponential term in the decomposition rate equation used in the numerical model should be reduced for improving agreement between the model and the experimental results.

(17)Joseph A. Bonometti, Clark W. Hawk

High Temperature Solar Absorber Material Measurement Technique

Journal of Solar Energy Engineering Volume 123, August 2001

Reflectivity is highly dependent on surface conditions, integrating spheres are typically used to obtain reflectivity values. They normally cannot evaluate the hot samples of interest to STUS. Temperature dependence has been investigated but at levels below 2000 K. Recent STUS research heated samples to 1500 K using electric resistive elements. Specular measurements were made at these temperatures and evaluated with a monochromatic laser. The system developed in this study enables to be subjected to conditions approximating those found in space solar absorber, being applicable to temperatures above 3000 K. It also allows the total reflectivity to be calculated. It is considered more suited for an absorber cavity than the silver or rhodium samples used for secondary concentrator components.

Basic material properties determine the amount of solar energy that is absorbed, transmitted or reflected and these values will often change with differing temperatures. This investigation developed a new approach to evaluate the material properties (i.e., reflectivity, absorptivity) of a solar absorber wall and experimentally tested the method using sample coupons. The reflectivity was measured both at ambient and elevated temperatures over a range of angles from 0 to 90 degrees. The same experimental data set was used to calculate the sample's total reflectivity, by uniquely integrating the recorded intensities over a hemisphere. The test methodology uses the incident solar energy as the heating source, while directly measuring the reflected light (an integrated value over all visible wavelengths) and is suitable for test samples over 3000 K.

The technique facilitates simultaneous measurement of the properties. These key absorber properties are critical to thermal and optical computational design codes for such devices. It is desirable to test representative materials manufactured from typical processes to obtain more accurate data for use in hardware design calculations.

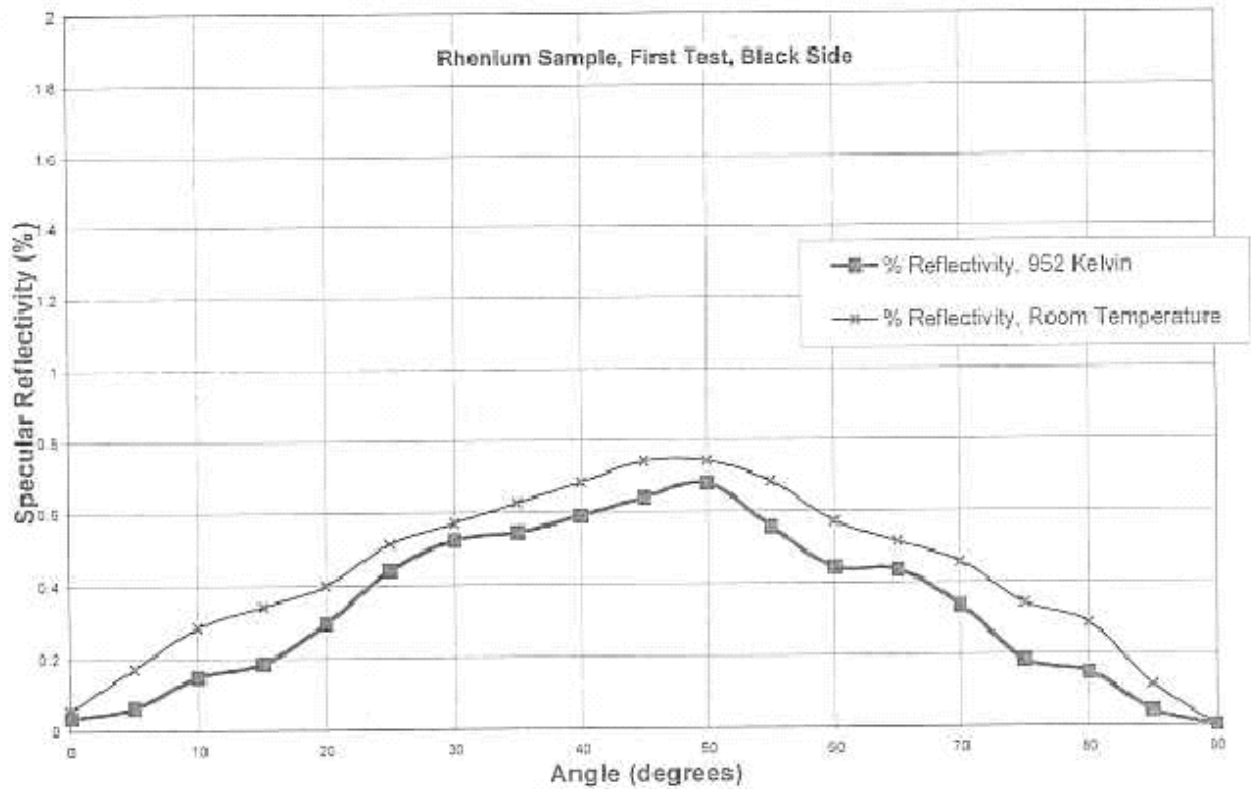


Fig. 2 Reflectivity at temperature

Fig. 2.17

(18)Reiner Buck, Thomas Bräuning, Thorsten Denk Markus Pfänder, Peter Schwarzbözl and Felix Tellez
Solar-Hybrid Gas Turbine-based Power Tower Systems (REFOS)
 Journal of Solar Energy Engineering Volume 124 February 2002

Solar hybrid power plants have a significant potential for cost reduction when the solar energy is introduced into a gas turbine of Combined Cycle systems (CC). The introduction into gas turbine systems could be realized with pressurized volumetric air receivers heating the compressed air of the gas turbine before it enters the combustor. A scheme of the concept is shown in following figure :

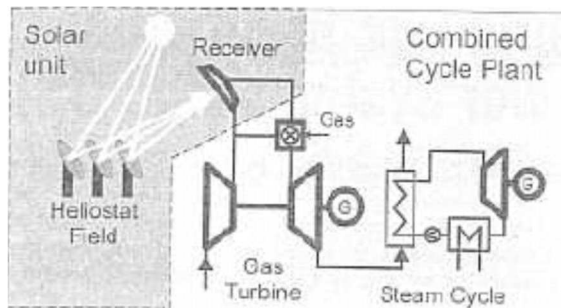


Fig. 2.18.1 Solar air preheating system

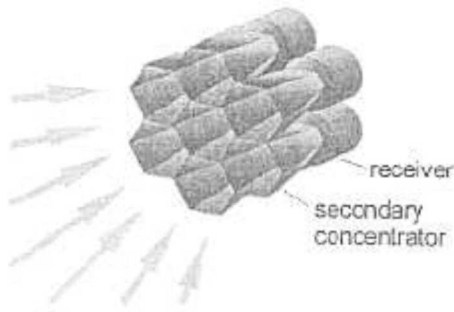


Fig. 2.18.2 Modular receiver arrangement

Solar air preheating offers superior performance, as the solar energy absorbed in the heated air is directly converted with the high efficiency of the CC plant. This results in reduced heliostat field size and thus less overall investment cost for the solar part as compared to solar system generation. This concept can be applied to wide range of power levels (1 to 100 MW) A receiver module, consisting of a secondary concentrator and a volumetric receiver unit, was tested at the Plataforma Solar de Almería, Spain.

The technical goals of the receiver system demonstration were

- *absorbed thermal power(design conditions) : 350 KW
- *operating pressure (absolute) : 15 bar
- *air outlet temperature : up to 800 °C
- *receiver efficiency (including improved secondary concentrator) : 80%

A schematic of a receiver module is shown below:

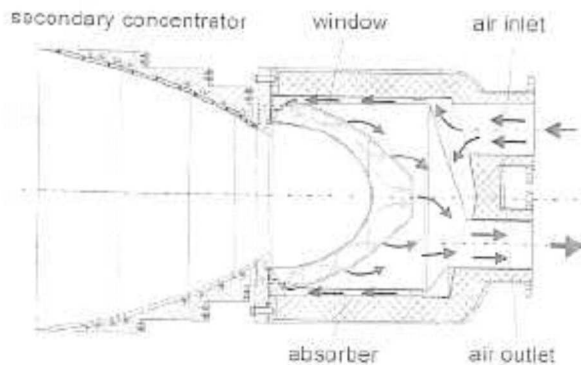


Fig. 2.18.3 - REFOS Receiver Module

Air exit temperatures up to 815°C and power levels of 410 kW were achieved. Total solar test time summed up to 400 hours. Receiver efficiencies were in the range of 70%. A new secondary concentrator with improved efficiency was designed and built. Based on an inexpensive manufacturing technology, the secondary concentrator geometry was optimized to reduce the optical losses. Performance tests with this new secondary concentrator and a cold-water calorimeter proved the expected increase in efficiency of about 10%. Maximum operation power was 450 kW at the exit aperture. The dependency of performance on the incidence-angle showed good agreement with the predictions, as well as the results of a special photographic measurement campaign. Several configurations of solar-hybrid gas turbine cycles in the low to medium power range are examined for performance and costs. The results confirm the promising potential of this technology to reach competitiveness in certain power markets;

Comparative performance of REFOS and ISCCS

Figures of Merit	Day-Time Operation		Full Time Operation	
	REFOS	ISCCS	REFOS	ISCCS
(1) Solar thermal efficiency %	47.3	47.7	47.4	47.7
(2) Thermal solar share %	28.6	12.5	15.0	7.1
(3) Incremental solar share %	25.4	8.4	11.3	4.1
(4) Incremental solar thermal to electric efficiency %	38.3	35.2	32.3	30.9
(5) Incremental total solar to To electric efficiency %	18.1	16.8	15.3	14.7

ISCCS → Integrated solar combined cycles system

Solar thermal efficiency : $\eta_{th,sol} = (Q_{sol,th})/DNI* AAP$

Thermal solar share: $f_{ss} = (Q_{sol,th})/(Q_{sol,th} + E_{fuel})$

Incremental solar share : $\Delta_{ss} = (E_{el} - \eta_{ref} \cdot E_{fuel})/E_{el}$

Incremental solar thermal to electric efficiency: $\eta_{\Delta} = (E_{el} - \eta_{ref} \cdot E_{fuel})/Q_{sol,th}$

Incremental total solar to electric efficiency : $\eta_{\Delta,t} = (E_{el} - \eta_{ref} \cdot E_{fuel})/DNI* AAP$

DNI : annual direct normal insolation

AAP : area receiver aperture

$Q_{sol,th}$: annual solar thermal energy to cycle

E_{fuel} : annual fuel energy to cycle

E_{el} : annual electricity production

η_{ref} : efficiency of the reference cycle

(19)Doerte Laing and Magnus Pålsson

Hybrid Dish/Stirling Systems: Combustor and Heat Pipe Receiver Development

Journal of Solar Energy Engineering Volume 124, May 2002

A hybrid sodium heat pipe receiver has been developed within the project HYHPIRE, funded 50% by the European Commission. The hybrid receiver was designed for the SBP/LCS 10-kWel dish/Stirling system with the SOLO-161 Stirling engine. The SBP/LCS 10 KW dish/Stirling system with the SOLO-161 Stirling engine is an advancement of the SBP 9-KW dish/Stirling system which has accumulated 29000 operating hours.

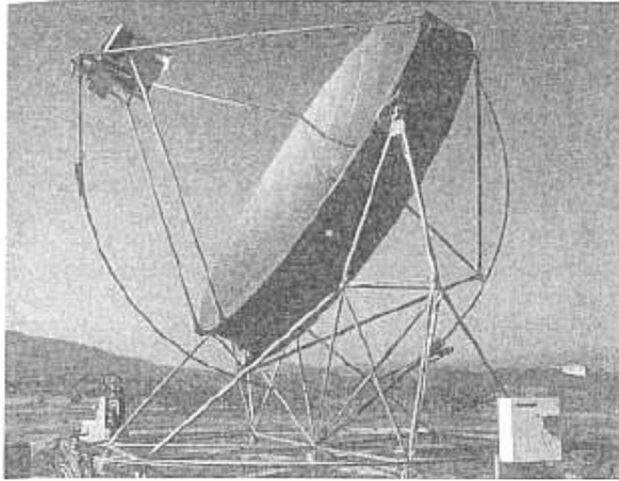


Fig. 2.19.1 - SBP/LCS 10 KW Dish/Stirling system

These systems use a directly irradiated tube-type receiver. Successful market penetration of dish/Stirling systems is much supported by a hybrid system which will allow Stirling engine operation driven by solar and/or combustion heating ,to harmonize energy production and demand. Therefore, the receiver has to be provided with an additional combustion system.

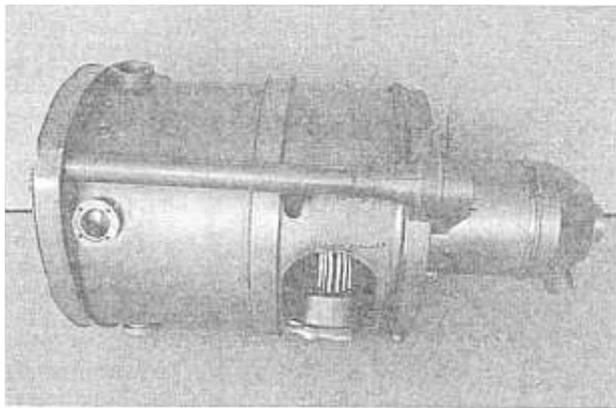


Fig. 2.19.2 Hybrid heat pipe receiver with combustion system

The use of a heat pipe receiver makes it much easier to integrate such a combustion system than with a tube-type receiver because the heat pipe allows a separation of a different heat transfer surfaces, absorber surface, Stirling heater head and gas heat exchanger. This gives more freedom in designing all three components according to their specific requirements. In addition, it has the advantage of excellent heat transfer, thus non-uniform heat fluxes can be tolerated much better than with the tube-type receiver. The system has been tested successfully in all operation modes.

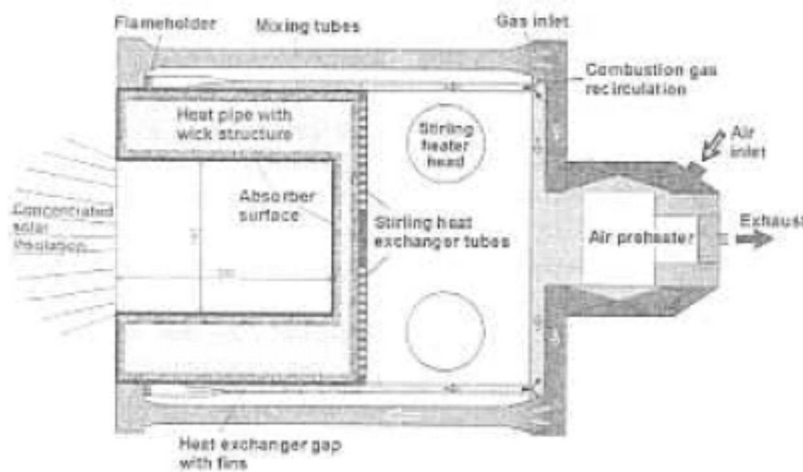


Fig. 2.19.3 Scheme of hybrid heat pipe receiver

The heat pipe was designed for a total thermal load of 45 kW at 700C-850C sodium vapour temperature. This would be the maximum power for 1000 W/m² insulation. Maximum thermal load needed for the Stirling engine is 30 kW. Therefore the gas heat exchanger was designed for a heat transfer of 30 kW. If solar irradiation exceeds this load, the excess heat will be automatically rejected by ventilating cold air through the gas heat exchanger. This is done with the fan of the combustion system, by-passing the preheater.

The heat pipe is built up as a double walled pot. Solar heat input, combustor heat input, and heat output to Stirling heater is realized by using three different heat transfer surfaces on the heat pipe. The inner cavity serves as absorber surface. The first 50 mm of the cavity are shaded by a ceramic ring, with an inside aperture of 180 mm. The outer heat pipe mantle, equipped with 400 fins, serves as heat transfer surface for the gas heat flow. The 3 mm diam Stirling heater tubes are brazed into grooves in the outer rear plate of the heat pipe, which serves as the condenser zone of the heat pipe. The two heating zones—namely the internal cavity receiving concentrated solar radiation and the external cylindrical wall which is heated by the combustion system—can be loaded. A combination of axial webs and a surface covering structure is used inside the heat pipe. All capillaries structures of the heat pipe are made up of 600 screen, spotwelded in place. The heat pipe container parts are made of Inconel 625.

The flame holder is located in the front part of the heat pipe, just behind the sodium pool, and the combustion gas leaves the heat exchanger at the rear end of the heat pipe.

The expansion cylinder head is connected to the hybrid receiver through a single duct, the regenerator housing through a bundle of thin tubes, to allow for thermal expansions that cannot be taken up by the flexible gas collar of the engine. The heat pipe is located in front of the Stirling cylinders, while the preheater lies behind the cylinders. The whole hybrid receiver is fixed over three bearings into a frame that is rigidly connected to the engine. The bearings allow the movements of the receiver due to thermal expansion in axial and radial direction.

The hybrid heat pipe receiver has been successfully developed and tested.

(20) Abraham Kogan, Meir Kogan

The Tornado Flow Configuration—An Effective Method for Screening of a Solar Reactor Window

Journal of Solar Energy Engineering Volume 124, August 2002

In volumetric solar receivers used for effecting chemical reactions the working fluid must be contained within a sealed enclosure provided with a window transparent to incident solar radiation, which arises when it operates at a pressure different from atmospheric pressure. To

prevent the destruction of the window by local overheating, it is necessary to prevent the solid particles from contacting the window surface. The use of a curtain of an auxiliary gas flow in the vicinity of the inner surface of the reactor window to screen the window against contact with the main fluid flow.

The working fluid in solar receivers, utilized for effecting chemical reactions, is usually flown through a sealed enclosure provided with a quartz window. When one of the reactants or products of reaction is a powder, care must be taken to prevent contact of the incandescent powder particles with the window, in order to obviate its destruction by overheating. Attempts made in the past to screen the window against particle deposition by a "curtain" of an auxiliary gas stream showed that very substantial flow rates of auxiliary gas (30—80% of the main stream flow rate) were necessary for perfect window screening. The heat absorbed by the auxiliary gas stream represented a major loss of energy. In an effort to reduce the auxiliary stream flow rate to a minimum, a certain flow pattern akin to the natural tornado phenomenon has recently been developed in our laboratory. It enabled effective reactor window screening by an auxiliary gas flow rate less than 5% of the main gas flow rate. The tornado effect is discussed and demonstrated by a smoke flow visualization technique.

The whirling flow system which has been described appears to be an ideal solution for the window screening job. It requires an auxiliary gas flow rate of less than 5% of the main gas flow rate. Its effectiveness is not limited to small size windows. The auxiliary gas sweeps the window surface as a thin and very fast film that covers the surface completely. It also cools effectively the window material, due to the high heat transfer coefficient of the rapid boundary layer flow. Since the auxiliary stream doesn't detach from the window surface and doesn't mix appreciably with the main stream, it doesn't remove much process heat from the reacting gas.

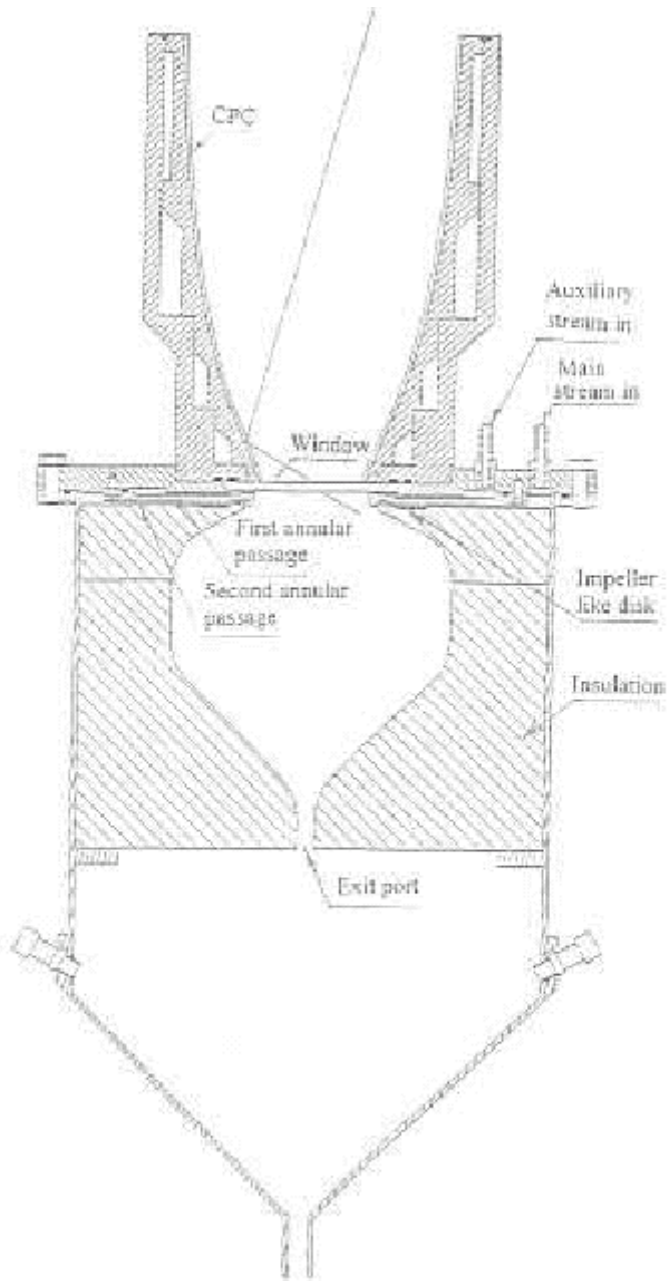


Fig. 2 Reactor model M2b-CPC assembly

Fig. 2.20.1

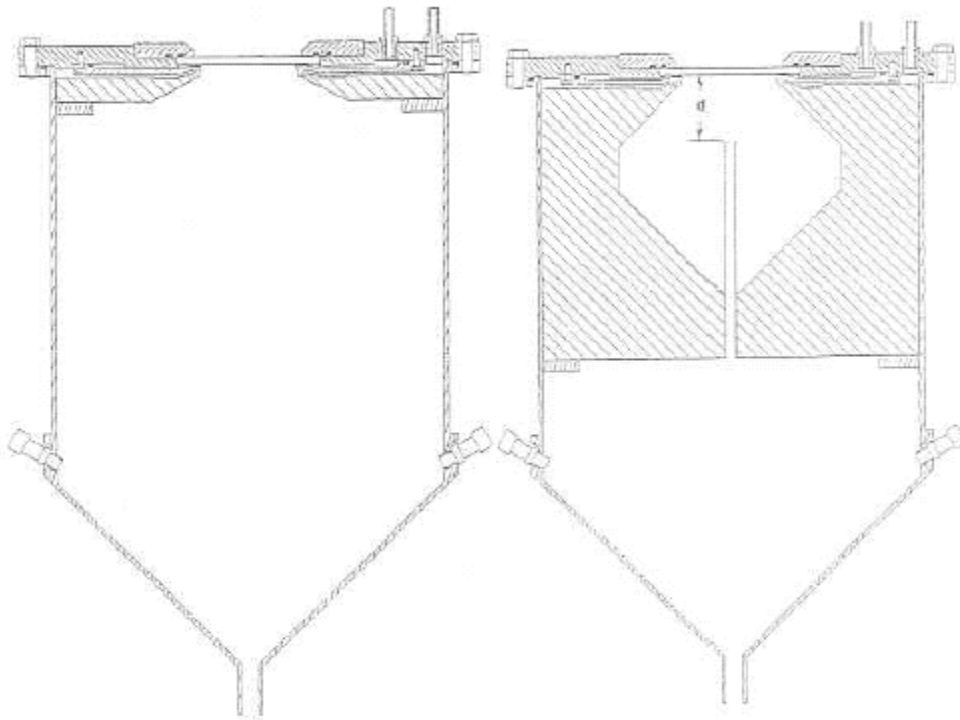


Fig. 11 Reactor model M2c

Fig. 12 Reactor model M2d

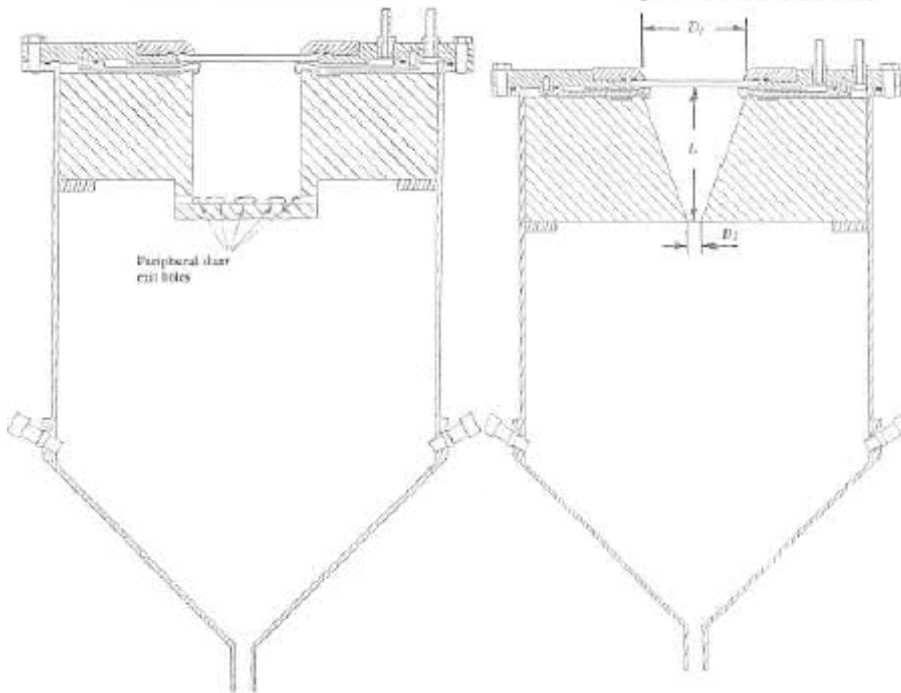


Fig. 14 Reactor model M2e

Fig. 4 Reactor model M2a

Fig. 2.20.2

(21)Abraham Kribus, Andreas Timinger

Optical In-Situ Assessment of a Non-imaging Secondary Concentrator in a Solar Tower

Journal of Solar Energy Engineering Volume 124, August 2002

Nonimaging reflective concentrators are used for concentration of solar radiation, especially as second stage concentrators for high temperature solar power plants. Secondary concentrators may be relatively small devices when the primary is a parabolic dish or large devices intended for solar tower systems. The use of secondary concentrators can increase the flux incident on the solar receiver relative to the use of only one concentrator stag, because the potential of a two-stage system may approach the thermodynamic limit of concentration. Reaching a high incident flux is important in high temperature applications since it provides higher receiver efficiency. The performance of a nonimaging concentrator is sensitive to the geometric accuracy of its reflective surfaces.

A method for remote optical measurement of the geometry of non-imaging concentrators is presented. A concentrator installed in a solar tower was measured by observation of transmission patterns from the heliostat field, and comparison of the measured patterns to a ray tracing simulation. The actual geometry of the concentrator was derived from optimization of the match between real and simulated patterns. The measurement was sensitive and accurate enough to detect small errors in the concentrator geometry, such as 1mm in linear dimension and 0.1° in concentrator tilt angle. The measurement procedure is simple and can be easily adapted to a wide range of non-imaging optical systems. Compared to an integral calorimetric test of a concentrator, the remote optical method provides much more geometric information and much higher accuracy. The remote optical measurement enables measurement of devices with deep geometry and a non-uniform number of reflections, and does not require contact with or manipulation of the reflective surfaces. This method can complement photo-grammetry used for primary concentrators, to provide a complete solution for characterization of two-stage optical systems.

The analysis described can be partly automated but manual intervention and control for the high-level decisions are recommended. For a given type of concentrator some expertise will be needed in order to define the decoupling and optimization order of the parameters and to identify which features in the pattern should be matched for specific parameters. This is important when the method is applied for a complex concentrator with a large number of degrees of freedom and of observation points, since the amount of computation for a fully automatic optimization could be prohibitive. As the heliostat field increases in size, the concentrator inlet aperture will also increase by roughly the same ratio.

(22)Alejandro Londoño-Hurtado, Alejandro Rivera-Alvarez
Maximization of Exergy Output From Volumetric Absorption Solar Collectors
Journal of Solar Energy Engineering Volume 125, February 2003

A Volumetric Absorption Solar Collector is a solar collector that uses a semitransparent medium to collect solar radiation through a semitransparent solid or liquid volume. In a VASC solar radiation is absorbed and delivered to the user as heat transfer. This heat is extracted from the collectors bottom at an amount that can be greater than, smaller than, or equal to the radiation delivered at the bottom. The temperature varies with depth.

A model has been developed to study the behaviour of Volumetric Absorption Solar Collectors (VASC) and the influence of the design parameters on the performance of the collector. The model's approach is based on the use of several dimensionless numbers, each of them having a clear physical significance, which play a key role in the analysis of the collector. The model is then used to conduct a thermodynamic optimization of VASC, which gives the optimal design parameters that maximize the exergy output of the heat extracted

from the collector. The results agree with the findings made by other authors who have studied flat plate solar collectors.

In the no depth limit, equations for a VASC become the equations for the flat plate collector. From a VASC can be extracted much more exergy that can be extracted from a flat plate collector. In this sense a VASC is thermodynamically superior to a flat plate collector. The improving thermodynamic performance of the collector has constraints given by the allowance of high temperatures of the medium. A VASC that uses a water medium gives to the collector the capacity of extracting high amounts of exergy. The main disadvantage of water is its low boiling point. A VASC that uses ordinary glass medium has no problem handling high temperatures but its low transparency and high conductivity makes it a bad choice. Therefore it is necessary to develop or search for available materials to be used as the appropriate semitransparent medium. The ideal medium would be one with a transparency similar to or higher than water's transparency, conductivity similar or lower than the water's conductivity and a high temperature allowance.

Further work must be done concerning the implementation of more complete models for a VASC in search for more realistic finite-time thermodynamical limits for the operation of the VASC. These models should take into account factors like reradiation losses and spectral absorption.

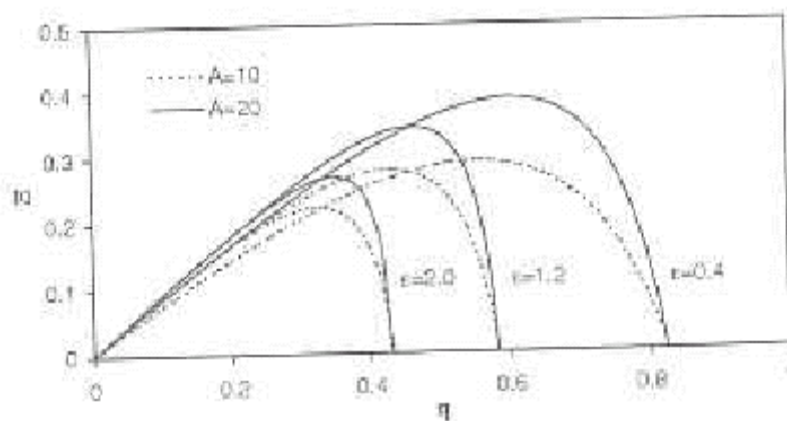


Fig. 3 Variation of the exergy output with efficiency for $B=0.06$

Fig. 2.22.1

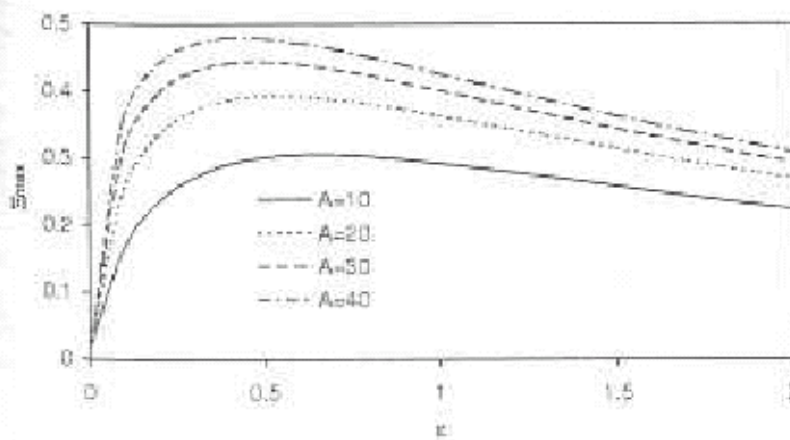


Fig. 6 Variation of the maximum exergy output with dimensionless depth for $B=0.06$

Fig. 2.22.2

(23)Pai-Chuan Liu

Temperature Distribution in a Porous Medium Subjected to Solar Radiative Incidence and Downward Flow: Convective Boundaries

Journal of Solar Energy Engineering Volume 125 May 2003

The knowledge of steady-state temperature distribution is known a priori for natural convection stability analysis. The present study determines the temperature profiles in an infinite horizontal layer of fluid filled with saturated porous medium confined between two convective surfaces subjected to external radiative incidence and imposed downward convection. The investigation concentrates on the influences of the thermal boundary condition (Biot number), internal and external Rayleigh numbers, Peclet number, optical thickness, and surface reflectivity.

The temperature distribution within a fluid-saturated porous medium confined between two parallel layers subjected to external thermal irradiation while both surface exchange energy with the external environment were presented. In general, the temperature of the lower boundary surface is higher than that of the upper boundary surface due to accumulated incoming energy from the top. The temperature distribution is almost parabolic in nature when plotted as a function of the non-dimensional location within the fluid layer. The temperature profile reduces to the standard linear curve when the above influential factors were absent from the porous medium. The increase of energy absorption, surface reflectivity, and external incident energy increase the nonlinearity of the temperature distribution. The temperature gradient decreases with an increase of energy exchange. The least stable situation exists when the surface is insulated such that all incoming energy is retained and absorbed within the fluid layer.

An exception in this trend occurs for increasing the externally imposed downward make-up water. The rationale is that less energy is accumulated and retained within the system as the water velocity increases, which causes less thermal disturbance in the fluid layer. As external energy is accumulated within the fluid, the temperature rises and the location of the maximum temperature lies near the lower portion of the fluid layer.

The result presented in this study should provide useful information for actual stability computation in applications such as solar pond and industrial fluidized bed designs. Future investigation should study the effects of temperature dependent properties, which are important in many engineering applications.

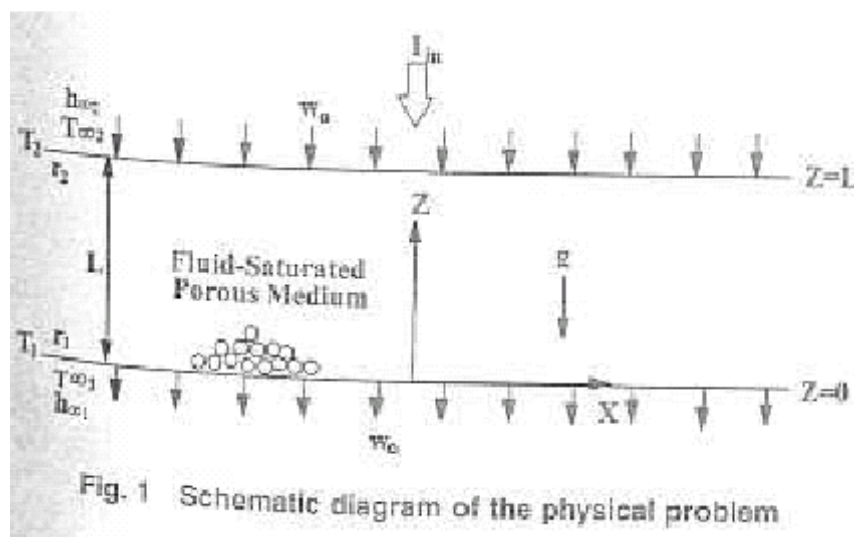


Fig. 1 Schematic diagram of the physical problem

Fig. 2.23

(24)Thomas Mancini, Peter Heller, Barry Butler, Bruce Osborn, Wolfgang Schiel, Vernon Goldberg, Reiner Buck, Richard Diver, Charles Andraka, and James Moreno
Dish-Stirling Systems: An Overview of Development and Status

Journal of Solar Energy Engineering May 2003 Volume 125 Issue 2 pp 135-151

Solar thermal power systems, which are also sometimes referred to as concentrating solar power systems, utilize the heat generated by concentrating and absorbing the sun's energy to drive a heat engine/generator and produce electric power. Dish-engine systems comprise a parabolic dish concentrator, a thermal receiver, and a heat engine/generator located at the focus of the dish to generate power.

Dish-Stirling systems have demonstrated the highest efficiency of any solar power generation system by converting nearly 30% of direct-normal incident solar radiation into electricity after accounting for parasitic power losses, producing more than 3000 suns concentration, and operating at temperatures of 750C at annual efficiencies of 23%. Dish-Stirling systems track the sun and focus solar energy into a cavity receiver where it is absorbed and transferred to a heat engine/generator.

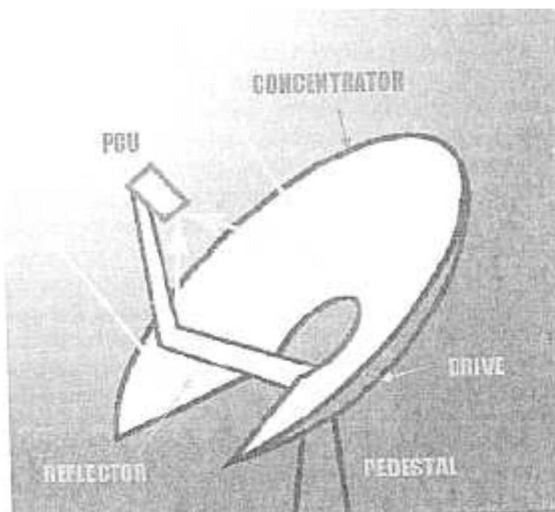


Fig. 2.24.1 - Dish Stirling system components

Although a Brayton engine has been tested on a dish and some companies are considering adapting micro-turbine technology to dish engine systems, kinematic Stirling engines are currently being used in the four Dish-Stirling Systems being developed today.

Dish Stirling systems are modular i.e. each system is a self-contained power generator, allowing their assembly into plants ranging in size from a few kilowatts to tens of megawatts. The near-term markets identified by the developers of these systems include remote power, water pumping, grid-connected power in developing countries and end-of-line power conditioning applications.

The receiver is a key component in a Dish-Stirling system because it must convert the concentrated solar energy to heat and transfer it to the engine working fluid at high-flux conditions from 75 to 100W/cm² and temperatures of 700-800C. The advanced receivers that are currently being developed include heat-pipe receivers, hybrid receivers, and a volumetric receivers

Heat Pipe Receivers

Heat pipe receivers use sodium or a mixture of sodium and potassium to transfer heat from the surface of the receiver to the engine heater head. Heat pipes utilize a capillary wick to

distribute the liquid metal over the back surface of the absorber. The liquid metal evaporates, vapour is transported to the engine heater head where it condenses, and the liquid metal refluxes to the absorber. In these receivers, the liquid metal condenses at the constant temperature thereby providing uniform heating to the Stirling engine, unlike DIR receivers that can experience large temperature differences between quadrants or along the tubes of the receiver. Since the receiver materials typically limit the peak receiver temperature and thus the performance, in a heat pipe receiver the peak temperature is the average temperature, which raises the achievable working gas temperature considerably. The increased working gas temperature balance among the four cylinders of the engine, and overall simplicity resulted in a 20% increase in system efficiency

Bio Dish Hybrid Receiver

A schematic of the BioDish receiver design is shown in Fig. 2.24.2. The absorbing part of the receiver is designed as the ceramic half bowl with internal channels. The concentrated solar radiation illuminates and is absorbed on the inner surface of the bowl. Through the rotationally symmetric design, the flux distribution and the heat transfer to the working gas of the Stirling engine are optimized. The heater heads, which are also made of ceramic, connect the receiver to the engine and allow for the higher temperatures and the higher cycle efficiencies than current metallic heads. The biogas combustion system consists of a combustor, located on the centre axis and surrounded by a cylindrical air pre-heater and a ceramic shell for ducting the combustion gases. Combustion occurs between the receiver and the shell while combustion gases flow through the pre-heater heating incoming combustion air. To meet the requirements of hybrid operation, the power output of the combustor has to be quickly adjustable. This is accomplished by controlling the combustion air flow. To limit emissions from the combustion system, the maximum temperature of combustion is limited to 1400C

Volumetric Receiver

The pressurized volumetric receiver is shown schematically in Fig 2.24.3. The concentrated solar radiation enters the receiver through a domed quartz window, which closes the opening of the pressure vessel. Inside the vessel, the volumetric absorber, made with highly porous ceramic foams or similar materials, is heated by the incident radiation. The air passes through the porous absorber where it is heated by forced convection before going to the gas turbine. The hot air from the receiver is ducted to the gas turbine combustor where, if necessary, it is further heated by combustion of fossil fuel. These receiver is operated under the conditions similar to those required for a recuperated gas turbine cycle

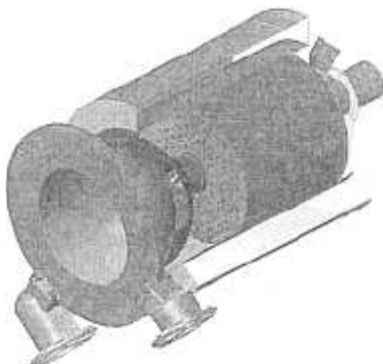


Fig 2.24.2 – Bio-Dish hybrid receiver

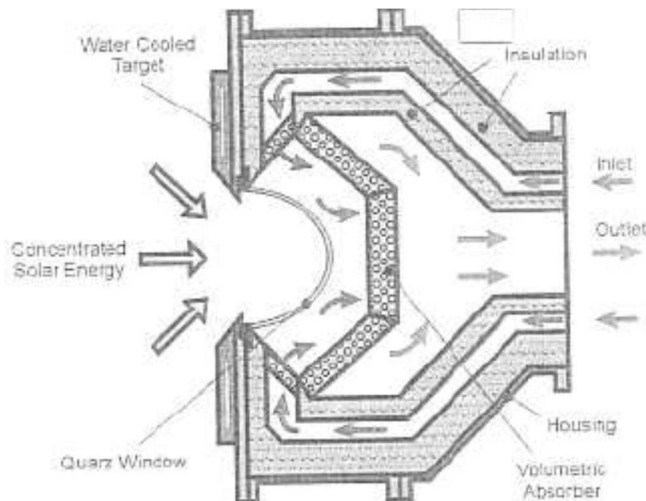


Fig. 2.24.3 DLR pressurized volumetric air receiver

(25) Bertocchi R., Karni J., Kribus A.

Experimental evaluation of a non-isothermal high temperature solar particle receiver

Energy 29, 2004

A solar particle receiver is presented. Concentrated irradiation was converted into thermal energy in a gas flow by a cloud of radiation absorbing sub-micrometer carbon particles. The carbon particles, when exposed to concentrated solar irradiation, heat up rapidly and transfer their gained heat to the surrounding gas. Additionally, the particle cloud shields the receiver cavity's wall from the concentrated irradiation, alleviating some of the structural and material limitations normally associated with conventional volumetric receivers.

For the discussed experimental evaluations, cloud particle mass fractions were in the range of 0.2–0.5%. The developed solar particle receiver accumulated over 12 net hours at operating temperatures exceeding 1700 K without any major failures. Particle mass loadings in the cloud were around 5 g/m³ gas. Exit gas temperatures exceeding 2100 K were measured for nitrogen. The most intriguing results were the heating of air to 1980 K at an influx of 755 W/m², showing that the particle/gas heat transfer matches the kinetics of carbon particle oxidation. CO₂ was heated to 1900 K. The average steady wall temperature was typically 100 K lower than that of the exit gas, in the plane of the exit gas sensor location, which alleviates some of the material limitations associated with the receiver design. The results also showed that the wall temperatures for the heating of air were very similar to the case of nitrogen, indicating that the heat transfer was completed in the front part of the receiver, before oxidation of the particles, maintaining intact the shielding effect of the particle cloud on the receiver walls.

Conversion efficiency exceeds 80% at mass flow rates > 4.59 kg/hr with CO₂. Tests for determining the conversion efficiency at high mass flow rates with an inert gas will be performed in the next test phase. The re-radiation losses through the entrance aperture ranged from 40% of the total influx at the lowest mass flow rates to 11% at the highest mass flow rates. The compact design of the receiver kept the surface losses from the receiver's external housing to 3–4%, almost independent of mass flow. Future work will focus on achieving higher exit gas temperatures, increasing the allowable mass flow rate, evaluate different particle cloud injection configurations and add a capability for chemical analysis of the exit

gases' composition.

The developed solar particle receiver is intended for applications using a process gas at temperatures of 1500–2000 K, where the use of electricity or combustion of fossil fuels to heat the gas is either inefficient or prohibitive by emission regulations.

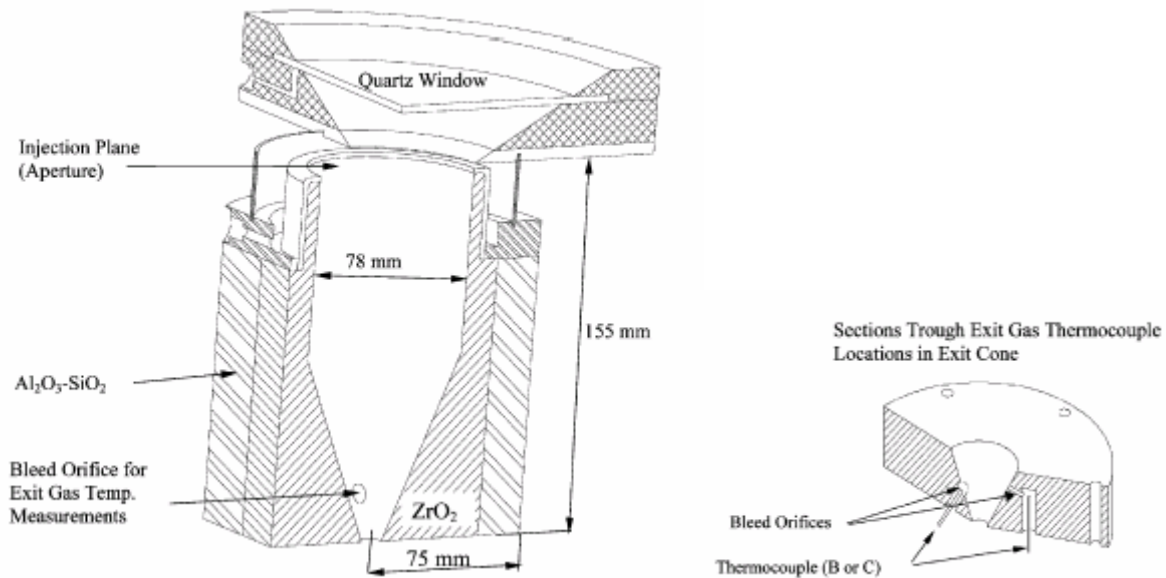


Fig. 2.25 - Geometric layout of solar particle receiver. Quartz window is seated between two water-cooled flanges. Cavity wall thermocouples are not shown. Enlarged view shows how hot gas was bled to the recessed thermocouples located adjacent to the gas exit port, via two different flow geometries.

(26) Rachamim Rubin, Jacob Karni

Chemical Kinetics Simulation of High Temperature Hydrocarbons Reforming in a Solar Reactor

Journal of Solar Energy Engineering Volume 126, August 2004

This study is aimed at developing a simulation model of a solar volumetric reactor for hydrocarbon reforming, operating at high temperature and pressure. It will then be used to optimize the reactor design and analyze its performance. The model development utilizes previous and on-going experimental work on volumetric receiver and catalyst development. The reaction's kinetics are computed, using the CHEMKIN II simulation package. The chemical kinetic modeling of the relevant C-H-O system is based on: (i) Definition of the relevant computation domain and parameters: temperature, pressure, reactant compositions, residence time, and catalyst load, (ii) Utilizing laboratory measurements at 700–1400 K and 1–4 bar. to quantify the kinetic parameters for both, H_2O , and CO_2 reforming of CH_4 and for the Reverse Water Shift reaction. Calculated and measured data are compared for three representative cases, showing a good agreement. The results indicate that the Arrhenius method can be a viable and practical way to predict the behaviour of steam and CO_2 reforming over a range of temperatures and pressures. Furthermore, it is shown that the present approach can provide a method for estimating the desirable dimensions of the reactor for reforming of

CH₄. Additional, on-going computational and experimental work, which would provide a more accurate simulation, can easily be implemented using the present numerical model. The results indicate that the Arrhenius method can be viable and practical way to predict the behaviour of steam and CO₂ reforming over a range of temperatures and pressures. Using CHEMKIN with the obtained parameters, and with a representative module of the computational control volume in the receiver, provide a method for estimating the desirable dimensions of DIAPR reactor for reforming CH₄. The RWS reaction reaches equilibrium much faster than either CO or steam reforming reactions. Calculations indicate that the DIAPR type receiver can be used as the basic design for a solar reformer. Also, increasing the operating pressure would lead to a smaller reactor size. Modeling side reactions such as those causing carbon formation, and substantiating their kinetic parameters by laboratory measurements would help greatly in the reactor design.

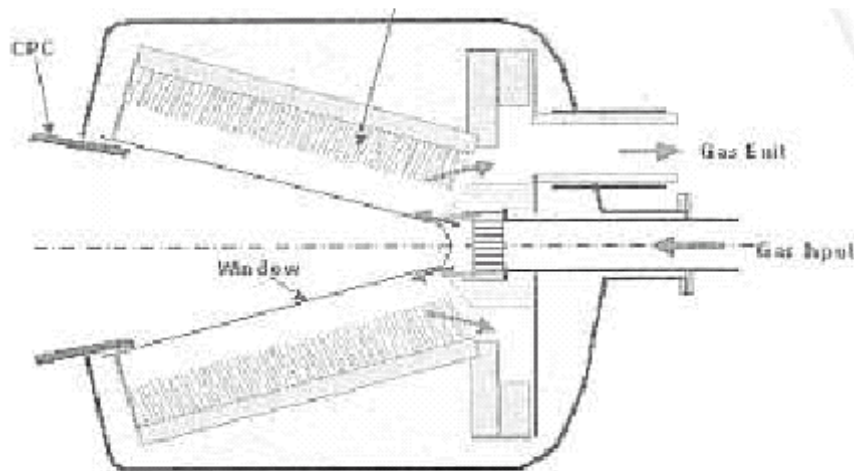


Fig. 13 Schematic view of a DIAPR-type reformer

Fig. 2.26.1

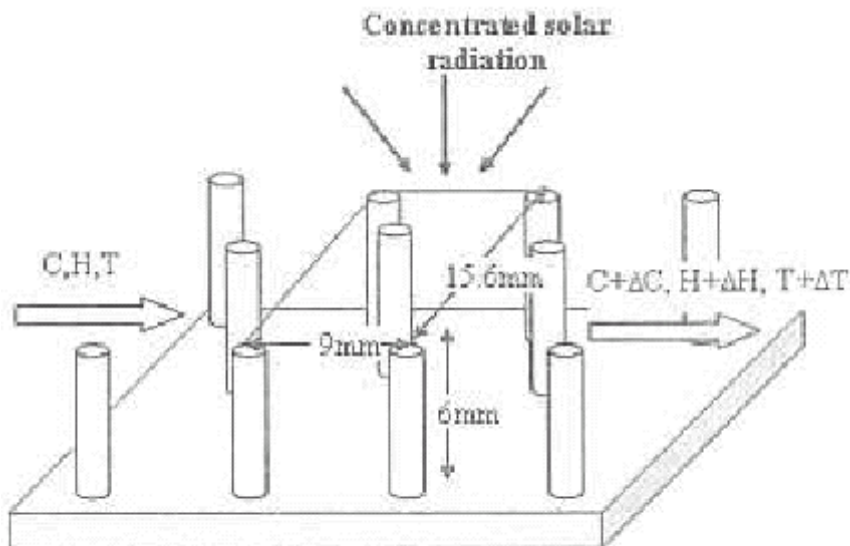


Fig. 14 Representative module (unit cell) of the computational control volume in the Porcupine absorber; C is the concentration, H is the enthalpy and T is the temperature

Fig. 2.26.2

(27)Jaimee K. Dahl, Alan W. Weimer, Andreas Z'Graggen and Aldo Steinfeld
Two-Dimensional Axi-Symmetric Model of a Solar-Thermal Fluid-Wall Aerosol Flow Reactor

Journal of Solar Energy Engineering February 2005 Volume 127 Issue 1 pp 76-85

A solar-thermal fluid-wall reactor consisting of three concentric vertical tubes : (an outer quartz tube(ID 0.048m OD 0.053m) , a central solid graphite tube (ID 0.021m OD 0.026m), and an innermost porous graphite tube (ID 0.012m OD 0.018m)) is constructed to dissociate methane to hydrogen and carbon black using concentrated solar power. Argon is fed into the annular space between the quartz tube and the solid graphite tube to sweep oxygen away from the hot graphite tube. A separate stream of argon is fed into the annular space between the two graphite tubes and it is forced to the porous tube wall to act as an aerodynamic blanket for protecting the inner wall of the porous tube from the carbon particle deposition. Methane is fed into the top of the porous tube and dissociates to form carbon black and hydrogen. The reaction products and the fluid-wall argon exit the bottom of the porous tube as shown in following figure:

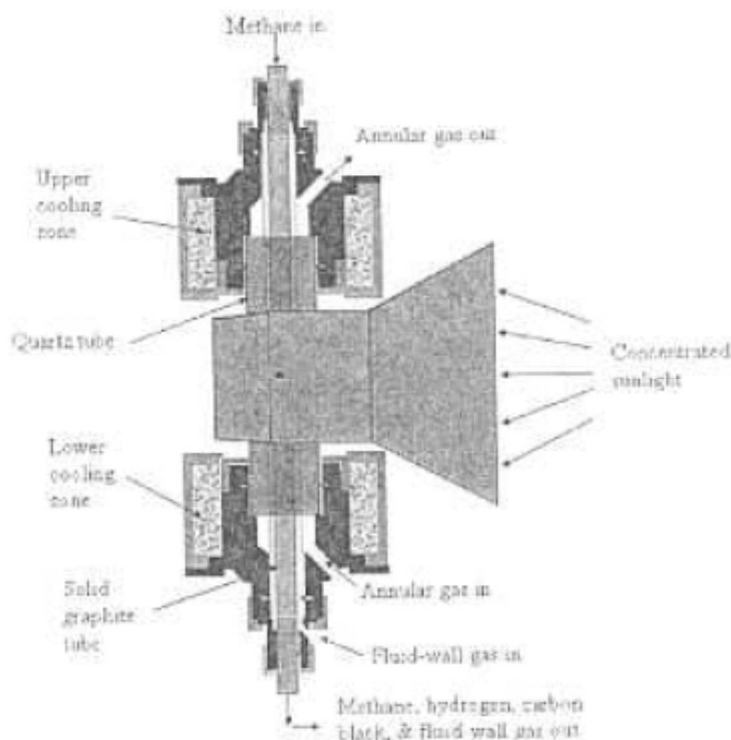


Fig. 2.27 Schematic of solar thermal fluid wall aerosol flow reactor

The reactor is placed at the focal point of the primary concentrator that can deliver upto 10 KW of solar power. A secondary concentrator enveloping the reactor augments the incident solar power flux from the primary concentrator and allows stagnation temperatures greater than 2000K to be achieved

The deposition of carbon black on the porous tube wall in the hot zone of the reactor is a technical problem when a full-scale reactor is operated continuously

Several aspects of the design are modelled for scaling the system up: the heat transfer and its effect on the integrity of the materials, and the fluid flow of all gas streams within the reactor.

The solar reactor is modelled by decoupling two domains .For the “outer domain” both argon and hydrogen are fed into the annulus region between the solid graphite tube and the quartz tube at initial velocities of 0.01 and 0.45 m/s. For argon flow , the quartz tube reaches 1500K

at the center of the hot zone where the graphite tube is at 2200K. The dominant heating source for the quartz tube is IR radiation emitted by the graphite tube. For the hydrogen flow at an initial velocity of 0.01m/s, the quartz tube reaches approximately 1650K in the center of the hot zone, approaching the temperature at which the quartz softens. Thus if hydrogen is to be fed into the annulus, the flow rate should be maintained above $3.73 \times 10^{-6} \text{ m}^3/\text{s}$.

It is determined that the inlet gas temperatures, mass flow rates, and permeability of the porous wall affect the gas flow profile through the porous tube wall. By increasing the inlet gas temperature and/or the tube permeability in the hot zone section of the reactor, a more uniform flow profile can be obtained along the length of the tube.

(28)Anton Meier, Enrico Bonaldi, Gian Mario Cella and Wojciech Lipinski
Multitube Rotary Kiln for the Industrial Solar Production of Lime

Journal of Solar Energy Engineering August 2005 Volume 127 Issue 3 pp 386-395

Lime and cement manufacturing are energy intensive processes that proceed at temperatures above 1200-1600K. The principal component of lime, or quicklime, is calcium oxide (CaO). It is produced by the thermal decomposition of limestone, a naturally occurring mineral that consists mainly of calcium carbonate (CaCO₃).

About 1.8 t of limestone are required to produce 1 t of quicklime

A scaleable solar multitube rotary kiln to effect the endothermic calcination reaction $\text{CaCO}_3 \rightarrow \text{CaO} + \text{CO}_2$ at above 1300 K is designed and tested.

The novel indirect heating rotary kiln consists of a tilted cylindrical steel drum lined with ceramic insulation and comprising a multitube reaction chamber made from high-temperature resistant SiC. The rotary kiln works with any conventional external heat source in place of concentrated solar radiation, allowing for continuous operation in case of missing or insufficient solar irradiation.

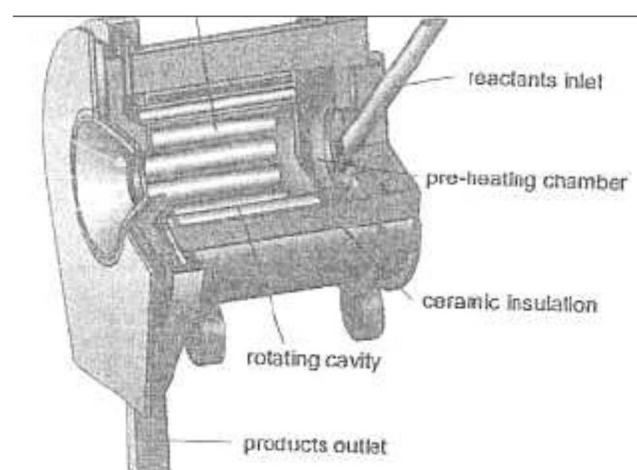


Fig. 2.28 Schematic representation of the indirect heating the multitube rotary kiln

The indirect heating 10-kW reactor prototype processes 1–5 mm limestone particles, producing high purity lime of any desired reactivity and with a degree of calcination exceeding 98%. The reactor's efficiency, defined as the enthalpy of the calcination reaction at ambient temperature (3184 kJ kg^{-1}) divided by the solar energy input, reached 30%–35% for solar flux inputs of about 2000 kW m^{-2} and for quicklime production rates up to 4 kg h^{-1} .

The kiln prototype operated reliably for more than 100h, withstanding thermal shocks that occur in solar high temperature applications. The next step will be the scale-up of the solar

lime reactor and the demonstration of the solar production of lime at a power level of 0.5-1 MW . An economic assessment indicates that the cost of solar lime produced in an industrial solar calcinations plant of 20-25 MW solar input is about 2-3 times the current selling price of conventional lime.

The use of concentrated solar energy in place of fossil fuels as the source of process heat has the potential of reducing by 20% CO₂ emissions in a state-of-the-art lime plant and by 40% in a conventional cement plant.

(29)Irina Vishnevetsky, Michael Epstein, Rahamim Rubin

Simulation of Thermal and Chemical Processes in Annular Layer of ZnO–C Mixtures

Journal of Solar Energy Engineering Volume 127, August 2005

A special setup, electrically heated, enabling the simulation of the process conditions encountered in a solar chemical reactor, is described. The setup allows us to study the thermal and chemical processes in different solid (powder or granules) reactant layers from the beginning of the heating until the reaction is completed, in a heating condition typical for indirectly, externally heated solar reactors. The particular case of the ZnO carboreduction process is analyzed in this paper as an example. Tests were executed using different powder mixtures of ZnO–C to demonstrate the layer-wise nature of the process

The productivity of the annular reactor with fixed incident flux strongly depends on its outer to inner diameter ratio and must be preferably intensified with its height increasing. Annular layer thickness b can be increased together with its inner radius, resulting with increasing of the radiation losses. Reactivity investigations of different mixtures with various kinds of ZnO powders and carbon agents both with deficiency and surplus of carbon allowed making the following conclusions :

Reactivity of carbonaceous reducing agent increases with decreasing of their oxidation temperatures. Oxidation ability and reactivity is better for nongraphitizing carbons with a larger amount of impurities. The selection of a candidate for reduction agent can be made based on a simple test of oxidation on the air. Using a low active carbon agent in under-stoichiometric mixtures leads not only to the decreasing of the reaction rate but also to inferior reaction quality caused by a strong back reaction. The characteristics of the reaction rate of mixtures with different ZnO powders and the same carbon agent demonstrate their linear dependence on mixture bulk density within the measurement accuracy. <the screening effect of residual carbon in over stoichiometric mixtures apply heating resistance especially in the later stage of the reaction while significantly prolongs its full completing, but improves the reaction quality by depressing the back reaction. The Molar amount of surplus of carbon needed for the optimization depends on its reactivity. It decreases with the increases of the carbon reactivity.

The results show that the reactivity and the behaviour of mixtures strongly depend on their components structures, impurities, and stoichiometry. This method can be generally applied for studying endothermic chemical reactions involving other solid reactants.

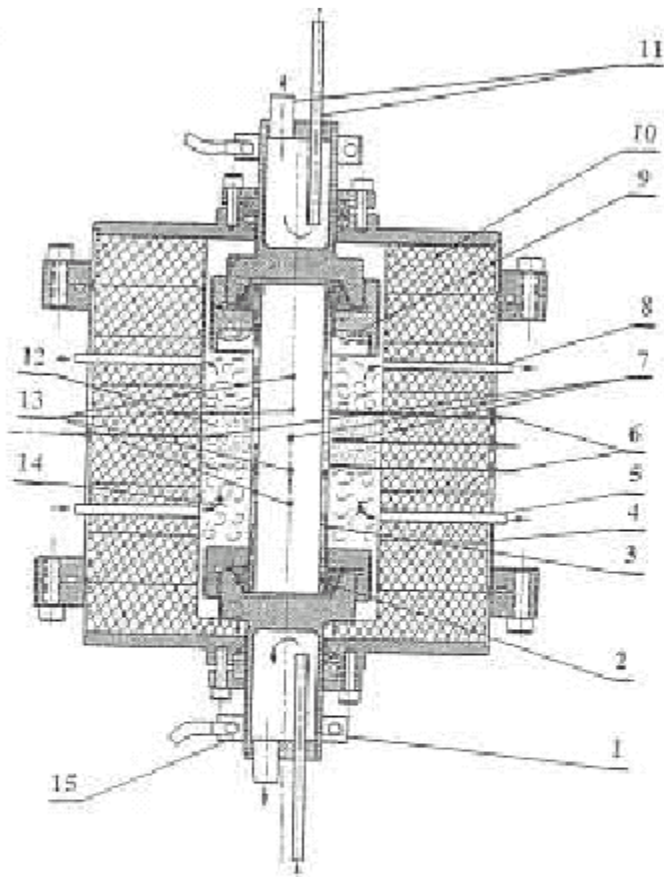


Fig. 1 Principle scheme of the electrical setup. (1) Water-cooled current feeder; (2) graphite packing; (3) SiC heater; (4) hermetic frame; (5) vacuum and inert gas inlet tubes; (6) electrical contacts; (7) radial thermocouples; (8) gas outlet tubes; (9) Zn condenser; (10) high-density alumino-silicate (Dura-board) rings; (11) water-cooling tubes; (12) reaction powder; (13) axial thermocouples; (14) insulated blanket; (15) current clips

Fig 2.29.1

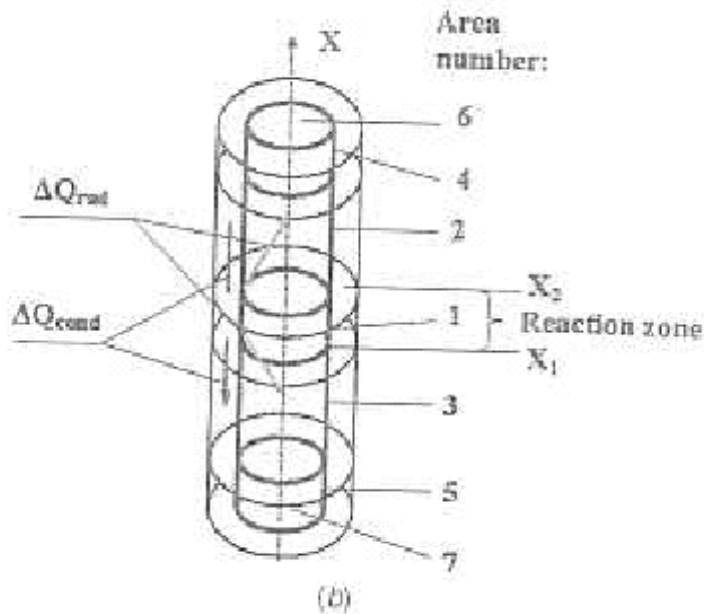


Fig. 2 Typical axial temperature distributions of the heater obtained at different times during the heating process (a) and principal scheme of the axial thermal losses; thin line—outer heater surface, thick line—inner heater surface (b) (for ΔQ_{rad} $t_6 = t_7 = 20^\circ\text{C}$, $t_4 = t_5 = 100\text{--}300^\circ\text{C}$, t_1, t_2, t_3 are averaged in the areas 1, 2, 3 using axial temperature curve fitting, $\epsilon = 0.9$).

Fig. 2.29.2

(30) Aceves S.M., Nakamura H., Reistad G.M., Martinez-Frias J., Tsuyoshi Hatamachi, Tatsuya Kodama, Yuki Isoke, Daisuke Nakano, Nobuyuki Gokon
Double-Walled Reactor Tube with Molten Salt Thermal Storage for Solar Tubular Reformers

Journal of Solar Energy Engineering Volume 128, May 2006

The development of the solar reformer aimed at increasing the capability to convert concentrated solar thermal energy. Three types of solar reformer, a tubular reformer with an integrated heat exchanger, a directly irradiated metal tubular reactor, and a volumetric receiver, reactor, have been developed and tested at a level of a few hundreds of kW of solar input. The directly irradiated tubular reactor was scaled up to a solar input level of 480 kW. It was installed on the tower for operation at the Weizmann institute of science. The reformer was shaped in a pentagon containing eight reaction tubes, this reformer attained chemical methane conversion of 71-94 % and chemical storage efficiency of 33-44%. A major limitation factor for scaling up these tubular reformer to a multi-megawatt level is placing a large and heavy reformer on top of the solar tower. A new reformer concept allows a multi-megawatt tubular reformer to be built on the ground, due to the newly developed solar reflective tower or beam-down optics.

This paper proposes a novel-type of "double-walled" reactor tube with molten-salt thermal storage at high temperatures for use in solar tubular reformers. The prototype reactor tube is

demonstrated on the heat-discharge and chemical reaction performances during cooling mode of the reactor tube at laboratory scale. The Na_2CO_3 composite material with MgO ceramics was filled into the outer annulus of the double-walled reactor tube while the Ru-based catalyst particles were filled into the inner tube. The heat discharge from the molten Na_2CO_3 circumvented the rapid temperature change of the catalyst bed, which resulted in the alleviation of decrease in chemical conversion during cooling mode of the reactor tube. The double walled reactor with the Na_2CO_3 composite material effectively prolonged the reforming period with a high chemical conversion level over 90% during cooling mode. The reforming period with the high level chemical conversion was prolonged by more than 10 minutes for the wide GHSV range. It is interesting that the prolonged period of time increased rather the space velocity of the reactant increased. This would be due to the fact that the reforming reaction kinetics in the inner tube was controlled by the diffusion limiting of the reactant gas at the GHSV range and the catalyst bed temperature range of 700-920° C. The porous sintered ceramic network, appeared to be developed to some extent in the Na_2CO_3 composite material.

The application of the new reactor tubes to solar tubular reformers is expected to help realize stable operation of the solar reforming process under fluctuating insolation during a cloud passage.

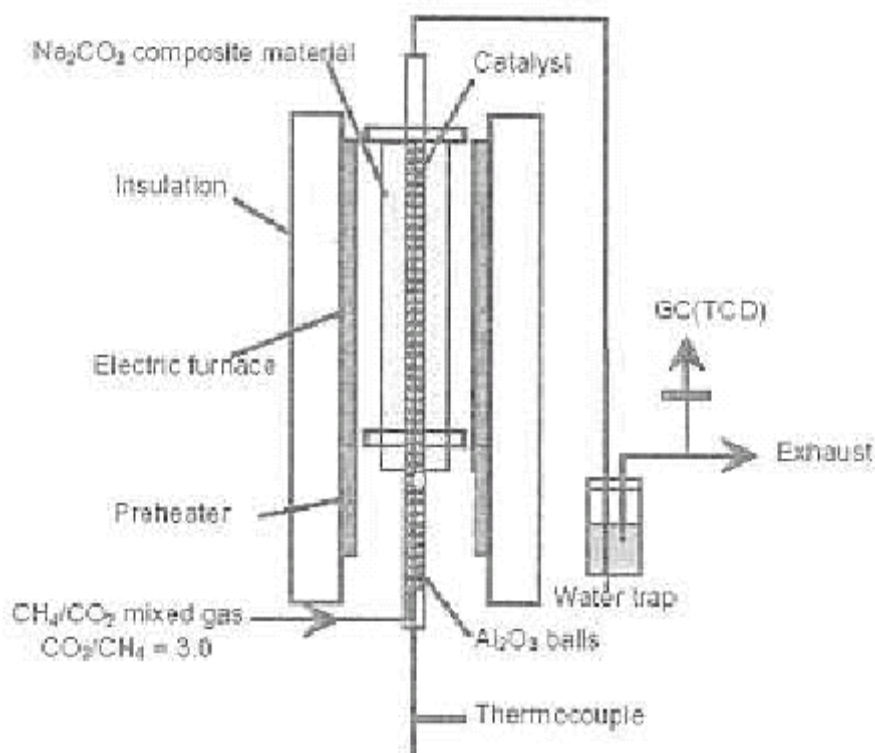


Fig. 1 Experimental setup for CO_2 reforming by the double-walled reactor tube with the Na_2CO_3 composite material

Fig. 2.30

(31) Martin Roeb, Christian Sattler, Ruth Klüser, Nathalie Monnerie, Lamark de Oliveira, Athanasios G. Konstandopoulos, Christos Agrafiotis, V. T. Zaspalis, L. Nalbandian, Andrew Steele and Per Stobbe
Solar Hydrogen Production by a Two-Step Cycle Based on Mixed Iron Oxides

A promising method for the conversion and storage of solar energy into hydrogen is the dissociation of water into oxygen and hydrogen, carried out via a two-step process using metal oxide redox systems such as mixed iron oxides,

These metal oxide redox systems are coated upon multi-channelled honeycomb ceramic supports capable of absorbing solar irradiation, in a configuration similar to that encountered in automobile exhaust catalytic converters. With this configuration, the whole process can be carried out in a single solar energy converter, the process temperature can be significantly lowered compared to other thermo-chemical cycles and the recombination of oxygen and hydrogen is prevented by fixing the oxygen in the metal oxide.

The receiver-reactor has been developed and installed in the solar furnace in Cologne, Germany.

A highly compact reactor structure is that of a honeycomb monolith consisting of a plurality of channels on the surface of which active compounds can be coated. SiC-based ceramics in particular have shown superior thermal properties and can be coated with a variety of traditional and novel techniques. Therefore SiC has been selected for the solar water spilling reactor.

The reactor (Fig. 2.31) contains a ceramic support structure that is able to host different coated structures in order to compare different redox pair systems. The ceramic honeycombs tested were made from two kinds of silicon carbide : recrystallized and siliconized (Re-SiC and Si-SiC, respectively). The housing is made of stainless steel and the reactor has a quartz window to allow a volumetric heating of a space closed to the environment.

The reactor is designed to withstand temperatures up to 1673 K. It is connected to an exhaust treatment system to analyze and thereafter dispose of the gases.

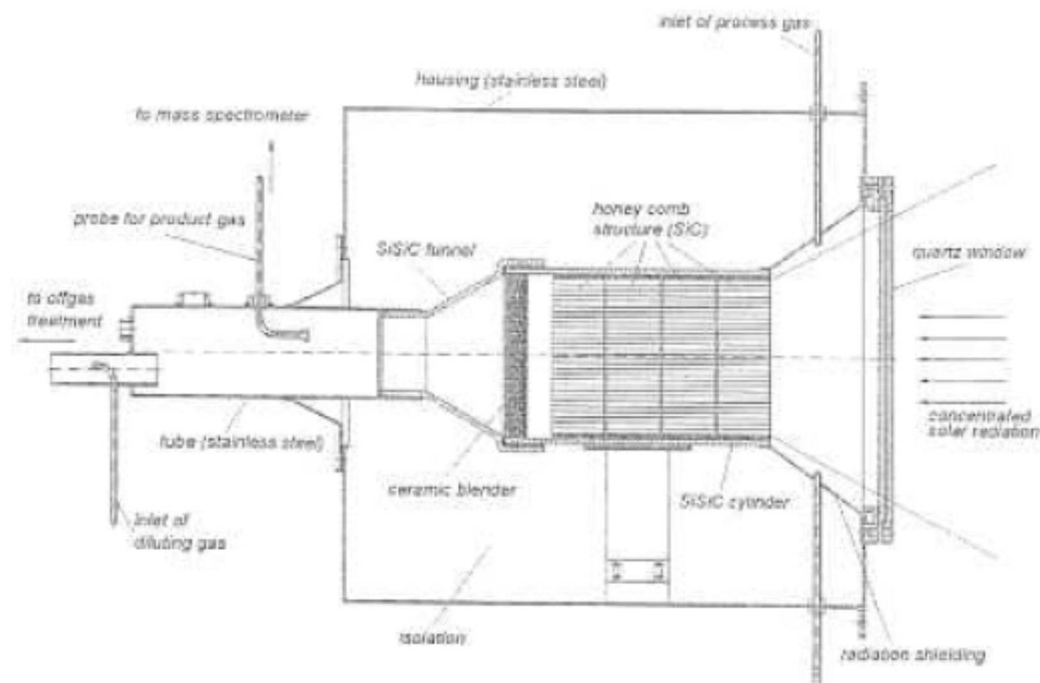


Fig. 2.31 Solar test reactor at DLR in Cologne ,Germany

. It was proven that solar hydrogen production and water splitting is feasible by this process demonstrating that multi-cycling (upto 10) of the process and achievement of a uniform

temperature profile of 1473 K was possible in principle. The analyses indicate that there is potential to reduce the production cost of hydrogen down to 10-12 eurocent/KWh and is expected to lower further.

(32)Lock, J.P. , Peterson, B.L. and Weimer, A.W., Pitts, R.J. , Bingham, C.E. and Lewandowski, A.A.

Aluminum nitridation in a solar-heated vibrating fluidized bed reactor

Journal of Solar Energy Engineering Volume 121

Aluminium nitridation is highly exothermic and has a significant activation energy and the process doesn't occur before the temperature of 850C.but the melting point of aluminium is 660C.secondly the heat generated by the reaction raises the temperature high enough (2200C) to cause dissociation of AlN to its precursors

By mixing a carrier in the precursor mixture, a less sintered powder is formed. A carrier prevents the coalescence of aluminium by providing a surface for the molten metal to cover. This causes a higher surface area of aluminium to be exposed to the nitrogen, which leads to a better conversion of aluminium to AlN. The carrier material also acts as a diluent and helps to control the exothermic nature of the reaction AlN itself is used as a carrier eliminating the need for a separation step to remove the carrier from the product material. The problem of thermophoresis is solved by directly heating the center upper surface of bed of fluidized particles avoiding the wall deposition by preventing the fine powders from reacting adjacent to a conventional hot wall.

A vibrating fluidized bed reactor was constructed and interfaced with the High-Flux Solar Furnace at the National Renewable Energy Laboratory in Golden, CO.

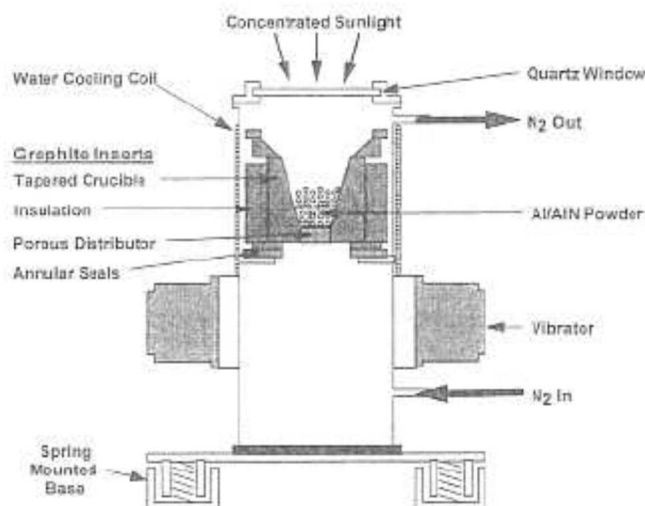


Fig. 2.32.1 Schematic of the fluidized bed reactor assembly



Fig. 2.32.2 Actual reactor assembly interfaced with the NREL solar furnace

Various precursor mixtures of aluminium and aluminium nitride were heated for approximately 10 to 15 minutes using focused sunlight with an intensity as high as 2,000 kW/m. Particles ranging in size from 2 micrometer to 10 micrometer were produced with the heating and fluidization process. High conversion was also achieved using multi-pass processing.

A schematic of the reactor assembly and a corresponding picture of the actual reactor as installed are shown in Figs. 2.32.1 and 2.32.2 respectively.

A high-temperature 14.6 cm I.D.(internal diameter) X 15.2 cm tall graphite crucible is enclosed with graphite fiber insulation. It is contained in a 25.4 cm nominal diameter X 61 cm tall RA310 stainless steel outer shell. The gas distributor is fabricated from porous graphite. This crucible has a tapered design to promote the fluidization of the reacting powders. It is held in place using a lower stainless steel support ring, three graphite annular rings, and an upper pressure plate that is pressed downward with screws through the stainless steel top plate. A 0.32 cm thick quartz window that has a diameter of 22.9 cm is mounted in the center of the top plate and allows the 4 cm diameter focused solar radiation beam to enter the reactor from above. The actual reaction zone in the crucible is placed 49.5 cm below the quartz window since this coincides with the actual focal point of the solar beam. A turning mirror is used to redirect the solar beam downward along a vertical axis. The reactor assembly is mounted to a 30.48 cm X 60.96 cm steel base plate fitted with four spring mounts at the corners.

3. State of The Art Solar Engines

3.1 Introduction

The solar dynamic power system collects the sun's rays onto a solar collector which in turn focuses the light into a chamber known as the receiver. This results in heating of the receiver which in turn heats a fluid, helium-xenon, that powers a turbo-alternator / compressor resulting in the production of electrical energy. The solar receiver is also designed to transfer energy to the fluid during the sun phase, and to store energy for operation during the shade phase. The fluid is then cooled by the radiator that rejects waste heat to space.

During the past 30 years SD component technologies have been developed which are now available for near-Earth orbit applications. However, several technical challenges were identified which can be resolved in ground-based tests. These key issues are:

Flux tailoring

Control methodology

Transient mode performance

Concentrator facet fabrication and manufacturing techniques,

Thermal energy storage (TES) canister fabrication and manufacturing techniques, and

Scalability to the 20 to 25 kW. range.

The main components of the test facility are:

1) Solar Simulator

2) Solar Dynamic System :

a) Concentrator Subsystem

b) Receiver Subsystem :

c) Power Conversion Unit (PCU) Subsystem

d) Waste Heat Subsystem

e) Power Control and Conditioning Unit (PCCU) Subsystem

Studies have shown that solar dynamic power with thermal energy storage can provide significant savings in life cycle costs and launch mass when compared with conventional photovoltaic power systems with battery storage for providing continuous electric power in near-Earth orbits. Applications include potential growth for ISS Alpha, communication and earth observing satellites, and electric propulsion. An aerospace government/industry team is working together to show that we can do it "cheaper, better, faster" to successfully demonstrate solar dynamic power for space.

3.2 List of Articles (Solar Engines)

Authors, Topic, Journal

Page No.

(1) Miles O. Dustin, Joseph M. Savino, Dovie E. Lacy, Robert P. Migra,69

Albert J. Juhasz and Carolyn E. Coles

Advanced Solar Dynamic Space Power System Perspectives

Requirements and Technology Needs

Solar Energy Conference March 22-27, 1987.

(2) Lee S. Mason, Carlos D. Rodriguez, Barbara I. McKissock,73

James C.Hanlon, and Brian C.Mansfield SP-100 Reactor with Brayton Conversion for Lunar Surface Application Ninth Symposium on Space Nuclear Power Systems Jan 12-16, 1992	
(3)Kim K. de Groh, David M. Roig, Christopher A. Burke,..... Dilipkumar R. Shah Performance and Durability of High Emittance Heat Receiver Surfaces for Solar Dynamic Power Systems 1994 ASME International Solar Energy Conference, March 1994	75
(4)Carol M.Tolbert..... Selection of Solar Simulator for Solar Dynamic Ground Testing 29th Intersociety Energy Conversion Engineering Conference Aug 7-12 1994	77
(5)Kent S. Jefferies..... Solar Simulator for Solar Dynamic Space Power System Testing ASME International Solar Energy Conference 1994	78
(6)Richard K.Shaltens..... Overview of the Solar Dynamic Ground Test Demonstration Program at the NASA-LEWIS Research Centre March 1995	80
(7)Thomas W. Kerslake and James Fincannon..... Analysis of Solar Receiver Flux Distributions for US/Russia Solar Dynamic System Demonstration on the MIR Space Station. 30th Intersociety Energy Conversion Engineering Conference July 31-Aug 1,1995.	83
(8)Donald A. Jaworske, Kent S. Jefferies, and Lee S. Mason..... Alignment and Initial Operation of an Advanced Solar Simulator Journal of Space Crafts and Rockets Nov-Dec'96	85
(9)Robert L. Dreshfield..... Long Time Creep Rupture of Haynes TM Alloy 188 Eighth International Symposium on Super-alloys, September 22-26,1996	88
(10)Dennis Alexander..... 2 kWe Solar Dynamic Ground Test Demonstration Project Volume I: Executive Summary NASA CR-198423, Vol. I, February 1997	89
(11)Dennis Alexander..... 2 kWe Solar Dynamic Ground Test Demonstration Project, Volume II: Design Report NASA 3-26605 February 1997	91
(12)Dennis Alexander..... 2 kW Solar Dynamic Ground Test Demonstration Project Volume III: Fabrication and Test Report	92

NASA Contractor Report 198423, Vol. III, February 1997

(13)Carsie A. Hall, III, Emmanuel K. Glakpe, Joseph N. Cannon,93
Thomas W. Kerslake
Modeling Cyclic Phase Change and Energy Storage in Solar Heat Receivers
NASA Technical Memorandum 107487, June 1997

(14)Thomas W. Kerslake, Lee S. Mason, Hal J. Strumpf.....95
High Flux High Temperature Thermal Vacuum Qualification
Testing of a Solar Receiver Aperture Shield
32nd Intersociety Energy Conversion Engineering Conference July 27-Aug 1, 1997

(15)Staff of Solar Dynamic Power System Branch, Lewis97
Research Centre, Cleveland, Ohio, NASA
Solar Dynamic Power System Development for Space Station FREEDOM

**(1)Miles O.Dustin, Joseph M.Savino, Dovie E.Lacy, Robert P.Migra, Albert J.Juhasz
and Carolyn E.Coles**

**Advanced Solar Dynamic Space Power System Perspectives Requirements and
Technology Needs**

Solar Energy Conference March 22-27, 1987.

In Advanced Solar Dynamic Space Power System (ASD), two module sizes were chosen as representative of the large variety of future missions,7 and 35 kW. Larger power requirements would use multiple modules

Two thermodynamic cycles are being considered at this time for the ASD systems, Brayton and Stirling cycle

Brayton Cycle

The working fluid, a mixture of helium and xenon heated to a high temperature, by focussing solar energy carries the energy to the turbine where the thermal energy is converted to shaft work by expansion through the turbine. The balance of the waste heat is given up in the heat exchanger and radiator. An alternator connected to the turbine shaft furnishes the electrical power. The gas is compressed and returned to the recuperator to recover some of the waste heat before returning to the receiver.

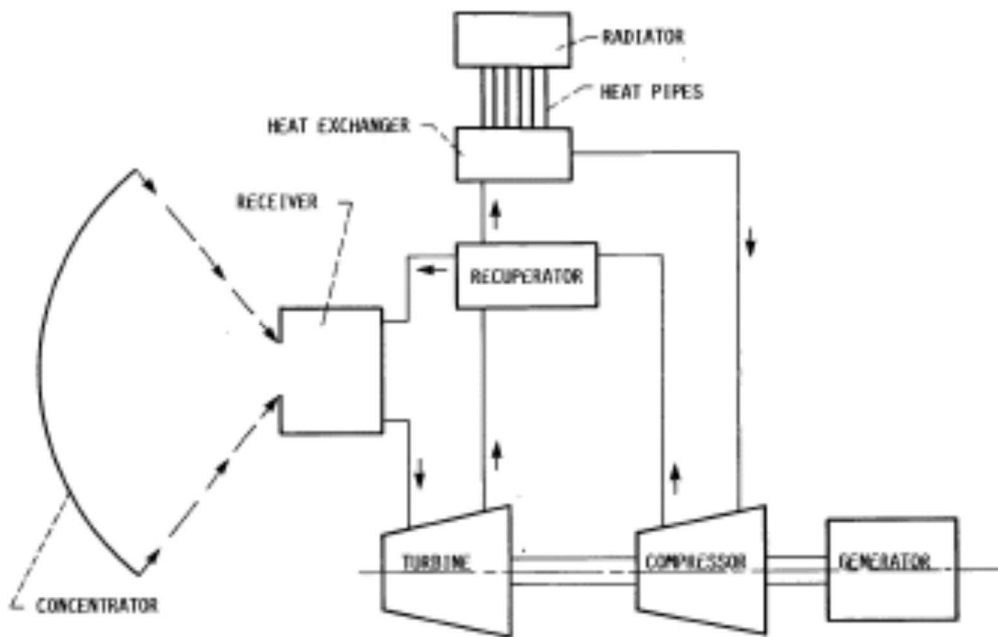


Fig. 3.1.1 BRAYTON CYCLE SPACE POWER SYSTEM

Stirling Cycle

This scheme shows heat pipes being used to deliver the thermal energy from the receiver to the Stirling engine heater. Liquid metal pumped loops can also be used to carry the waste heat to the radiator. As an oscillating free piston to convert the energy to useful work is used, a linear alternator is the most straight forward means for generating the electrical power. Thermal energy storage systems utilizing the latent heat of fusion of a phase change material are used to supply the heat for eclipsic operation of the power system for both systems.

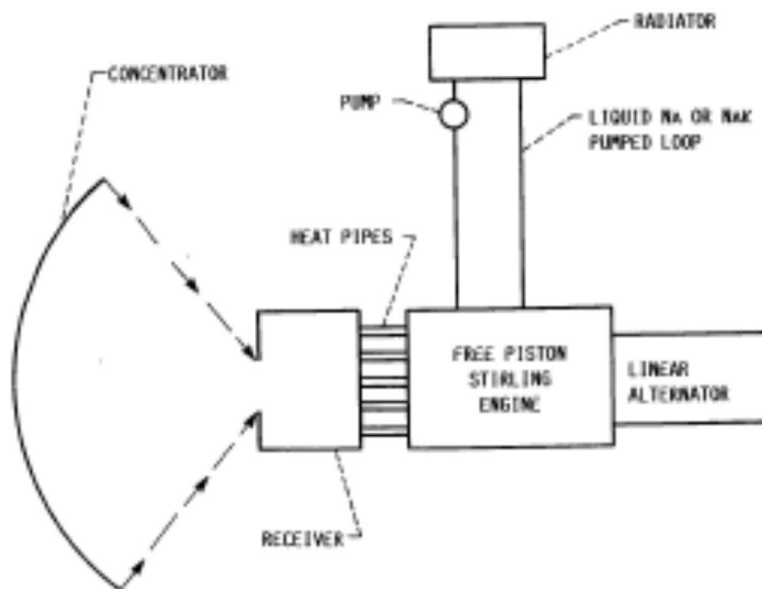


Fig. 3.1.2 STIRLING CYCLE SPACE POWER SYSTEM

It has been shown that high gains in ASD system performance will be derived from operating at a higher TES material melting point.

Receiver

Space power receivers differ from terrestrial receivers in several important areas. Terrestrial receivers do not utilize energy storage to enable the system to continue to produce power during periods of no sun energy. A space system on the other hand must store enough energy during the sun period to allow the production of power during the eclipse portion of the orbit. This amounts to about 36 min in a low-earth orbit (LEO). In a solar dynamic system, thermal storage in either a latent heat or possibly a sensible heat system will be used. AiResearch has presented, as a baseline receiver, the receiver shown in Fig..

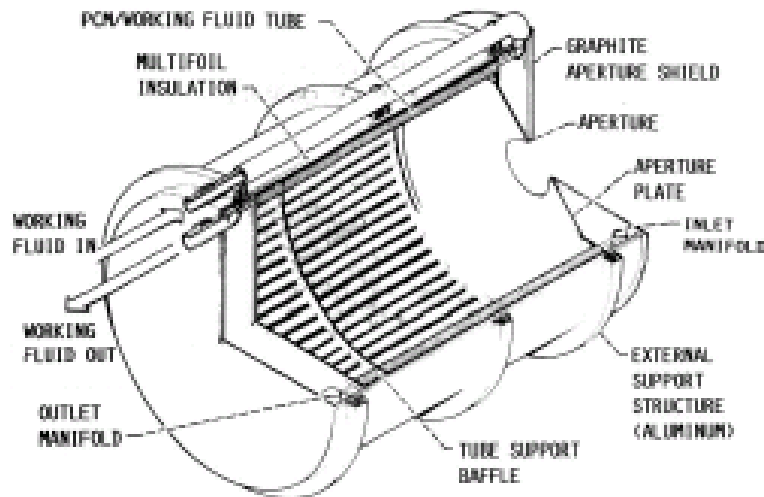


Fig. 3.1.3 - BASELINE RECEIVER

This receiver passes the working fluid through tubes in the walls of the receiver where it absorbs heat. The TES material surrounds the working fluid tubes. The TES system is fully charged during the sun period when the phase change material is fully melted. During the eclipse part of the cycle all of the energy has been extracted when the TES has completely solidified.

With most salts the volume of the salt increases when melting.. If this increase in volume is not properly designed for, so that melting first occurs adjacent to the void, serious damage to the containment vessel could result from overstressing experienced in each cycle (thermal ratcheting). In addition to being able to withstand the effects of the volume change of the TES material, the containment vessel must also be compatible with the TES material and it must be able to withstand high temperatures for extended periods of time. In the case of the ASD it must remain as a minimum, corrosion resistant for 7 to 10 yr which is one of the operational requirements for the program. It must also have a very low creep rate and must be able to withstand the space environment, i.e., atomic oxygen and ultraviolet radiation.

The thermal conductivity is crucial because phase change salt systems tend to have very low thermal conductivities requiring some form of enhancement. One method of enhancing the salts conductivity is to employ fins on the inner wall of the containment vessel to extend the heat transfer area and thus providing a conduction path for the heat out of the salt and into the cycle working fluid. Other methods include: (1) placing metallic wools or metallic felts inside the containment vessel with the TES material (2) employing what is known as a salt-metal or a slurry system where liquid metal is placed inside the containment vessel to co-exist with the salt, (3) encapsulating the phase change material in the void spaces of a porous ceramic matrix, (4) encapsulating the phase change material into small spheres for a pebble bed type concept or in a metallic capsule, and (5) using a pure metal instead of a salt as the phase

change material.

The other thermophysical properties which must be identified before the heat receivers TES subsystem can be completed are heats of fusion, melting point, density, specific heat, surface tension, vapour pressure.

Since the behaviour of the void, that results from the shrinkage of the TES when it freezes is fully dependent upon a continuous zero gravity field, tests on earth are not feasible. Therefore a flight experiment aboard the shuttle coupled with the development of analytical prediction techniques is being proposed. Extensive ground testing is also proposed.

NASA is also investigating the feasibility of using sensible heat as a means of thermal storage for the ASD program i.e. a solid sensible heat system, using beryllium, or a liquid sensible heat system, using liquid lithium in place of latent heat phase change designs.

(2) Lee S.Mason, Carlos D.Rodriguez, Barbara I. McKissock, James C.Hanlon, and Brian C.Mansfield

SP-100 Reactor with Brayton Conversion for Lunar Surface Application

Ninth Symposium on Space Nuclear Power Systems Jan 12-16, 1992

This study examines the potential for integrating Brayton-cycle power conversion with the SP-100 reactor for lunar surface power system applications. This study characterizes and models two different SP-100 Brayton systems.

The first system is sized for 100 kW and is designed to be self-deployable. It was assumed that this system would be one of the first elements delivered to the lunar surface and therefore could rely on no equipment or manpower for its installation. It was concluded that a design in which the power system is integrated with a lunar lander would best satisfy this requirement. This concept had been explored as an option for an easily deployable, self-contained power system for a periodically tended lunar observatory mission . An integrated lithium hydride/tungsten (LiH / W) enclosure shield is included for crew radiation protection. Although it was assumed that no infrastructure would be available for the deployment of the system, it was also assumed that crew members would be available to make the final electrical transmission line connections and to initiate system startup. A 10-year-equivalent, full-power system lifetime was assumed. Operation of the reactor at less than full thermal power could potentially extend the system's service life. The 100-kWe system is a safe, reliable design that requires minimal manpower for installation and uses relatively near-term technology. It is ideal for initial lunar base power requirements.

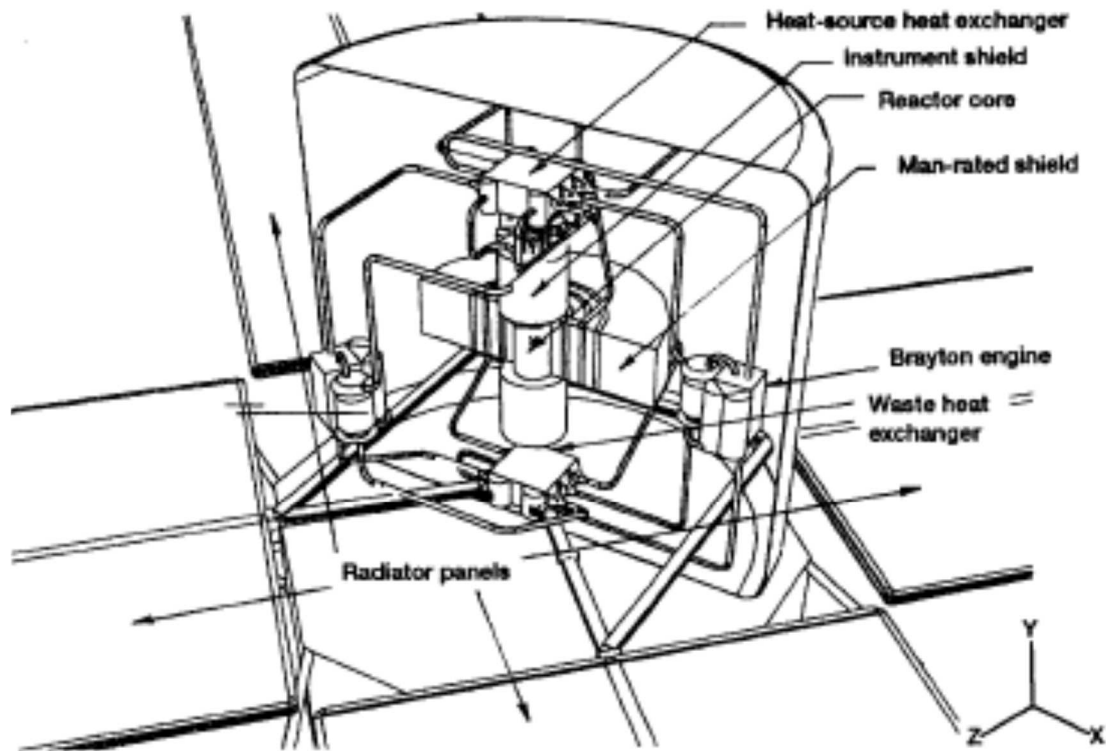


Fig. 3.2.1 - 100 kW SYSTEM DESIGN LAYOUT

The second system is sized for 550 kW. This system is assumed to be delivered to the Moon when power requirements have increased to account for a full operational liquid oxygen production facility. Because this system would be delivered once the base is established, it was assumed that a crew would be available for its installation. The basic concept consists of a single SP-100 reactor located in a cylindrical hole with surface-mounted Brayton engines and radiators. Man-rated radiation protection is provided through the emplacement of the reactor in the excavation. Despite the crew availability this power plant is designed for quick and easy assembly. It would be delivered to the site with all interface piping pre-connected and would only require the placement of the reactor in the excavation, installation of the radiator panels, and final electrical transmission line connections. As in the 100kWe case a 10-year-equivalent, full-power system life was assumed. The 550-kWs system is applicable when power requirements have increased to accommodate extensive in-situ resource utilization. Its design is consistent with the needs of an evolved lunar base: performance, safety, long life, and operational flexibility.

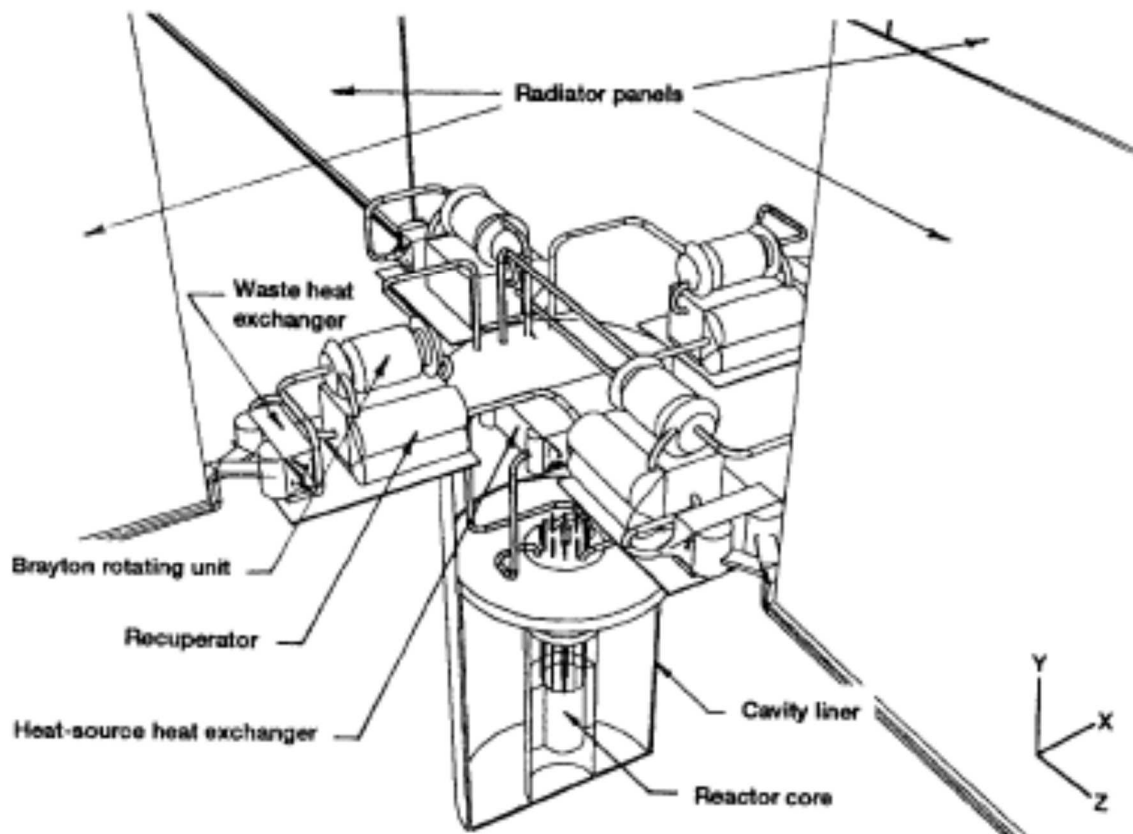


Fig. 3.2.2 - 550 kW SYSTEM DESIGN LAYOUT

(3)Kim K. de Groh, David M. Roig, Christopher A. Burke, Dilipkumar R. Shah
Performance and Durability of High Emittance Heat Receiver Surfaces for Solar
Dynamic Power Systems

1994 ASME International Solar Energy Conference, March 1994

Haynes 188, a cobalt-based superalloy, will be used to make thermal energy storage (TES) containment canisters for a 2 kW solar dynamic ground test demonstrator (SD GTD). Haynes 188 containment canisters with a high thermal emittance is desired for radiating heat away from local hot spots, improving the heating distribution, which will in turn improve canister service life. In addition to needing a high emittance, the surface needs to be durable in an elevated temperature, high vacuum environment for an extended time period. Thirty-five Haynes 188 samples were exposed to 14 different types of surface modification techniques for emittance and vacuum heat treatment (VHT) durability enhancement evaluation. Optical properties were obtained for the modified surfaces. Emittance enhanced samples were exposed to VHT for up to 2692 hours at 827°C with integral thermal cycling. Optical properties were taken intermittently during exposure, and after final VHT exposure. The various surface modification treatments increased the emittance of pristine Haynes 188 from 0.11 up to 0.86. Seven different surface modification techniques were found to provide surfaces which met the SD GTD receiver VHT durability requirement ($\epsilon \geq 0.70$ after 1000 hrs). Of the 7 surface treatments, 2 were found to display excellent VHT durability: an alumina based (AB) coating ($\epsilon = 0.85$ after 2695 VHT hrs) and a zirconia based coating ($\epsilon = 0.86$ after 2024.3 VHT hrs). The alumina based coating was chosen for the ϵ enhancement surface modification technique for the SD GTD receiver. Details of the performance and

vacuum heat treatment durability of this coating and other Haynes 188 emittance surface modification techniques are discussed.

Technology from this program will lead to successful demonstration of solar dynamic power for space applications, and has potential for application in other systems requiring high emittance surfaces. Surface modification was found to increase the emittance of Haynes 188 from 0.11 to between 0.28 and 0.86. Four techniques were found to increase the desired value of 0.80, or above. These techniques were: the application of an alumina based coating, carbon arc texturing, SiC arc texturing, and SiC grit blasting followed by air oxidation at 871°C. The resulting ϵ values obtained by these techniques are shown in Table 1.

Of the 35 emittance enhanced Haynes 188 samples, 12 samples corresponding to 7 surface treatments were found to meet the solar dynamic ground test demonstrator VHT durability requirement. None of the 12 samples tested were found to display any evidence of embrittlement or threat of spaling of the high emittance surface after VHT exposure with integral thermal cycling. Of the 7 surface treatments, 2 were found to display excellent VHT durability, (0.025 mm - 0.051 mm alumina based coatings and 0.254 mm zirconia based coatings).

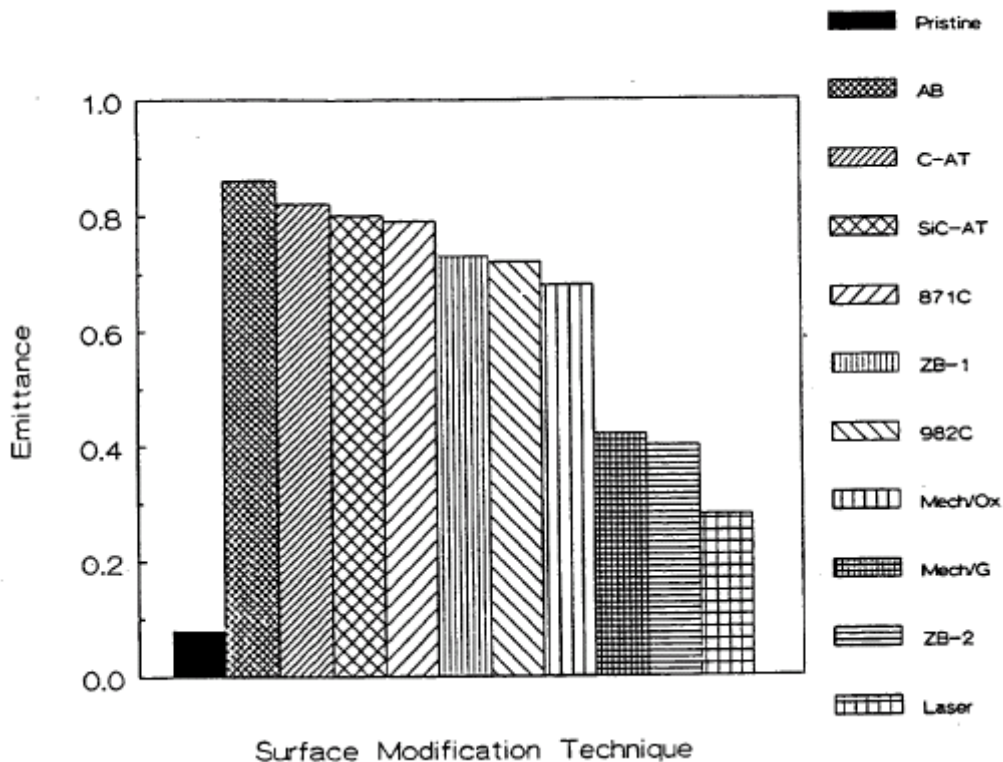


Figure 3.3. EFFECT OF SURFACE MODIFICATION ON THE EMITTANCE OF HAYNES 188.

Table 1. Summary of the Effect of Surface Modification on the Optical Properties of Haynes 188

Legend	Surface Treatment	$\epsilon_{827^\circ\text{C}}$	$\epsilon_{827^\circ\text{C}^*}$	α_s
Pristine	Pristine	0.14	0.08	0.370
AB	Alumina based coating (0.025 mm & 0.051 mm thick), ave. of 2	-	0.86	0.934
C-AT	Carbon arc textured	0.77	0.86	0.906
SiC-AT	SiC arc textured	-	0.80	0.914
871C	SiC grit blast & air oxidized (871°C: 3, 6 & 24 hrs), ave. of 3	0.79	0.80	0.905
ZB-1	Zirconia based coating, composition #1 (0.025 - 0.254 mm thick), ave. of 6	-	0.73	0.858
982C	SiC grit blast & air oxidized (982°C: 2, 4 & 16 hrs), ave. of 3	0.72	0.72	0.892
Mech/Ox	Mechanically indented & air oxidized (871°C, 24 hrs)	0.68	0.67	0.890
Mech/G	Mechanically indented w/ graphite application	0.42	-	0.516
ZB-2	Zirconia based coating, composition #2 (0.254 mm thick), ave. of 2	-	0.40	0.613
Laser	Laser Treated	0.28	-	0.774

Table 3.3 Summary of the effect of Surface Modification on Optical properties of Haynes 188

(4)Carol M.Tolbert

Selection of Solar Simulator for Solar Dynamic Ground Testing

29th Intersociety Energy Conversion Engineering Conference Aug 7-12 1994

In a solar dynamic power system, a solar concentrator collects and focuses the sun's light into the aperture of a heat engine. If a system based on a closed Brayton cycle is taken into consideration, a gaseous working fluid is heated by solar energy in the heat receiver, and converted to electricity by a power conversion unit.'

The solar simulator must illuminate the concentrator so that it can focus the light to the receiver aperture To properly test the SD system, the simulator must be capable of providing at least as much power as will be provided by the sun in Earth orbit.'

This solar dynamic power system test will be conducted in a simulated space environment and will require an artificial sun. To satisfy system requirements for the SD GTD experiment, the solar simulator needs to provide a uniform light flux to the SD concentrator, provide the light within a substance angle of one degree, and provide an intensity of one solar constant (1.37 kW /m) at air mass zero. Xenon lamps were chosen for the experimental campaign. They have a 5900 K blackbody curve spectral distribution which approximates the blackbody curve of the sun. These lamps require air and water cooling system.

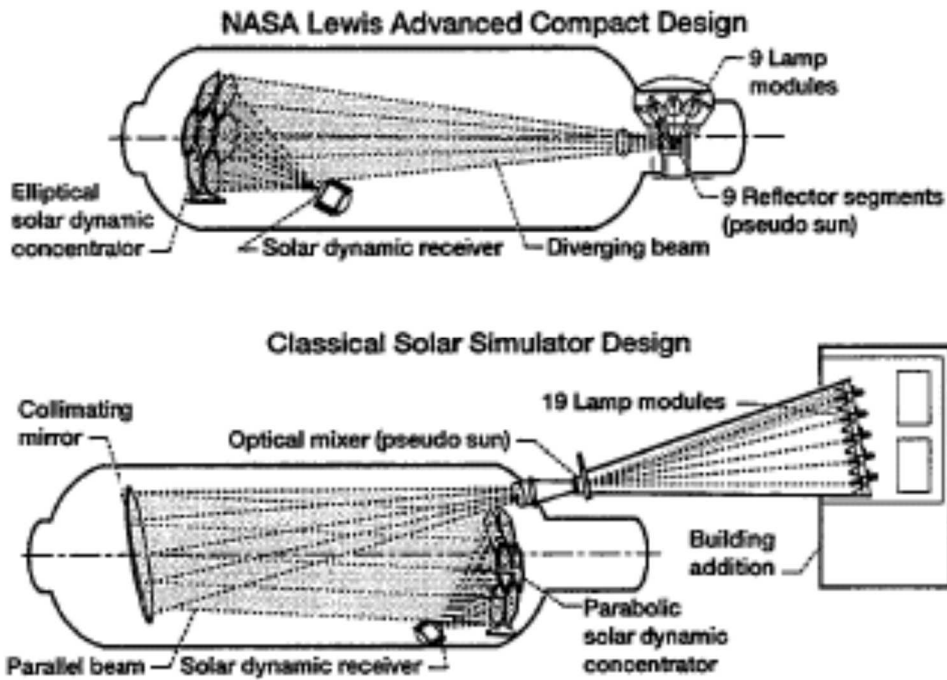


Fig. 3.4 - ADVANCED SOLAR SIMULATOR VERSES CLASSICAL SOLAR SIMULATOR

(5) Kent S. Jefferies

Solar Simulator for Solar Dynamic Space Power System Testing

ASME International Solar Energy Conference 1994

Planned vacuum tank testing of a solar dynamic space power system requires intense flux and that can be provided by a solar simulator because sunlight cannot be brought into the vacuum. The solar flux in space is more intense than sunlight that has been attenuated by the earth's atmosphere, to enable solar dynamic testing, the light source must subtend less than three times the 0.5 angle subtended by the Sun's diameter. The existing simulators didn't satisfy many requirements like subtense angle, i.e., the angular size of the apparent sun (as viewed from the experiment), of these solar simulators is too large to enable testing of solar dynamic systems. Therefore a new design was developed

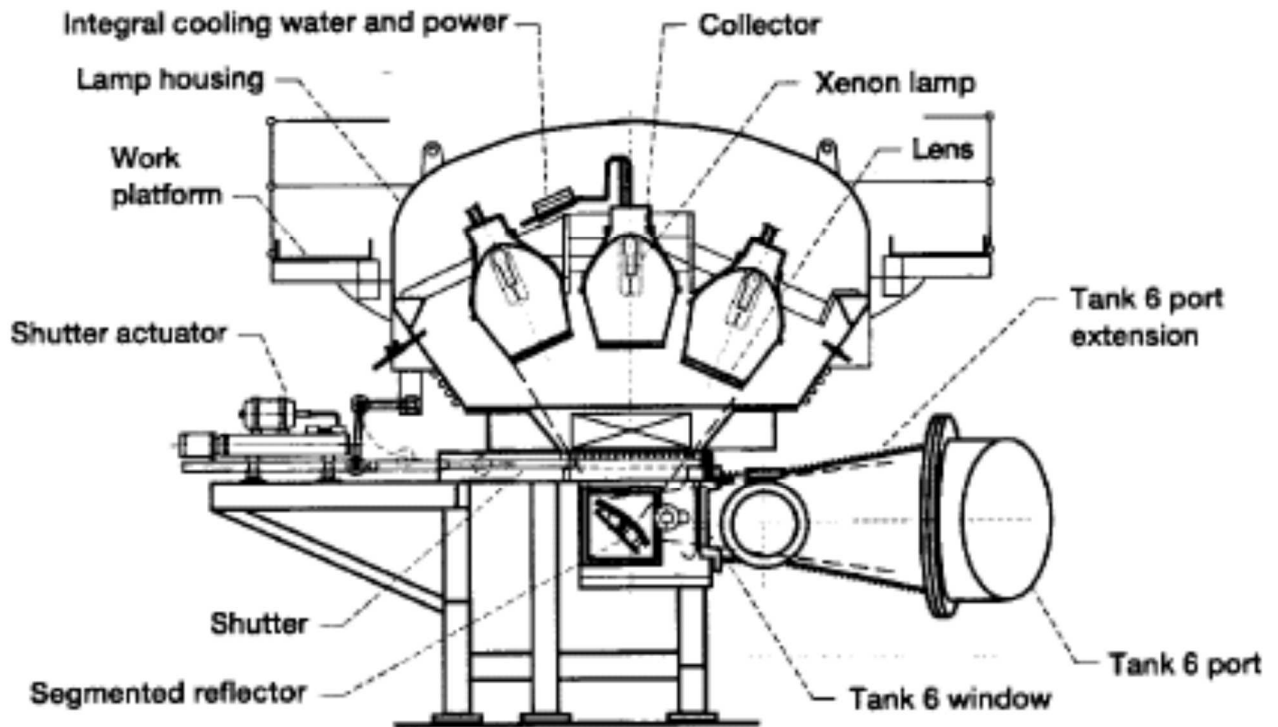


Fig. 3.5

Solar simulator characteristics	
Beam size	188.5-in. diam at 56-1/2 ft from apparent sun
Collimation	None - point source
Irradiance	1.8 kW/m ² (1.27 sun) max
Uniformity	±10%
Subtense angle	About 1 deg

Table 3.5 Solar Simulator Characteristics

Key features that enable this improved performance are: 1) elimination of the collimating mirror commonly used in solar simulators to transform the diverging beam into a parallel beam. It was accomplished by changing the solar dynamic concentrator optics to accept a diverging light beam, 2) a redesigned lamp module that has increased efficiency, and 3) the use of a segmented reflective surface to combine beams from several individual lamp modules at the pseudo-sun. The pseudo-sun is composed of nine reflective segments that are water cooled. This enables a reduction in length of the lamp house and provides much better cooling than classical simulators that have lenses at the pseudo-sun. Each segment has complex curvature to control the distribution of light. This advanced optical system is capable to analytically predict and control light intensity distribution. The optical efficiency improvement in a scaled unit can be analytically predicted in this design. In the new design the initial cost was cut by half, the efficiency was increased by 50% reducing the operating

cost by 1/3 and volume by a factor of 10. These benefits are the result of eliminating the large, expensive collimating mirror and eliminating its reflection losses, eliminating the expensive mixing lens array and its transmission and blockage losses, reducing the number of lamp modules, reducing the length of the lamp house, and increasing lamp module efficiency. This design has the potential to approach the goal of matching both the subtense angle and the intensity of the Sun.

(6)Richard K.Shaltens

Overview of the Solar Dynamic Ground Test Demonstration Program at the NASA-LEWIS Research Centre

March 1995

The NASA Office of Aeronautics and Space Technology initiated the 2 kW Solar Dynamic (SD) Space Power Ground Test Demonstration (GTD) Program which is managed by NASA Lewis Research Center (LeRC)[1,2,3]. The primary goal of this program is to conduct testing of flight prototypical components as part of a complete SD system in 1995. The SD space power system includes thermal energy storage in an environment simulating a representative low earth orbit (LEO).

In January 1994, the International Space Station Program Office initiated the joint U.S./Russian Solar Dynamic Flight Demonstration program which is also managed by the NASA Lewis Research Center. The primary goal of this program is to demonstrate the capabilities of the Solar Dynamic power system during orbital space flight on board the Russian Orbital Space Station (OSS) MIR. This flight demonstration is a stage in the development of the SD system for the International Space Station (ISS) Alpha [4]

A block diagram of a SD system is shown in Fig. The solar dynamic power system collects the sun's rays onto a solar collector which in turn focuses the light into a chamber known as the receiver. This results in heating of the receiver which in turn heats a fluid, helium-xenon, that powers a turboalternator / compressor resulting in the production of electrical energy. The solar receiver is also designed to transfer energy to the fluid during the sun phase, and to store energy for operation during the shade phase. The fluid is then cooled by the radiator that rejects waste heat to space.

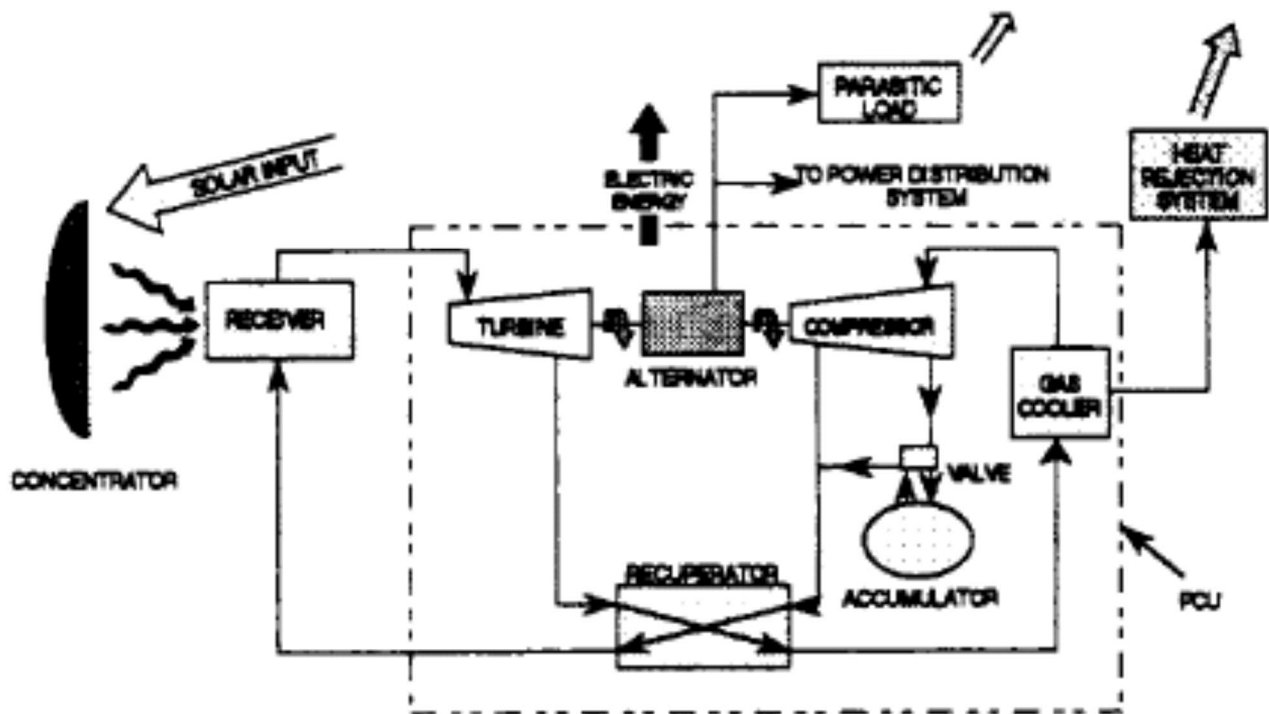


Fig. 3.6.1 - BLOCK DIAGRAM OF SD SYSTEM

NASA programs during the past 30 years have developed SD component technologies which are now available for near-Earth orbit applications. However, several technical challenges were identified during the Space Station Freedom (SSF) program which can be resolved in a ground-based tests). These key issues are:

- Flux tailoring - integration of the concentrator and receiver such that adequate solar flux is transferred into the cycle without excessive flux deposition in anyone area of the receiver,
- Control methodology - investigate methods of varying turboalternator compressor (TAC) speed and system management to maintain optimum system operation (energy management) as a result of long time period changes in insolation,
- Transient mode performance - evaluation of start-up and shutdown transients, and multiple orbit operations, including radiator thermal lag effects,
- Concentrator facet fabrication and manufacturing techniques,
- Thermal energy storage (TES) canister fabrication and manufacturing techniques, and
- Scalability to the 20 to 25 kW. range.

The SD GTD program will demonstrate a complete SO system in a thermal-vacuum environment, i.e. the large space environmental facility, known as Tank 6, at NASA LeRC. The Tank 6 facility includes a solar simulator, a liquid-nitrogen-cooled wall operating at 78 K to simulate the heat sink provided by the space environment, and an electric load simulator (ELS) capable of dissipating up to 4 kW of electrical power. Flight typical components are used in the SO system wherever possible to demonstrate the availability of SO technologies.

The main components of the test facility are:

- 1) Solar Simulator
- 2) Solar Dynamic System :
 - a) Concentrator Subsystem
 - b) Receiver Subsystem :

The solar receiver, shown in Fig., is used to both transfer the solar energy to the cycle working fluid and to store solar energy for system operation during eclipse. The receiver design is essentially a scale model from the SSF. The receiver uses the same thermal energy storage (TES) canister (full size) as was designed, built and tested during the SSF program. Manufacturing development and testing of the canisters has been completed by AlliedSignal ASE. The TES consists of the Haynes 188 canister, or hollow doughnut, filled with LiF-CaF₂ eutectic salt. The TES canisters will be placed in a scaled down receiver, which will have 23 tubes with 24 canisters per tube.



Fig. 3.6.2 - COMPLETE SOLAR HEAT RECEIVER

Surface modifications to improve thermal emittance characteristics of the Haynes 188 canisters is required to radiate heat away from local hot spots, improving heat distribution which result in improved service life. LeRC and AlliedSignal specialists evaluated 14 different types of surface modification techniques for emittance and vacuum heat treatment durability enhancements. An 0.025 mm thick alumina based coating was selected due to a very high emittance (0.85 after 2695 hrs with 32 thermal cycles) for the receiver canisters.

- c) Power Conversion Unit (PCU) Subsystem
- d) Waste Heat Subsystem
- e) Power Control and Conditioning Unit (PCCU) Subsystem

The 2 kW SD GTD program provides for the demonstration of a solar dynamic power system which is of sufficient scale and fidelity to ensure confidence in the availability of solar dynamic technology for Space. Studies have shown that solar dynamic power with thermal energy storage can provide significant savings in life cycle costs and launch mass when compared with conventional photovoltaic power systems with battery storage for providing continuous electric power in near-Earth orbits. Applications include potential growth for ISS Alpha, communication and earth observing satellites, and electric propulsion. An aerospace government/industry team is working together to show that we can do it "cheaper, better, faster" to successfully demonstrate solar dynamic power for space. The SD GTD program is ahead of schedule and within budget for completion in 1995.

(7)Thomas W. Kerlake and James Fincannon

Analysis of Solar Receiver Flux Distributions for US/Russia Solar Dynamic System Demonstration on the MIR Space Station.

30th Intersociety Energy Conversion Engineering Conference July 31-Aug 1, 1995.

The United States and Russia have agreed to jointly develop solar dynamic (SD) system for flight demonstration on the Russian MIR space station starting in late 1997.

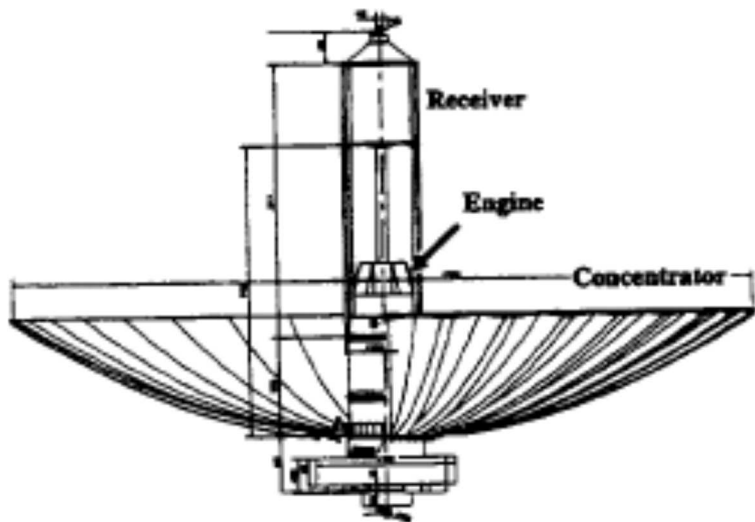


Fig. 3.7.1 - SOLAR DYNAMIC FLIGHT DEMONSTRATION HARDWARE

The heat receiver is supplied by the U.S and concentrator by Russia. A cylindrical, cavity-type heat receiver is located at the concentrator focal plane. The cavity is lined with heat exchanger tubes which store thermal energy and heat the working fluid

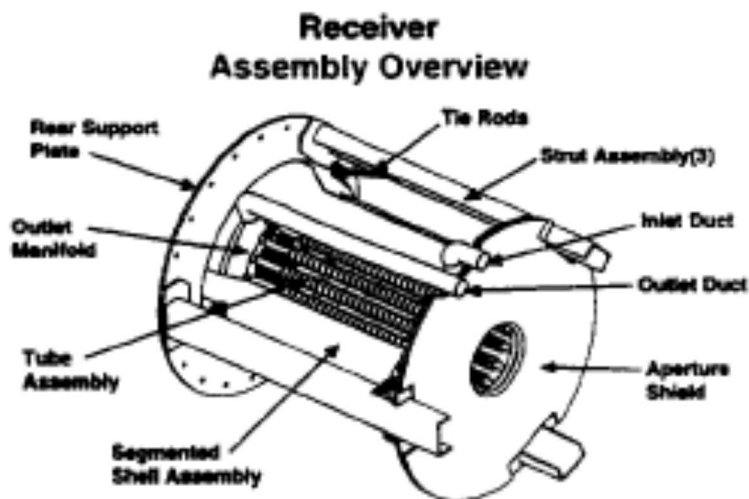


Fig. 3.7.2 - HEAT RECEIVER

A 0.24 m diameter circular aperture is centred at one end of the receiver cavity to admit concentrated solar energy. Energy not intercepted by the aperture is deposited on a segmented graphite aperture shield designed to protect the underlying metal structure from the excessive temperatures. Three steel c-channel support struts, 0.127 m wide by 0.063 deep, connect the receiver to the base of the concentrator.

Solar flux distributions must be calculated for the receiver cavity and the aperture shield to enable receiver thermal stress analyses. These analyses accounts for finite sun size with limb darkening, concentrator surface slopes and position concentrator thermal deformation, and the shading effects of the receiver support struts. The receiver spatial flux distributions are then combined with concentrator to the target receiver surfaces. These patterns vary with time depending on the chosen MIR flight attitude and orbital mechanics of the MIR spacecraft. The resulting predictions provide spatial and temporal receiver flux distributions for any specified mission profile.

The receiver cavity target was defined as a cylinder 0.483 m in diameter and 0.762 m in length. The surface was discretized into 0.0254 m segments along the length which correspond to the positions of individual phase change material thermal energy storage (TES) canisters located concentrically around each receiver tube. The cavity aperture plane is positioned coincident with the concentrator focal plane.

The receiver aperture plane target was defined by a 1 m diameter, flat circular disk located in the concentrator focal plane. The surface was discretized into 0.01 m radial increments. Solar energy incident on the target at a radius less than 0.12 m would be intercepted by the receiver aperture.

Optical analyses results were combined with concentrator shadowing predictions to define receiver flux distributions. These distributions are being used to design the receiver and Brayton cycle engine hardware. These distributions have also proved useful in SD system analyses to define acceptable system start-up and operating envelopes.

More refined optical analyses can be planned in future when as-built, concentrator petal thermal and optical properties are measured.

(8) Donald A. Jaworske, Kent S. Jefferies and Lee S. Mason
Alignment and Initial Operation of an Advanced Solar Simulator

Journal of Space Crafts and Rockets Nov-Dec'96

High power conversion efficiency, high energy storage efficiency, the elimination of batteries for storage, and other factors combine to make solar dynamic power an attractive alternative to existing space power systems. In ground test demonstration a solar simulator is needed to provide the radiant energy for operation in a thermal vacuum environment. Radiant energy from existing solar simulators is too diffuse to be concentrated into the solar dynamic heat receiver, thus to meet the specific needs of the solar dynamic system, a new solar simulator design is considered. A solar simulator utilizing nine 30-kw lamps can successfully power a fully integrated solar dynamic space power system in a thermal vacuum ground test facility for over 400 hrs. of operation.

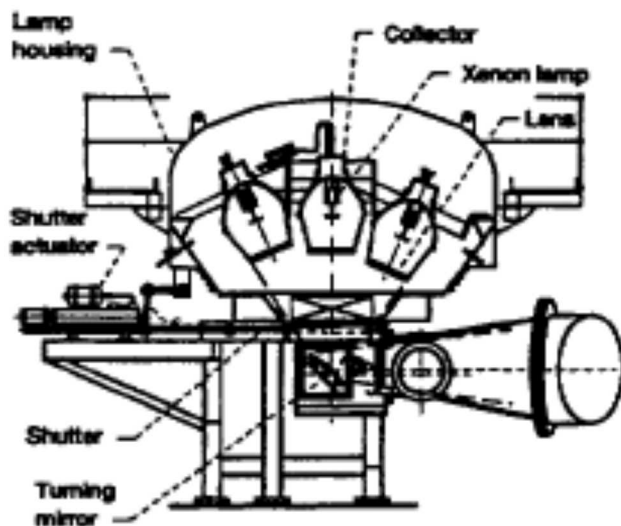


Fig. 3.8.1 - SCHEMATIC DIAGRAM OF SOLAR SIMULATOR

The nine lamp design utilizes a collector-lens combination that collects radiant energy from the fireball of each arc lamp. Nine turning mirrors are used to direct the energy into the vacuum tank and to superimpose them on the solar dynamic concentrator. One advantage to superimposing the nine beams is that in the event of a lamp failure during a ground test, the concentrator remains uniformly illuminated. There is enough margin in the solar simulator to

allow the remaining eight lamps to make up the shortfall.

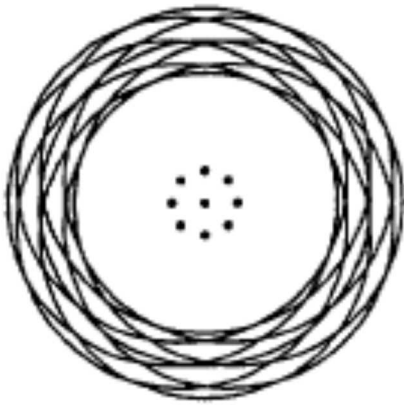


Fig. 3.8.2 - PATTERN OF THE NINE BEAMS OVERLAPPING AT THE CENTER

Another advantage of this design is that the angle of the beam converging from the individual lamp module towards its turning mirror equals the angle of the beam leaving the turning mirror and projecting into the tank. Because the angle of convergence is larger with this design than other solar simulator designs, the lamp modules are much closer, enabling a major reduction in the size of the solar simulator. The use of collector, lenses and turning mirrors enables this solar simulator to provide a combination of small subtense angle and high efficiency.

Alignment Procedure include one alignment and two focusing tasks 1)aligning each turning mirror to reflect light from the center of the concentrator,2)aiming each lamp module so that the secondary focus of the lamp module is at the center of its turning-mirror segment, and 3)positioning the fireball of each xenon arc lamp at the primary focus of its lamp module collector.

Optical characteristics of the solar simulator include 1)a subtense angle, i.e. the angular size of the simulated sun as viewed from the solar dynamic concentrator,(<1.5 deg);2)the ability to vary solar simulator intensity at the solar dynamic concentrator up to 1.7 kW/sq m;3) a beam diameter of 4.8 m at the solar dynamic concentrator; and 4) uniformity of illumination on the order of +/-10%.The spreadsheet program using 18*67 flux array for each lamp summed the flux distribution from each of the selected lamps and corrected the data for source distance and desired power setting The summation of average flux determined for each radial position multiplied by the spherical area of the radial segment at the optical control surface gave the total delivered power with all nine lamps at 20 kW total radiant power delivered to the optical control surface was 21.2 kW.

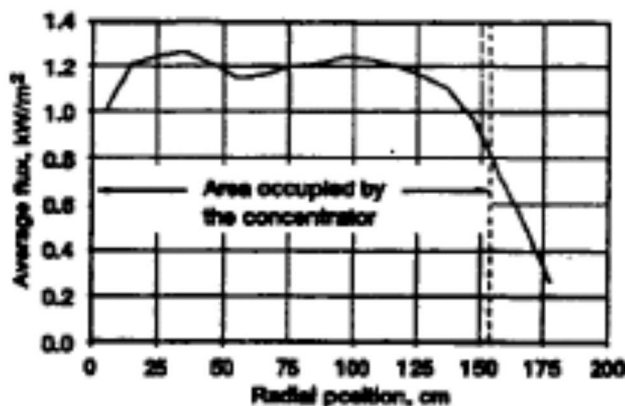


Fig. 3.8.3 - FLUX VARIATION WITH RADIAL POSITION(all nine lamps at 20 kW)

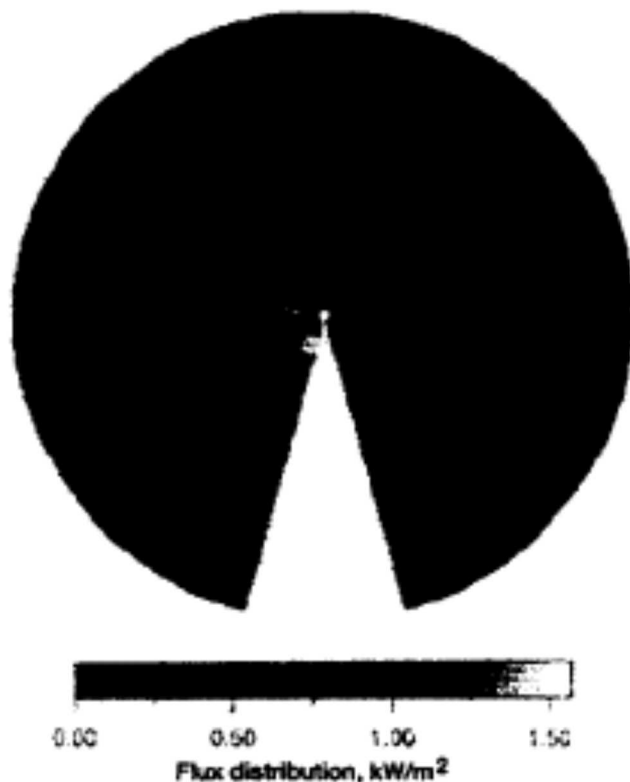


Fig. 3.8.4 - FLUX DISTRIBUTION AT THE OPICAL CONTROL SURFACE LOCATED AT THE CONCENTRATOR

The flexibility that this solar simulator provides in delivering radiant energy to a test article should make this facility useful for testing the performance of a wide variety of space power systems under various conditions.

(9)Robert L. Dreshfield

Long Time Creep Rupture of Haynes TM Alloy 188

Eighth International Symposium on Super-alloys, September 22-26,1996

The creep of Haynes Alloy 188 sheet in air was studied at temperatures of 790 °, 845 ° and 900 °C for times in excess of 30,000 h as part of a program to assure that Haynes Alloy 188 could be used in critical components of a solar dynamic power conversion system for Space Station Freedom. The rupture life and time to 0.5 and 1.0 percent creep strain of creep rupture specimens which had lives from about 6,000 to nearly 59,000 h are reported. A study was performed to evaluate the creep-rupture behaviour of Haynes Alloy 188 sheet at temperatures from 790 ° to 9130 °C and times in excess of 30,000 h. Comparison of the rupture data to previously published results suggests that the heat of material studied here is equivalent to the Haynes data at 845 ° and 9130 °C and somewhat superior at 790 °C. The time to 0.5 and 1 percent creep strain was comparable to that previously published by Haynes. While the sheet finishing technique had been changed, the slight difference between the lower temperature stress rupture behaviour can not be ascribed to that change because of the limited data in this study. Both welded and as-received specimens were tested. The welded specimen had essentially the same lives as the as-received specimens. Comparison of this data with

previously published results suggests that this material was similar in behaviour to that previously studied by Haynes except at 790 °C where the current sheet is somewhat stronger in stress rupture. Therefore the previously published data for Haynes Alloy 188 may be used in conjunction with this data to estimate the lives of components for a long life solar dynamic power system.

Three creep rupture tests were discontinued after 16,500 to 23,200 h and tensile tested at room temperature or 480 °C. The elongation of all three specimens was substantially reduced compared to the as-received condition or as aged (without applied stress) for 22,500 h at 820 °C. The reduction in elongation is thought to be caused by the presence oxidized pores found across the thickness of the interrupted creep specimens. The implications of the severe loss of ductility observed in tensile tests after prolonged creep test needs further study.

The TIG (tungsten inert gas welded) welded specimens in the present work had virtually the same creep rupture lives as non-welded material. Thus it appears that the engineering creep-rupture behaviour of welded Haynes Alloy 188 is the same as non-welded material. Three creep specimens were removed from test prior to fracture and subsequently tensile tested. Tests at both room temperature and at 480 °C showed extreme loss in ductility. The room temperature tests showing only about 1 percent elongation and the 480 °C test having only about 5 percent. This loss is believed to be associated with internal creep damage across the thickness of the sheet. While it is not likely to be of significance for the proposed Space Station application where the alloy will be exposed either to salt, vacuum or an inert gas, it would be prudent to study this phenomenon in greater detail if a long-life solar dynamic system is to be deployed.

In closing it is appropriate to comment that a 2.0 kW solar dynamic conversion system using many components of the system which was originally developed for Space Station Freedom has been successfully tested in a vacuum tank using a solar simulator at the Lewis research center.

(10)Dennis Alexander

2 kWe Solar Dynamic Ground Test Demonstration Project

Volume I: Executive Summary

NASA CR-198423, Vol. I, February 1997

The Solar Dynamic Ground Test Demonstration (SDGTD) successfully demonstrated a 2kW solar-powered closed Brayton cycle system in a relevant space thermal environment except for microgravity. The Brayton cycle is an all-gas-phase cycle and is not effected by the presence or absence of gravity.

The receiver developed for this purpose is suspended from a structure attached to the tank floor. The light energy is projected through the aperture by the concentrator during the sunlight portion of the orbit. *This* energy falls directly on the canister surfaces and is absorbed. The temperature of the canisters is raised and the salt heated and melted. Gas from the power conversion system flows through the tubes and absorbs heat from the inner surface of the canisters. During the eclipse portion of the orbit, heat stored in the canisters, both sensible and latent, continues to provide energy to the gas until the eclipse portion of the orbit ends. In rough terms, the eclipse period is one-third of the orbit. Therefore approximately two-thirds of the incoming light energy is transferred through the canisters to the gas during the sunlit portion of the orbit and the remaining one-third is stored in the canisters for the eclipse period.

It consists of a segmented graphite aperture plate to

- allow solar "walk on," which would occur in an actual flight system where acquisition of the sun would require the hot spot to be moved into the aperture
- absorb the "spillage" of light from the concentrator which is not directed through the aperture (approximately 4-5 percent of reflected sunlight).

The engine was operated for 48 hours producing a maximum of 2080 watts of ac power. An efficiency in the range of 14 to 17 percent was demonstrated during the test. This efficiency is available user dc energy divided by solar energy projected at concentrator averaged for an entire orbit, including the eclipse portion.

The design and manufacturing technologies necessary to produce optical facets and thermal energy storage canisters consistent with 25 kW sized systems have been demonstrated. System efficiency of greater than 15 percent (all losses fully accounted for) was achieved.

The next step in the development of solar dynamic space power will be a flight test.

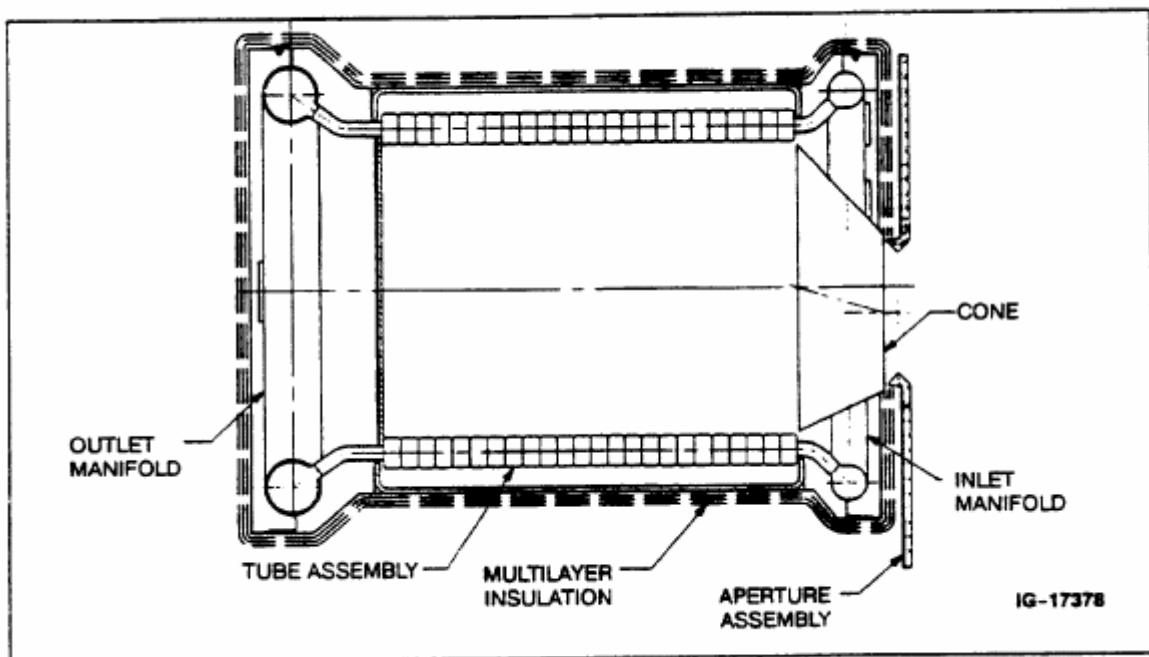


Fig 3.10.1 - receiver cross section

CONTAINMENT CANISTER CONFIGURATION

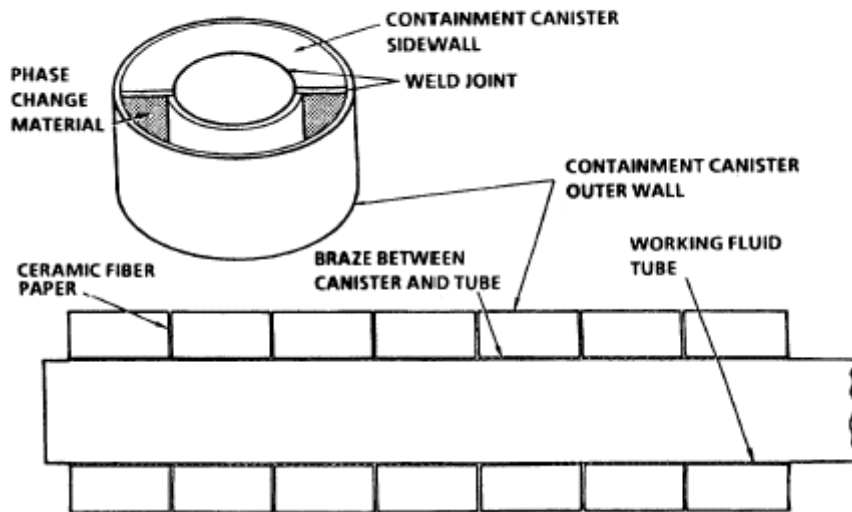


Fig. 3.10.2

(11)Dennis Alexander
2 kWe Solar Dynamic Ground Test
Demonstration Project, Volume II: Design Report
NASA 3-26605 February 1997

The receiver design comprises a cylindrical receiver cavity, the walls of which are lined with a series of tubes running the length of the cavity. The receiver incorporates integral thermal storage, using a eutectic mixture of lithium fluoride and calcium difluoride as the thermal storage solid-to-liquid phase change material (PCM). This thermal storage is required in order to enable power production when the solar simulator is off (equivalent to an eclipse period for a typical low-earth orbit).

The eutectic has a melting point of 767°C . The working fluid flows through a finned annular region in the tubes. The PCM is contained in a series of hermetically sealed metal containment canisters. The canisters are stacked and brazed to the working fluid tube. The receiver cavity walls consist of a metallic shell with an inner ceramic cloth liner. The shell is externally insulated.

The receiver configuration combines three functional components—the heat receiver, the heat source heat exchanger, and the thermal storage device—into a single unit. The working fluid from the recuperator flows to a toroidal manifold at the aperture end of the receiver. The manifold distributes the fluid to the individual tubes. The flow is collected in the outlet manifold and sent to the turbine.

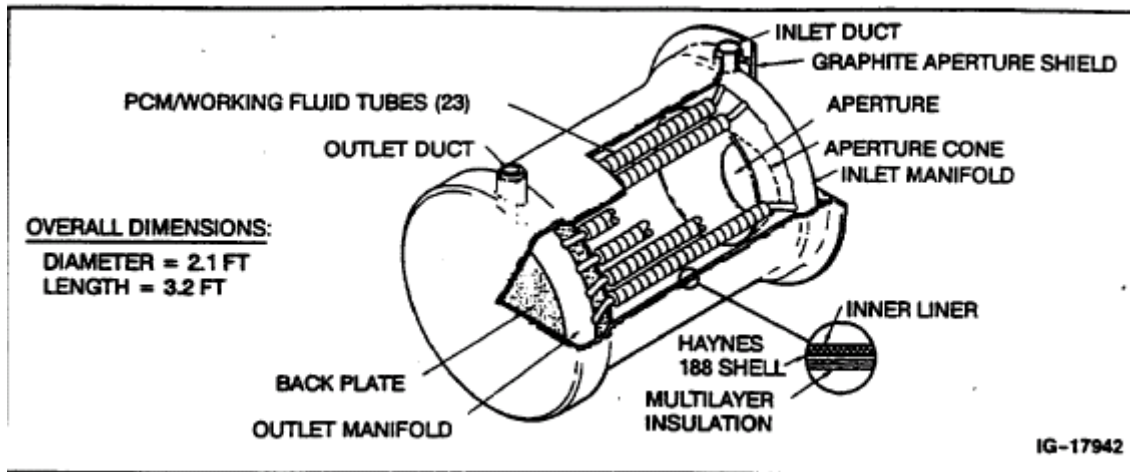


Fig. 3.11.1 – SDGTD receiver

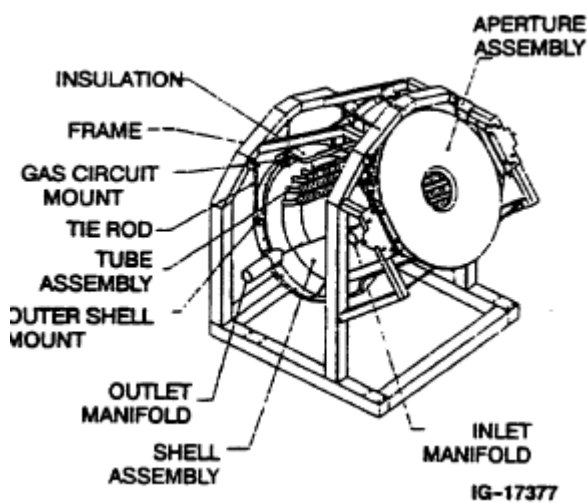


Fig. 3.11.2 – Receiver assembly overview

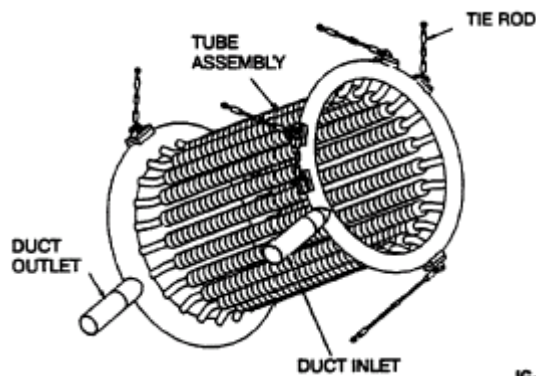


Fig. 3.11.3 - Receiver gas circuit

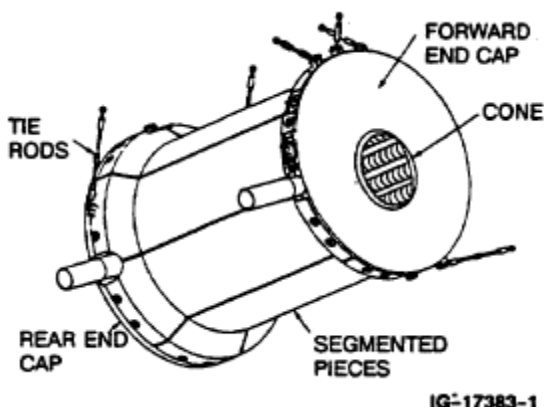


Fig. 3.11.4 – Outer shell assembly

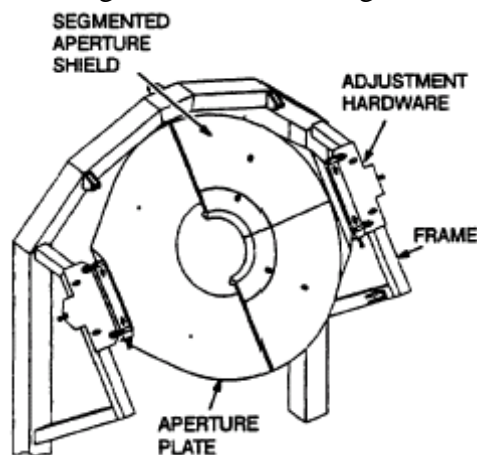


Fig. 3.11.5 – Receiver aperture assembly

(12)Dennis Alexander
2 kW Solar Dynamic Ground Test Demonstration Project
Volume III: Fabrication and Test Report

NASA Contractor Report 198423, Vol. III, February 1997

The receiver is made up of four subassemblies. The gas loop subassembly consists of toroidal manifolds, gas transport tubes, and salt containment canisters. Exterior to the gas loop is the outer shell subassembly, consisting of a thin metal shell covered on the outside with multilayer insulation and on the inside with a refractory shielding. At the aperture opening to the receiver is the heat shield subassembly, consisting of a graphite heat shield with its support and adjustment hardware. These three subassemblies are independently fastened to the support frame subassembly.

The use of individual containment canisters for the PCM is a key attribute of the receiver design. This configuration affords a readily fabricated and highly reliable design. Failure of a canister would affect only that individual canister, and have minimal impact on receiver operation. The compartmentalization also reduces the chance of failure by localizing void formation upon freezing (due to the lower density of the liquid as compared to the solid), minimizing the likelihood of high stress buildup. The receiver cavity walls consist of a metallic shell with an inner ceramic cloth liner. The shell is externally insulated. The receiver gas circuit, outer shell assembly, and aperture assembly are each independently mounted to a support frame, using tie rods. The approach minimizes weight-induced and thermally-induced stresses by off-loading weight from the gas circuit and allowing thermal growth.

(13)Carsie A. Hall, III, Emmanuel K. Glakpe, Joseph N. Cannon, and Thomas W. Kerlake

Modeling Cyclic Phase Change and Energy Storage in Solar Heat Receivers

NASA Technical Memorandum 107487, June 1997

Solar heat receivers employing encapsulated phase change materials (PCMs) have the advantage over sensible heat receivers of requiring less mass while producing higher energy storage densities. This makes them ideal candidates for energy storage in the space environment where temperatures are sufficiently high and PCMs with high latent heats of fusion become indispensable. Numerical results pertaining to cyclic melting and freezing of an encapsulated phase change material (PCM), integrated into a solar heat receiver, have been reported. The cyclic nature of the present melt/freeze problem is relevant to latent heat thermal energy storage (LHTES) systems used to power solar Brayton engines in microgravity environments. Specifically, a physical and numerical model of the solar heat receiver component of NASA Lewis Research Center's Ground Test Demonstration (GTD) project was developed and results compared with available experimental data. Multi-conjugate effects such as the convective fluid flow of a low-Prandtl-number fluid, coupled with thermal conduction in the phase change material, containment tube and working fluid conduit were accounted for in the model. A single-band thermal radiation model was also included to quantify reradiative energy exchange inside the receiver and losses through the aperture. The eutectic LiF-CaF₂ was used as the phase change material (PCM) and a mixture of He/Xe was used as the working fluid coolant.

PCM melting was induced by thermal radiation from a heater sleeve surrounding the canister and PCM freezing was induced by shutting the power to the heater and opening the shutter, thus, allowing the stored energy to conduct to the central rod and onto a radiator disc to reject the heat to space. solar heat receiver. The PCM melting and freezing processes are modeled using a hybrid enthalpy/temperature formulation with mushy zone prediction capability.

Numerical and experimental results are compared for balanced orbit and steady-state modes, and in both subcooled and latent (two-phase) regimes. Results show that while maximum and average canister outer surface temperatures are relatively insensitive to changes in receiver

gas inlet temperatures, receiver gas exit temperatures are very sensitive to changes in receiver gas inlet temperatures, particularly for operation in the subcooled regime. HOTTube predictions also show very good agreement with GTD experimental data for subcooled and latent steady-state modes.

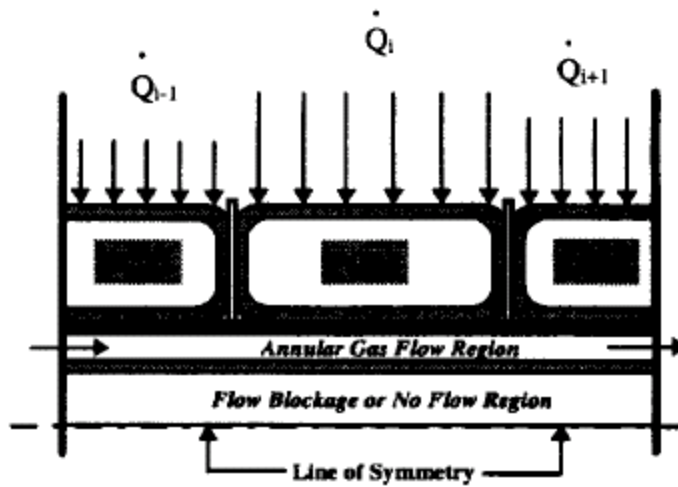


Fig. 3 Schematic of encapsulated PCM tube configuration with annular gas flow.

Fig. 3.13.1

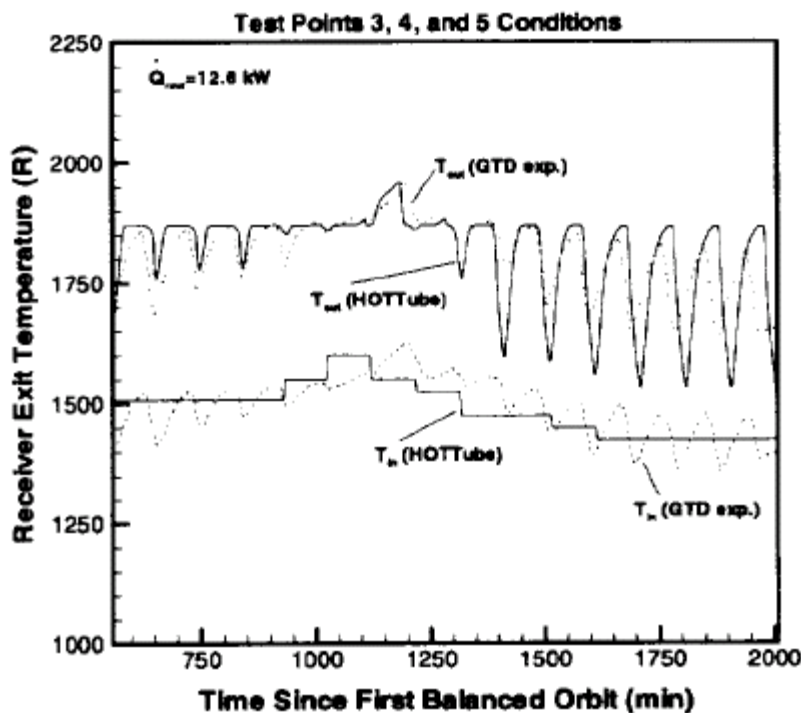


Fig. 9 Comparison of numerical and experimental results for the receiver gas exit temperature.

Fig. 3.13.2

(14) Thomas W. Kerslake, Lee S. Mason, Hal J. Strumpf
High Flux High Temperature Thermal Vacuum Qualification Testing of a Solar Receiver Aperture Shield

32nd Intersociety Energy Conversion Engineering Conference July 27-Aug 1, 1997

NASA Lewis Research Center (LeRC) and the Russian Space Agency (RSA) teamed together to design, build and flight test the world's first orbital Solar Dynamic Power System (SDPS) on the Russian space station Mir.

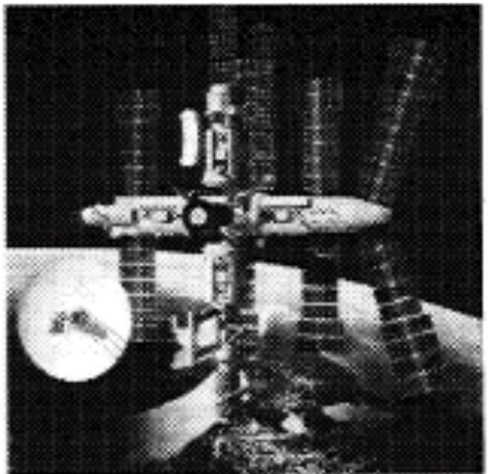


Fig. 3.14.1 SDFD hardware on moon

The aperture shield comprises the front face of the cylindrical cavity heat receiver and is located at the focal plane of the solar concentrator. It is constructed of a 0.0095-m thick stainless steel plate with a 1-m outside diameter, a 0.24-m inside diameter and covered with high-temperature, refractory metal multi-foil insulation (MFI) i.e. 40 layers of tungsten and molybdenum foil screen layers (see fig).The aperture shield must meet 3 primary requirements:1) minimize heat loss from the receiver cavity,2) provide a stiff, high strength structure to accommodate shuttle launch loads and 3) protect receiver structures from highly concentrated solar fluxes during concentrator off-pointing events.

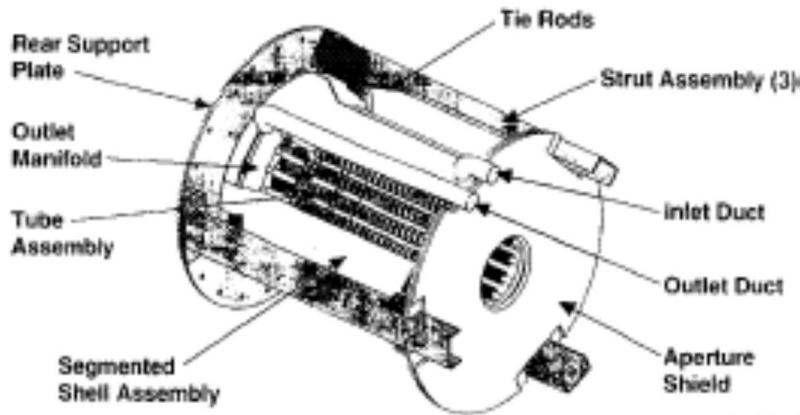


Fig. 3.14.2 SDFD Receiver

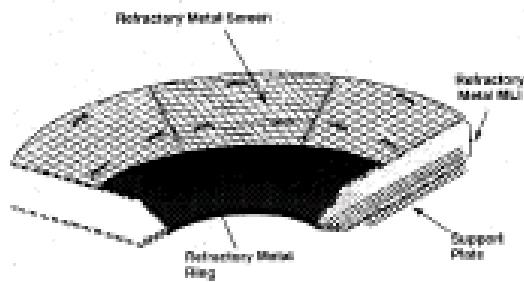


Fig. 3.14.3 SDFD Aperture Shield

The SDPS functions by pointing a parabolic reflecting concentrator at the Sun and focusing solar energy into a heat receiver located at the focal point. The receiver transfers heat to a working gas that drives a turbo alternator to produce electric power. Waste heat is radiated to space via a heat rejection system. To satisfy Mir operational safety protocols, the aperture shield was required to accommodate direct impingement of the intensely concentrated solar image for 1 hour period.

To verify thermal-structural durability under the anticipated high-flux, high-temperature loading, an aperture shield test article was constructed and underwent a series of two tests in a large thermal vacuum chamber configured with a reflective, point focus solar concentrator and a solar simulator.

The primary objective of the test was to demonstrate the structural adequacy of the aperture shield outer multi-foil insulation(MFI) layers and structure under severe solar thermal loading. Several thermal loading was defined as a one-time exposure to an incident solar flux of 80 W/cm² for a period of 60 min in a vacuum environment. The testing would be considered successful if all of the following criteria were met: (1) the test article was exposed to the required flux levels for at least 30 minutes with 60 minutes as the goal, (2) all required test article data and inspection results were properly recorded, (3) test article sustained no significant surface blistering or warpage and (4) test article sustained no significant screen or foil breakage.

In the first test, a near equilibrium temperature of 1862 K was attained in the center of the shield hot spot. In the second test, with increased incident flux, a near equilibrium temperature of 2072 K was achieved. The aperture shield sustained no visible damage as a result of the exposures.

With a peak incident flux goal of 80 W/m², the actual peak flux achieved was estimated to be 70+ -10 W/m².

These results show that this aperture shield would be tolerant of significantly higher fluxes and temperatures.

(15)Staff of Solar Dynamic Power System Branch, Lewis Research Centre, Cleveland, Ohio, NASA
Solar Dynamic Power System Development for Space Station FREEDOM

Introduction

This report gives a detailed description of a solar dynamic power system developed for the space station FREEDOM program.

Heat Receiver

For this ambitious program two heat receiver designs have been developed the baseline design and the advanced development design.

1.) Baseline Receiver Design

Design Description

The heat receiver accepts concentrated solar energy from the concentrator and directly transfers a fraction of this energy to a closed Brayton-cycle working fluid circulating through the receiver. The remaining solar energy is absorbed by a thermal energy storage (TES) phase-change material (PCM) located within the receiver. TES permits continuous heat engine operation through orbital eclipse periods when solar insolation is not available.

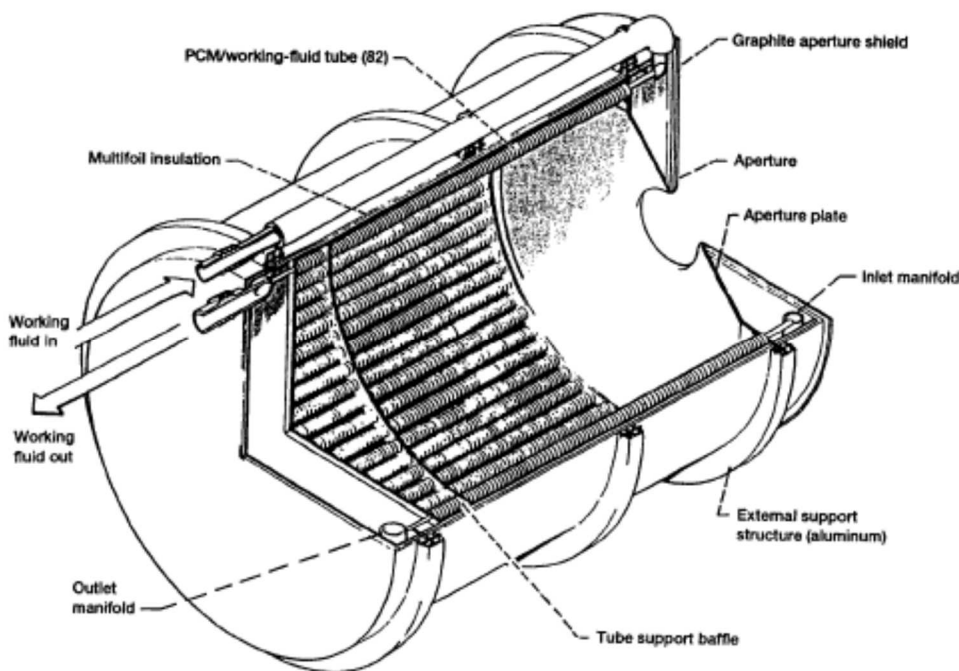


Fig 3.15.1 Solar Heat Receiver concept Diameter 6.1 ft Length 9.8 ft

The heat receiver concept is shown in figure 1 and is shown in cross section in figure 2. The receiver is an insulated cylindrical cavity lined with multiple working-fluid tubes. The cylinder is closed at one end and has a circular aperture at the other end to admit concentrated solar energy. Relatively cool working fluid flows through an external duct to a toroidal inlet manifold at the aperture end of the receiver. After making a single pass through the individual tubes, hot working fluid is collected in a toroidal outlet manifold and is sent to the heat engine turbine. Various receiver design attributes and a receiver mass breakdown are given in tables 1 and 2, respectively.

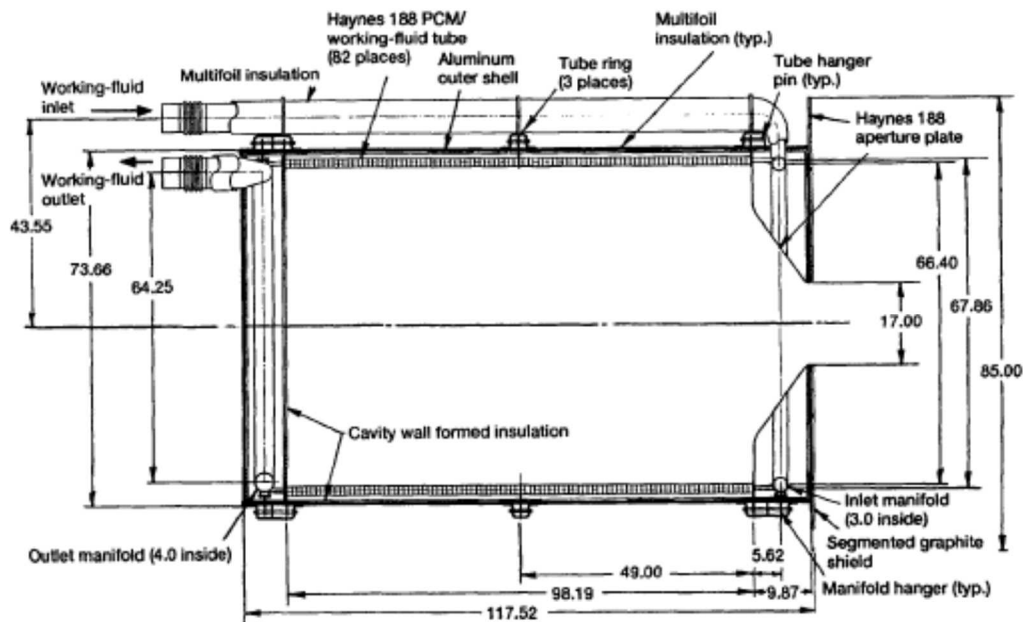


Fig 3.15.2 Solar Receiver Layout (Dim in inches)

Solar dynamic module user power, kW	25
Receiver incident thermal rating, kWt (max.)	209
Working fluid	He/Xe (MW=40)
Receiver inlet temperature range, °F	975–1040
Receiver outlet temperature range, °F	1340–1400
Tube material	Haynes 188
Containment canister material	Haynes 188
Tube support ring material	Haynes 188
Aperture shield material	Graphite
Piping and header material	Haynes 188
External support structure material	Aluminum
Formed insulation	(a)
Multifoil insulation	Nickel, aluminum

Table 3.15.1 : CBC Receiver Design Attributes

Component	Weight, lbm
Phase-change material	750
Working-fluid tube	240
Containment canisters	1538
Inlet/outlet manifolds	117
Insulation	438
Shell and structure	516
Aperture plate and shield	263
Total	3862

Table 3.15.2 : CBC Receiver Mass Summary

Each working-fluid tube is surrounded by multiple PCM containment canisters that are constructed of the cobalt-base superalloy Haynes 188 as shown in figure 3.and 4.

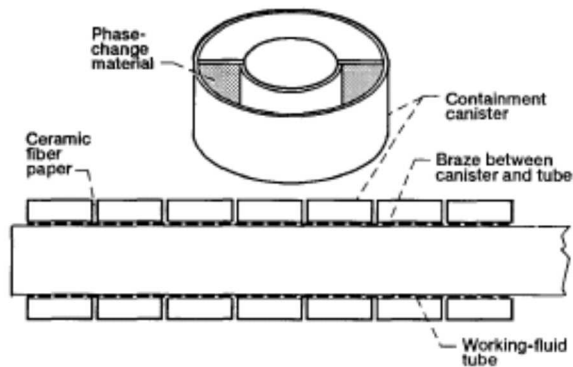


Fig 3.15.3 Receiver Tube Configuration

The PCM is a eutectic mixture of lithium fluoride-calcium fluoride (LiFCaF₂) salt, which has a melting point of 768C Each canister is individually filled with PCM and hermetically sealed by electron beam welding

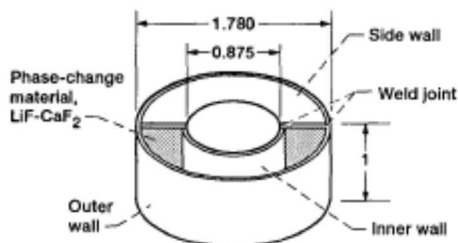


Fig. 3.15.4 PCM Containment Canister

The canisters are stacked on each working-fluid tube with ceramic paper spacers between adjacent canisters and then brazed to the working-fluid tube

The primary purpose of the braze joint is to conduct heat from the canister to the working-fluid tube. The receiver cavity walls consist of a layer of formed insulation. Energy is reflected and radiated off the cavity side wall to the back side of the receiver tubes to provide relatively uniform heat input circumferentially around the tubes. Blankets of nickel and aluminium multifoil insulation are wrapped around the formed insulation. The insulated cavity walls are enclosed in an aluminium support structure. The tubes are supported in baffles that are connected to reinforced regions of the outer support structure. Tubes fit loosely in the baffles, thereby allowing unconstrained thermal expansion. The cavity back wall moves as the tubes expand, and tube expansion is accommodated by two external baffles. The inlet manifold and the receiver support structure are protected from incident solar flux by a segmented graphite shield. The shield is designed to prevent damage from nominal on-Sun flux spillage and short-duration solar beam track-on and detrack events.

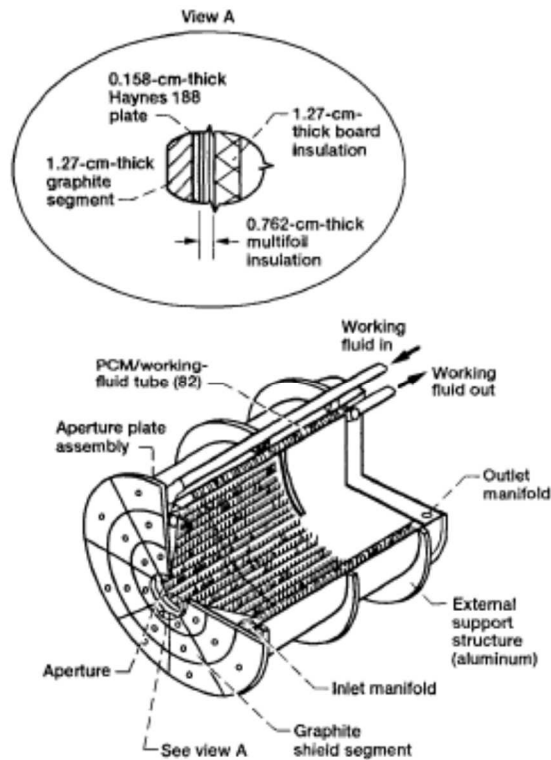


Fig 3.15.5 Solar Receiver with Aperture Plate Assembly Overall Dimension Diameter 1.86m Length 2.99m

Design Rationale

Major design constraints include the given flux input distribution from the offset, segmented surface concentrator the allowable working-fluid pressure drop, the cost, and the allowable mass or volume consistent with NSTS (national space transportation system) launch packaging requirements

The receiver cavity length and diameter were chosen to be consistent with the constraints. The aperture diameter was optimized to maximize the net energy that would be retained by the receiver over an orbit. This optimization involved the following time-dependent heat balance terms: solar flux admitted through the aperture, solar spillage flux on the aperture plate, reflected solar flux out of the receiver cavity, and infrared flux radiated out of the receiver cavity. The total mass of PCM employed was determined iteratively on the basis of the minimum PCM mass required to make performance (i.e., to deliver the required thermal power to the heat engine).

The PCM selected, a eutectic composition LiF-CaF₂ salt, was chosen on the basis of melting temperature, high heat of fusion, compatibility with the containment material, and experimentally demonstrated, stable thermophysical properties. Other PCM's considered, but eventually dropped, were LiF and the eutectic composition lithium fluoridemagnesium fluoride (LiF-MgF₂). LiF was dropped from consideration because its melting temperature was deemed too high, and LiF-MgF₂ was dropped because of its lack of stable, repeatable properties during thermal cycling tests.

The diameter, length, wall thicknesses, and number of working-fluid tubes and PCM containment canisters were chosen to satisfy several design considerations. Design

considerations include adequate heat transfer rates to the salt and the working fluid, conservative canister ullage or void volume to allow for liquid salt expansion, low thermal stresses, low working-fluid pressure drop, and salt compartmentalization. Placing the salt in small volumes or compartments serves two purposes: void volume is localized to accommodate salt melting expansion and thus minimize stress buildup in canister walls, and in the event of a canister leak, only a small portion of salt is lost, reducing the effect of salt contamination and insignificantly reducing receiver thermal storage capacity.

The working-fluid tube and canister material Haynes 188, was selected for its excellent high-temperature structural properties and its excellent compatibility with the LiF-CaF₂ salt and vacuum environment. Haynes 188 is also readily fabricable and weldable and is available in the required product forms. The nickel-base superalloy Inconel 617 is considered a close backup material to Haynes 188.

2.) Advanced-Development Receiver Design

Design Description

The advanced-development receiver design, which is considered an alternative or backup to the baseline receiver design, is similar to that design in size, mass, design approach, and overall thermal performance. However, the advanced development receiver design is distinctively different from the baseline design in two areas: the TES container design and the working-fluid tube manifolding design.

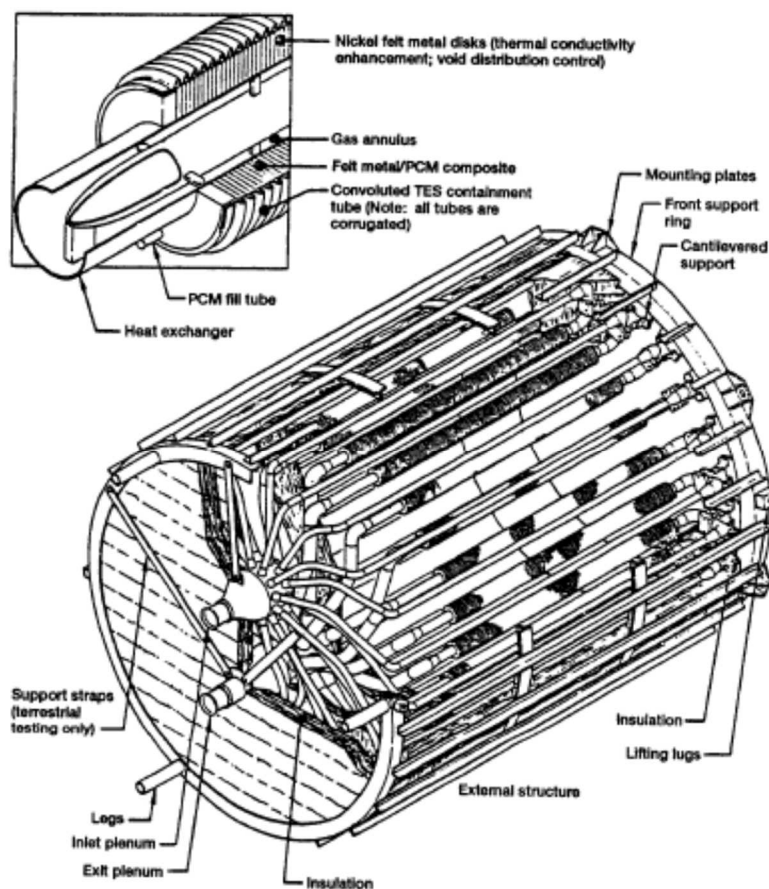


Fig 3.15.6 Advanced Developer Receiver Design Configuration

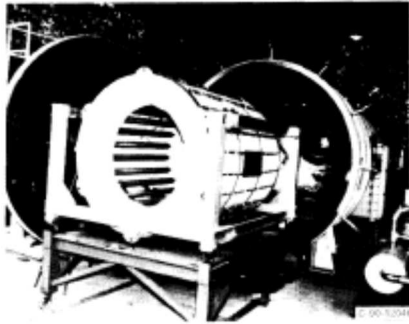


Fig 3.15.7 Advanced Development Receiver prior to testing in vacuum chamber

The advanced-development receiver design employs 24 long, tube-like annular PCM containers constructed of Inconel 617 instead of approximately 7800 short canisters made from Haynes 188. A single TES receiver tube has been taken into consideration.

The annular tube space is filled with 20-percent-dense nickel-felt matrix material that is impregnated with an eutectic composition LiF-CaF₂ salt. The outer tube wall consists of a X - in.-pitch bellows that is designed to accommodate large thermal strains. The heat engine working fluid, a 40 molecular-weight helium-xenon gas mixture, flows around a .0254m.-diameter cylindrical spud positioned inside the inner receiver tube. The spud effectively increases the gas Reynolds number, thereby increasing the forced-convection heat transfer coefficient while incurring a slight pressure drop penalty.

The working-fluid manifold design consists of long, spider plumbing runs from domed, cylindrical inlet and outlet plenums as shown in the figure.8



Fig 3.15.8 Receiver manifolding

This is in direct contrast to the baseline receiver design, which utilizes toroidal inlet and outlet headers and short, straight plumbing runs. The cylindrical plenums distribute flow uniformly between receiver tubes with a very low pressure drop (i.e., 2.5 percent of the inlet pressure (92 psi), The long plenum radial extension piping readily accommodates differential expansion between receiver tubes. To accommodate gross thermal expansion, the entire receiver tube and manifold assembly is cantilever supported at the aperture end by saddle clamps attached to the front structural ring. The receiver structure consists of stainless steel front, midspan, and back structural rings connected by longitudinal angle irons as shown in figure 9. The receiver tubes are insulated by ceramic fiber blanket insulation that also forms the cavity walls.

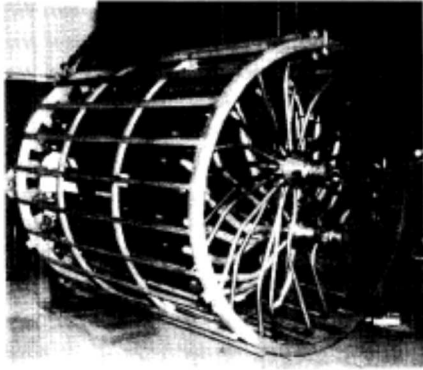


Fig 3.15.9 Receiver Structure

A third, perhaps more subtle, difference in the respective receiver designs is that the advanced-development receiver was designed to meet early SD program requirements and was fabricated as a ground test article (with a 1000-hr test life). As such, the advanced-development receiver design was based on solar input from a continuous surface Newtonian concentrator and on a constant working fluid inlet temperature and did not have to accommodate peaking or startup operating modes. An aperture plate assembly was not designed or built because an internal cavity heat source would be used during ground vacuum testing. Additionally, less expensive materials were permitted for fabricating receiver insulation, structure, and working-fluid plumbing and manifolding hardware. Its dimensions, a thermal performance summary, and a mass breakdown are given in tables 3,4 and 5 respectively.

Subsystem	Component or parameter	Dimensions	
		mm	in.
Receiver cavity	Cavity diameter	1778	70
	Cavity length	2032	80
	Receiver outer diameter (OD)	2184	86
	Total receiver length	2794	110
	Aperture diameter	330	17
Heat exchanger	HX/TES tube centerline diameter	1575	62
	HX tube OD	51	2
	Spud tube OD	25	1
	HX tube wall thickness	1.5	0.06
Corrugated TES containment tube	Wall thickness	0.25	0.01
	Convolution OD	100	3.94
	Convolution ID	91	3.58
	Convolution pitch	6.4	0.25

Table 3.15.3 Receiver Dimension

Total solar input to receiver, kW	184.9
Minimum receiver efficiency, percent	91.3
Maximum receiver thermal loss, kW (percent of total)	13.7 (7.4)
Reflection	0.8 (0.4)
Reradiation	9.0 (4.9)
Conduction through insulation	3.9 (2.1)
Sensible energy source, kW (percent of total)	2.4 (1.3)
Temperatures (nominal quasi-steady operation), °C (°F):	
Control of turbine inlet temperature	705 (1300); -9 (-15); 16 (30)
Maximum TES containment temperature	896 (1645)
Maximum TES temperature gradients:	
Circumferential	72 (162)
Axial	116 (241)
Maximum heat exchanger tube temperature	822 (1512)
Maximum insulation temperature	955 (1751)
Pressures:	
Pressure loss, percent of inlet	2
Maximum variation between heat exchanger tubes, percent	0.4

Table 3.15.4 Receiver Thermal Performance Summary

Receiver subsystem or component	SDHRT ^a weight		Flight weight	
	kg	lb	kg	lb
Heat exchanger/TES heat storage tubes:	759	1673	759	1673
PCM/LiF-CaF ₂	319	703	319	703
Nickel felt-metal disks	298	657	298	657
TES containment	46	101	46	101
Heat exchanger tubing	96	212	96	212
Receiver insulation	454	1000	227	500
Heat exchanger tubing and pipe	338	745	49	108
Inlet and exit plenums	82	181	82	90
Receiver structure	545	1202	272	600
Total receiver weight	2178	4801	1389	2971

Table 3.15.5 Receiver Mass Breakdown

Design Rationale

The key feature of the advanced-development receiver is the TES tube design. The motivation for using the felt-metal matrix material in the PCM containment volume is twofold. First, the nickel felt enhances conduction (and radiation) heat transfer through the otherwise poorly conducting salt. This reduces the temperature gradients (and associated thermal strains) dictated by TES tube charge and discharge requirements. Second, the nickel felt localizes salt freezing and void formation due to individual fiber wetting characteristics. Because the felt-metal wicking height (against gravity) is greater than the .1016m outer diameter of the TES tube, the liquid salt uniformly wets the entire volume of felt metal. In addition, the felt metal eliminates buoyancy-driven flows within the liquid salt. Thus, the salt melting and freezing behaviour is essentially independent of gravity when ground tested in a horizontal orientation. Hence, by means of ground tests (in normal gravity), flight performance (in microgravity) can be readily verified without the need for expensive flight testing.

Other benefits of the advanced-development receiver TES tube design approach (when compared with the baseline receiver approach) include fewer PCM containers to be filled and less welding and inspecting of both PCM containers and working-fluid plumbing and manifolding. However, both these benefits come at the expense of less redundancy in the TES subsystem (i.e., fewer salt containers) and an arguably more involved salt-filling procedure

4. CONCLUSIONS

4.1 RESULTS & DISCUSSIONS FOR SOLAR REACTORS

A current development program carried out by a consortium including Boeing, Rotem Industries, Ormat Industries and the Weizmann Institute, is developing a larger partitioned receiver system (Yogev *et al.*, 1999). This system includes a large DIAPR rated at 500 kW, and several preheaters that bring the total receiver system output to about 800 kW. In the design of this system, more care was given to minimizing the partitioning losses such as the pressure drop in series connection of receivers. This receiver system will supply thermal energy to a small gas turbine in hybrid (solar fuel) operation. This system is still small relative to large grid-connected power plants, but can serve as a demonstration of small sub-megawatt off-grid plants that are needed in many applications around the world. Larger plants can be constructed by modular assembly of several side-by-side DIAPR receivers as the high-temperature stage within a partitioned system.

Future work regarding the developed solar particle receiver will focus on achieving higher exit gas temperatures, increasing the allowable mass flow rate, evaluate different particle cloud injection configurations and add a capability for chemical analysis of the exit gases composition.

The rectangular concentrator is a practical and relatively low-cost solution for central receiver systems, in addition to its optical advantages. The significance of this demonstration is not just for this particular field layout. An appropriate non-regular optical solution can be derived for many types of asymmetric fields using the optimized receivers. The severe restrictions placed on high-performance field design by symmetric secondary concentrators are therefore alleviated, and additional degrees of freedom are now available for field design and optimization.

The main losses of energy from a high-temperature solar receiver are by thermal emission re-radiation and convection through the aperture. All other losses can, in principle, be made in which significant. These aperture losses can be minimized by a partitioning approach (Ries *et al* 1995; Doron and Kribus, 1996). The losses are reduced by dividing the total aperture area into parts that are exposed to different irradiance flux levels, while energy transfer from the high temperature to the lower temperature parts is prevented. The working fluid gradually heated as it passes through a sequence of receiver elements with increasing irradiance levels. In this way, the highest fluid and absorber temperatures are reached only near the end of the working fluid's path, and the losses over much of the total aperture area are relatively low. Partitioning fits naturally with the common distribution of radiation that a heliostat field creates on the target plane: higher flux at the center, lower flux away from the center. It also fits quite naturally with the convective heat transfer to the receiver's working fluid. The limiting case having minimum thermal energy losses and maximum receiver efficiency is an infinite number of small partitions (Ries *et al* ., 1995). This approach can significantly improve the use of an available irradiance distribution produced by the primary concentrator field, thus gaining the most benefit from the investment in concentration optics. The actual improvement in performance relative to a single receiver depends on the irradiance distribution and on the number of stages. An experimental system to demonstrate the partitioning approach was constructed at the Weizmann Institute.

Solar particle receivers can be used either to heat up a process gas or to perform chemical reactions on the particles themselves. The developed solar particle receiver is intended for applications using a process gas at temperatures of 1500–2000 K, where the use of electricity or combustion of fossil fuels to heat the gas is either inefficient or prohibitive by emission regulations.

For a solar reactor based on ceramic refractory honeycomb structure coated with active redox materials capable of achieving a uniform temperature profile of 1473 K, analysis indicates that there is a potential to reduce the production cost of hydrogen down to 10-12 Eurocent/kWh. Reduction of cost for the installation of the solar part of the plant, which is expected to proceed with the ongoing commercialization of solar thermal applications, may produce even lower cost.

Combustion system of the hybrid heat pipe receiver still needs some improvements to reach a more stable flame at all possible operation modes and to reduce CO-emissions.

The viability of using concentrated sunlight as a heat source to synthesize AlN in a high-temperature vibrating fluidized bed reactor has been proved, the process being environmentally benign. It involves no toxic chemical reactants, intermediates, or products. The solar coupled processing provides for a clean energy source to initiate and drive the high temperature reaction.

Future developments are estimated by extrapolating on the DIAPR technology. Many modern power generation cycles and thermo-chemical processes, such as fuel

production, require high temperatures in excess of 1,000°C and pressures of 10–30 bar. A solar receiver capable of operating at these conditions could be integrated with the most efficient power cycles available, such as the Combined Cycle of gas and steam turbines, which has a proven thermal-to-electricity efficiency of over 50%. Such a configuration, combined with the appropriate collector optics, could have performance and cost advantages over other solar thermal concepts, and may be competitive with conventional fuel plants in certain markets .

4.2 RESULTS & DISCUSSIONS FOR SOLAR ENGINES

The interest in space solar engines solutions develops because technical solutions utilized for these purposes (receiver configuration, storage system etc.) could be applied for terrestrial applications, too.

The Solar Dynamic Ground Test Demonstration (SDGTD) successfully demonstrated a 2 kW solar-powered closed Brayton cycle system in a relevant space thermal environment. In addition to meeting technical requirements the project was completed 4 months ahead of schedule and under budget. The following conclusions can be supported:

- The component technology for solar dynamic closed Brayton cycle technology has clearly been demonstrated.
- The thermal, optical, control, and electrical integration aspects of systems integration have also been successfully demonstrated. Physical integration aspects were not attempted as these tend to be driven primarily by mission-specific requirements.
- System efficiency of greater than 15 percent (all losses fully accounted for) was demonstrated using equipment and designs which were not optimized. Some pre-existing hardware was used to minimize cost and schedule.

In closing it is appropriate to comment that a 2.0 kW solar dynamic conversion system using many components of the system which was originally developed for Space Station Freedom has been successfully tested in a vacuum tank using a solar simulator at the Lewis Research Center.

The success of finding a very high emittance coating which is durable to VHT will help to ensure successful demonstration of solar dynamic power generation for space applications, and has potential for applications in other systems requiring high emittance surfaces. Based on these findings, the alumina based coating has already been chosen for emittance enhancement for the SD GTD parasitic load radiator in addition to the heat receiver canisters.

Results show that while maximum and average canister outer surface temperatures are relatively insensitive to changes in receiver gas inlet temperatures, receiver gas exit temperatures are very sensitive to changes in receiver gas inlet temperatures, particularly for operation in the subcooled regime. HOTTube predictions also show very good agreement with GTD experimental data for subcooled and latent steady-state modes.

There are two primary reasons for the interest in the solar dynamic system as the source of growth power. A photovoltaic/solar dynamic hybrid system offers the flexibility of a power system with two types of sources, thus ensuring an uninterrupted power supply in the unlikely event of a major or systematic problem in either type of source. But even more compelling is the potential cost saving that can be realized with solar dynamics. Solar dynamic power generating and storage components have longer lifetimes than photovoltaic arrays and batteries. Long lifetimes result in substantial savings in hardware replacement, launch, and on-orbit installation costs. Because of the significantly higher solar-to-electric power

efficiency of a solar dynamic system, its solar collection area is only about 25 percent of that for a photovoltaic system for a given power output. Therefore, it will have lower aerodynamic drag and lower reboost requirements. For constant-drag operation, solar dynamic systems would allow operation at lower altitudes. This would permit the National Space Transportation System (NSTS) orbiter to rendezvous with Freedom at lower altitudes, significantly increasing the orbiter's payload capacity and lowering the launch cost per pound to orbit.

Studies have shown that the various operations and hardware cost savings resulting from the use of solar dynamic power rather than photovoltaic power for growth would amount to a reduction in life-cycle costs of several billion dollars over the 30-year life of Freedom station.

Further receiver development is required in the following areas: canister design and fabrication, cavity and TES tube design, working-fluid flow loop design, aperture plate assembly design, thermal "state-of-charge" determination techniques, and long-term, high-temperature component life assessment techniques.

Further canister fabrication development is needed to refine canister metal-forming operations, weld joint design and welding parameters, weld inspection techniques and approaches, and salt-fill-hole closure weld design. Canister production salt-filling techniques need further work to ensure that a repeatable process is developed which precludes salt contamination and distillation. In addition, a braze material must be selected and a brazing technique developed for attaching the canisters to the working-fluid tubes. The braze joint must provide high thermal conductance between the canisters and the working-fluid tube for the 3D-year design life of the receiver.

Further heat transfer analyses are needed to refine the receiver cavity design by studying the effects of cavity length-to-diameter ratio, variable cavity diameter, tube-to-tube spacing, and internal cavity wall radiative properties. In conjunction with these studies, TES tube design refinements could be made to maximize the total mass of PCM melted and to minimize the receiver cavity orbital temperature variation. Tube performance increases could be achieved by considering, as a function of tube length, variable canister diameters, wall thicknesses, contained PCM masses, and void volume fractions

The design of the receiver working-fluid flow loop needs further development. Design attributes that require special attention include low fluid pressure drop through ducts and manifolds, high structural compliance to accommodate differential and gross thermal expansion, and working-fluid containment. Although low pressure drop is extremely important for heat engine efficiency, fluid containment is the most important design feature of the fluid flow loop because loss of working fluid constitutes a SDPM single-point failure. Therefore, highly compliant manifold designs that minimize the number and size of weld joints should be developed to preclude large thermal stresses that could fail weld joints. In addition, double containment designs for manifolds and ducts should be considered to further reduce the likelihood of working-fluid leaks.

The aperture plate assembly design requires further development in the areas of material selection, thermal performance, and structural design. The specific graphite shield material chosen requires testing to verify its capacity for withstanding high temperatures, large temperature gradients, and the low-Earth-orbit environment of vacuum and atomic oxygen. The design must incorporate a highly effective, multilayered insulation (composed of high temperature metal foils or another material) to protect the underlying receiver structural metal

from temperature extremes. The insulating performance of the aperture design must be validated through analyses and tests. Lastly, the aperture plate assembly layers must be mechanically supported to allow for unconstrained thermal expansion. This requirement is most critical for the shield layer, which directly receives the highly concentrated solar flux. Analyses and tests are required to determine the extent of shield segmentation and to evaluate a scheme to attach shield segments to the other aperture plate assembly layers.

Techniques are needed to determine the so-called receiver state of charge, or the quantity of stored thermal energy within the receiver. Knowledge of the receiver state of charge is necessary for SDPM operating modes including cold startup and peaking/recovery power production as well as for long-term energy balance maintenance. Basic areas needing further work include identification of robust, long-lived sensors, judicious selection of the receiver parameters to measure, and development of thermal control and state-of-charge algorithms.

In addition to the suggestions given in the preceding section four other recommendations are offered here concerning the development of the solar heat receiver. In short, the recommendations are as follows: modify the multiple layers of construction in the aperture plate assembly, emphasize integration of receiver components early in the receiver design cycle, emphasize integration of the receiver with the SDPM early in the receiver design cycle, and structure future receiver development programs to be hardware intensive (i.e., allocate a large fraction of program resources for the fabrication, inspection, testing, and documentation of full-scale test hardware

Because of limited program resources, TES tube engineering development was somewhat restricted, making this area fertile ground for more development work. Specific TES tube design features to further develop include the following:

(1) **Bellows:** Greater effective compliance and durability are required as well as an improved method for terminating the bellows at the tube end cap without affecting the bellows structural characteristics. The bellows design should also accommodate a continuous matrix material that completely fills the convolution volumes to mitigate matrix material deformation or translation and the adverse void effects that are encountered when using felt-metal disks.

(2) **Matrix material:** Long-term cycling tests are needed to demonstrate salt distribution stability within the matrix, matrix structural integrity, and matrix material chemical compatibility with salts. Matrix materials to consider include metal felts (other than nickel), ceramic and graphite fibers, and various material foams. These materials offer potentially lower mass and better wicking and thermal transport enhancement than nickel felt, which was chosen in large part due to advanced development receiver program constraints.

Given that the development work suggested in the preceding section showed promising results, it is recommended to directly incorporate the matrix material technology of the advanced-development receiver program into the baseline receiver design. The resulting hybrid receiver design would have fewer, larger TES canisters with thinner walls (when compared with the current baseline receiver design), would possibly even have bellows, and would contain a salt impregnated matrix material. This hybrid design conceivably would have lower mass and higher thermal efficiency than either the baseline or advanced-development receiver designs while maintaining gravity-independent operation and TES subsystem redundancy. Furthermore, if the number of canisters is sufficiently reduced, the number of

working-fluid tubes could be reduced to enable either manifolding approach (i.e., toroidal or cylindrical spider plenum designs).

Another recommendation, for future receiver hardware development programs, is to thoroughly document fabrication histories and fully inspect hardware before testing commences. An example of this would be a full pretest computed-tomography inspection of each TES tube to document the initial condition of the salt-impregnated matrix. This becomes very important for gaining needed information on the performance of the TES subsystem, whose detailed characteristics heretofore have not been well explored. This documentation also greatly simplifies post-test assessment of hardware thermal and mechanical performance. Although this appears to be a basic recommendation, it is one easy to overlook or relinquish when budgetary and schedule pressures are encountered during the planning and/or implementation stages of a program.
